Universidade de Aveiro

Ano 2018

Departamento de Engenharia de Materiais e Cerâmica

JOANA DANIELA FERREIRA GONÇALVES

DESENVOLVIMENTO DE NANOPARTÍCULAS MULTIFUNCIONAIS REVESTIDAS COM FUCOIDANA PARA TERAPIA COMBINADA DO CANCRO

DEVELOPMENT OF MULTIFUNCTIONAL FUCOIDAN-COATED NANOPARTICLES FOR COMBINED CANCER THERAPY

Universidade de Aveiro

Ano 2018

Departamento de Engenharia de Materiais e Cerâmica

JOANA DANIELA FERREIRA GONÇALVES

DESENVOLVIMENTO DE NANOPARTÍCULAS MULTIFUNCIONAIS REVESTIDAS COM FUCOIDANA PARA TERAPIA COMBINADA DO CANCRO

DEVELOPMENT OF MULTIFUNCTIONAL FUCOIDAN-COATED NANOPARTICLES FOR COMBINED CANCER THERAPY

Dissertação apresentada à Universidade de Aveiro para a obtenção do grau de Mestre em Materiais e Dispositivos Biomédicos, sob a orientação científica da Doutora Paula Celeste da Silva Ferreira, Equiparada a Investigadora Coordenadora do Departamento de Engenharia de Materiais e Cerâmica da Universidade de Aveiro e da Doutora Cláudia Sofia Cordeiro Nunes, Pós-Doutorada do Departamento de Engenharia de Materiais e Cerâmica da Universidade de Aveiro.

Este trabalho foi desenvolvido no âmbito do projeto CICECO-Aveiro Institute of Materials POCI-01-0145-FEDER-007679 (Refª. FCT UID/CTM/50011/2013) financiado por fundos nacionais através da FCT/MEC e quando aplicável cofinanciado pelo FEDER, no âmbito do Acordo de Parceria PT2020. Agradece-se o suporte financeiro do projeto PTDC/NAN-MAT/28785/2017.

Dedico este trabalho aos meus pais, irmãos e amigos.

o júri

Presidente	Professor Doutor Rui Ramos Ferreira e Silva professor associado, Departamento de Engenharia de Materiais e Cerâmica da Universidade de Aveiro
Arguente	Professor Doutor Vítor Brás de Sequeira Amaral professor catedrático, Departamento de Física da Universidade de Aveiro
Orientadora	Doutora Paula Celeste da Silva Ferreira equiparada a investigadora coordenadora do Departamento de Engenharia de Materiais e Cerâmica da Universidade de Aveiro

.

acknowledgments

In the first place I would like to thank my supervisors Dr. Paula Ferreira and Dr. Cláudia Nunes for their knowledge, support, and for their patience to help and guide me.

I want also to express my gratitude to: Eng. Marta Ferro and Eng. Célia Miranda from the Department of Materials and Ceramic Engineering of University of Aveiro that helped me in TEM and BET analyses respectively; Dr. Alvaro Mayoral and Dr. Qing Zhang both researchers associate professors in School of Physical Science and Technology in Shanghai for TEM analyses; Dr Rosário Soares and Dr. Manuela Marques from the Department of Chemistry of University of Aveiro for the help with XRD and elemental analysis, respectively. I also want to thank Prof. Margarida Cruz and Prof. Liliana Ferreira from the Physics Department of Faculty of Sciences of the University of Lisbon, for helping me with the magnetic measurements and magnetic hyperthermia studies.

I thank all my lab colleagues and, in special, I want to thank Mirtha, Ana, Mariana, Zélia and Manuel.

Last but not least, I want to thank my parents and all my friends and boyfriend for the support and motivation.

palavras-chave Hipertermia magnética, nanopartículas magnéticas, magnetite, co-precipitação, fucoidana.

resumo

As nanopartículas magnéticas, nomeadamente as nanopartículas (NP) de magnetite têm sido alvo de investigação e desenvolvimento para aplicação na área biomédica, em especial na hipertermia magnética como terapia para o cancro. As NP são frequentemente revestidas com diversos materiais, tais como sílicas e polímeros naturais ou sintéticos como a quitosana ou o polietilenoglicol (PEG), visando melhorar a biocompatibilidade mas também potenciar a sua estabilidade coloidal. A fucoidana é um polissacarídeo que tem sido bastante estudado para aplicações biomédicas devido principalmente à sua biocompatibilidade e propriedades antitumorais.

Neste trabalho foram desenvolvidas NP de magnetite revestidas com fucoidana e foi avaliado a seu potencial de aplicação em hipertermia magnética, com o intuito de poderem ser usadas na terapia do cancro, combinando a terapia por hipertermia magnética com as propriedades antitumorais da fucoidana. As NP foram sintetizadas pelo método de co-precipitação à temperatura ambiente e, posteriormente, sujeitas a um tratamento hidrotermal com diferentes condições de tempo (1, 2 e 3 h) e temperatura (150 ou 200 ºC). O revestimento das partículas com fucoidana foi feito utilizando duas metodologias: i) após a sua síntese (revestimento pós-síntese) e ii) simultaneamente com a síntese (revestimento *in situ*). No revestimento pós-síntese testaram-se diferentes concentrações de fucoidana para avaliar a sua influência nas propriedades físico-químicas e na eficiência térmica das NP. Nas sínteses com revestimento *in situ* para além de avaliar o efeito de diferentes concentrações de fucoidana, estudou-se ainda a influência da temperatura de reação na funcionalização da superfície das NP. As NP foram caracterizadas em termos de cristalinidade e tamanho de partícula, área superficial específica, morfologia, estabilidade coloidal e eficiência térmica. De uma forma geral, as NP sintetizadas e revestidas com fucoidana apresentaram uma morfologia quase esférica, e em termos de tamanho as NP com menor tamanho exibiram uma maior área superficial. O tratamento hidrotermal promoveu o aumento da cristalinidade e do tamanho das NP em função do aumento do tempo e temperatura do tratamento hidrotermal. Ocorreu também um aumento da polidispersividade que se traduziu numa diminuição da eficiência de aquecimento por hipertermia. O revestimento com fucoidana revelou ter influência na dispersão coloidal das NP, sendo que houve uma melhoria na estabilidade coloidal e, consequentemente, na sua eficiência térmica devido à redução das interações entre as NP. Para a sintese de NP por co-precipitação e revestidas pós–síntese, obtiveram-se os melhores resultados em termos de estabilidade, que se deverá ao facto de as NP obtidas *in situ* serem mais pequenas e possuirem uma maior tendência para se aglomerarem. A amostra que apresentou melhores resultados na libertação de calor foi a sintetizada por co-precipitação à temperatura ambiente e revestida pós-síntese com uma concentração de fucoidana de 2 mg/mL, apresentando um Poder de Libertação Intrínseco (ILP, do inglês *Intrinsic Loss Power*) de 2.6 nHm^2/kg, e que de acordo com a literatura estará na faixa considerada adequada para tratamentos por hipertermia magnética (2 a 4 nHm^2/kg). Adicionalmente, esta amostra possui NP com tamanho médio dentro da gama recomendável para a introdução no organismo (inferior a 20 nm) e em especial para a sua potencial aplicação em hipertermia magnética. No entanto, as NP sintetizadas e revestidas simultaneamente com 2 mg/mL de fucoidana apresentaram também uma eficiência térmica elevada (1.7 nHm^2/kg), sendo que o seu processo de preparação é mais simples. Por tudo, o descrito, os resultados obtidos neste trabalho demonstraram que as NP de magnetite revestidas com fucoidana têm potencial para a aplicação em hipertermia magnética podendo ainda ter, dadas as caracteristicas intrinsecas da fucoidana, actividade antitumoral, potenciando o tratamento do cancro.

keywords Magnetic hyperthermia, magnetic nanoparticles, magnetite, co-precipitation, fucoidan.

abstract

Magnetic nanoparticles, namely magnetite nanoparticles (NP) have been subject of research and development for application in the biomedical field, especially in magnetic hyperthermia as a therapy for cancer. NPs are often coated with various materials such as silicates and natural or synthetic polymers such as chitosan or polyethylene glycol (PEG), in order to improve biocompatibility but also to enhance their colloidal stability. Fucoidan is a polysaccharide extensively studied for biomedical applications mainly due to its biocompatibility and antitumor properties.

In this work, NP of magnetite coated with fucoidan are developed and evaluated for the application in magnetic hyperthermia for cancer treatment, combining magnetic hyperthermia therapy with the antitumor properties of fucoidan. The NP are synthesized by the co-precipitation method at room temperature and, afterwards, subjected to a hydrothermal treatment with different time (1, 2, and 3 h) and temperature (150 or 200 ºC) conditions. The coating of the particles with fucoidan are performed using two methodologies: i) after their synthesis (post-synthesis coating) and ii) simultaneously with the synthesis (*in situ* coating). Different concentrations of fucoidan are tested in the post-synthesis coatings to evaluate their influence on the physicochemical properties and the thermal efficiency of NP. In the *in situ* coating syntheses, in addition to evaluating the effect of different concentrations of fucoidan, the influence of the reaction temperature on the functionalization of the NP surface are also studied. NP are characterized in terms of crystallinity and particle size, specific surface area, morphology, colloidal stability and thermal efficiency. In general, NPs synthesized and coated with fucoidan have nearly round shape morphology, and in terms of size NPs with smaller size exhibited a larger surface area. The hydrothermal treatment promoted the increase of NP crystallinity and size as a function of the time and temperature of the hydrothermal treatment. There is also an increase in polydispersity which resulted in a decrease in heating efficiency by hyperthermia. The coating with fucoidan showed to improve the colloidal stability and, consequently, the thermal efficiency due to the reduction of the interactions between the NP. For the synthesis of NP by co-precipitation and post-synthesis coated, better results were obtained in terms of stability, due to the fact that the NPs obtained *in situ* are smaller and have a greater tendency to agglomerate. The sample giving the best results in the heat release was the one synthesized by co-precipitation at room temperature and coated post-synthesis with a concentration of fucoidan of 2 mg/mL, presenting an Intrinsic Loss Power (ILP) of 2.6 nHm^2/kg, which according to literature is considered sufficient in terms of thermal efficiency (2 to 4 nHm^2/kg). In addition, this sample had an average size within the recommended range for introduction into the body (less than 20 nm) mainly for its potential application in magnetic hyperthermia. However, NP synthesized and coated simultaneously with 2 mg/mL fucoidan also showed a high thermal efficiency (1.7 nHm^2/kg) and its preparation process is simpler. For all of the above described, the results obtained in this work demonstrated that NP of magnetite coated with fucoidan have potential for application in magnetic hyperthermia and may also have, as a consequence of the intrinsic characteristics of fucoidan, antitumoral properties, which allow to potentiate the cancer treatment.

Table of Contents

Index of figures

Index of tables

List of symbols

A_{BET}	Specific surface area (measured by BET).
D_{TEM}	Average nanoparticles size (measured by TEM).
D_{XRD}	Average crystallite size obtained from the X-ray diffraction pattern using Scherrer equation.
E_A	Magnetic anisotropy energy.
K	Anisotropy constant.
K_B	Boltzmann constant.
MNP	Magnetic nanoparticles.
NP	Nanoparticles.
P	Heat dissipation.
V_H	Hydrodynamic volume.
τ_N	Relaxation time through Néel relaxation mechanism.
τ_B	Relaxation time through Brownian relaxation mechanism.
τ	Total relaxation time.
μ_{at}	Dipole moment density.
χ	Magnetic susceptibility.
μ_0	Permeability of free space (vacuum).
Φ	Volume fraction of superparamagnetic MNP.

List of Abbreviatures

a.u.	Arbitrary units
AMF	Alternating Magnetic Field
BET	Brunauer-Emmett-Teller
CT	Chemotherapy
DGS	Directorate General for Health
XRD	X-Ray Diffraction
FCSP	Fucose Containing Sulfated Polysaccharides
FWHM	Full-Width at Half-Maximum
FT-IR	Fourier Transform Infrared
HT	Hyperthermia Therapy
ILP	Intrinsic Loss Power
IUPAC	International Union of Pure and Applied Chemistry
M	Magnetization
MHT	Magnetic Hyperthermia Therapy
MNP	Magnetic Nanoparticles
MRI	Magnetic Resonance Imaging
Ms	Magnetic saturation
NP	Nanoparticles
PEG	Poly(ethyleneglycol)
PIE	Isoelectric point
PLLA	Poly(lactic-co-glycolic acid)
PVA	Poly(vinyl alcohol)
PZ	Zeta Potencial
RT	Radiation Therapy
SAR	Specific Absorption Rate
SLP	Specific Loss Power
SPM	Superparamagnetic
SPION	Superparamagnetic Iron Oxide Nanoparticles
TEM	Transmission Electron Microscopy
VEGF	Vascular Endothelial Growth Factor

Chapter 1 Introduction

1.1 General aspects

Cancer is a disease characterized by out-of-control cell growth [1]. Regardless of efforts to find new therapies and considerable progress in medical research area, cancer is still one of the biggest causes of death in the world [2] having been registered 8.8 millions of deaths in 2015 [3]. In Portugal, and according to the Directorate General for Health (DGH) (from the Portuguese "*Direção Geral de Saúde"*), the incidence of new cases is expected to increase in the coming years. The prediction of the incidence of cancer up to 2035 can be visualized in Figure 1.1. An increase around 14.000 of new cases are expected by 2035 relatively to 2015 [4].

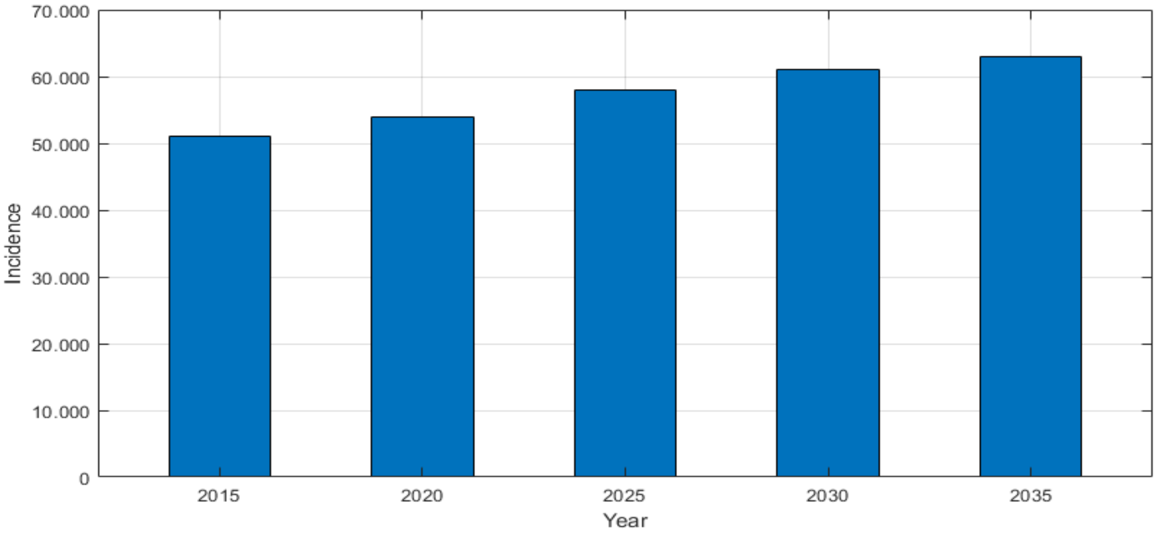

Figure 1.1: Predicted evolution of the cancer incidence in Portugal between 2015 and 2035 [4].

The aim of cancer treatment is the elimination of cancer cells, but without injuring the healthy tissues, or with as little damage as possible [5]. Unfortunately, conventional treatments such as chemotherapy, radiotherapy and surgery originate side effects such as hair loss, bleeding, edema, and fatigue [6], being extremely urgent the development of new treatments sought to overcome these drawbacks, with similar or improved efficiency against cancer.

Hyperthermia appears as an adjuvant alternative in the treatment of cancer. This treatment is grounded on the fact that normal cells have a higher resistance to heat than tumor cells, that are more sensitive to temperature increasing [7]. If temperature can be maintained accurately between 41 and 46 °C, tumor cells can undergo apoptosis [1], a natural process in which cells trigger their self-destruction in response to a molecular signal [7]. The cells of a normal tissue are not affected by this range of temperatures. Therefore, when the cells are exposed to temperatures above 46 °C, termed thermoablation treatment, they undergo necrosis (cellular death) instead of apoptosis [1]. However, using higher temperatures healthy cells may also be affected and damaged, being preferable to use temperatures that only cause apoptosis [7]. The currently available regional or local hyperthermia modalities have the difficulty of heating the tumor in a homogeneous way, originating a temperature gradient from the surface to the tumor core and reducing the treatment efficiency. Magnetic nanoparticle-mediated hyperthermia, also known as Magnetic Hyperthermia Therapy (MHT), has the potential to overcome this limitation, producing homogenous heating confined to the tumor tissue [8]. In addition, this therapy presents less side effects than conventional therapies as chemotherapy (CT), radiotherapy (RT) or surgery [9].

Magnetic nanoparticles (MNP), namely iron oxide nanoparticles, due to their differentiated properties such as biocompatibility, susceptibility to magnetic field and relatively easy synthesis, exhibit superparamagnetic behavior below a critical diameter, as well as the possibility of functionalization with biomolecules, allow to propose their application as heat mediators in hyperthermia treatments [10]. The most frequently used forms of iron oxide MNP in biomedical applications is magnetite (Fe_3O_4) and maghemite (γ-Fe_2O_3) [1]. Though, an inevitable issue associated with particles in this size range is their instability (they tend to aggregate over long periods of time) due to their large surface area-to-volume ratio [11], and also the magnetic attraction between dipole-dipole particles [10, 12]. In addition, metallic nanoparticles are easily oxidized in air, resulting in the loss of magnetism, undermining its efficiency in terms of heat generation. Therefore, it is crucial to develop strategies to stabilize MNP against degradation and agglomeration [11]. In order to attain this purpose and allow their use in MHT, MNP are often coated to improve their biocompatibility and stability [9]. In addition, the coating protects their surface from oxidation and enables also the functionalization with bioactive molecules (like anticancer drugs) producing multifunctional MNP [10]. Different coating materials have been used to modify the MNP surface including organic and inorganic coatings [9, 13].

Fucoidan is a sulfated water-soluble polysaccharide, which is the main constituent of brown algae and can also be found in some marine invertebrates (e.g. echinoderms) [14]. This polysaccharide has several properties, like anticancer activity [15, 16]. Fucoidan has been introduced in food supplements and drinks, being administered to patients with cancer in countries such as Korea, Japan and China. Fucoidan has been reported to be effective in different types of administration including oral, intraperitoneal, or intravenous [17].

It can be found in literature few reports of the use of fucoidan associated to NP as coating agent, aiming to improve the NP stabilization or taking advantage of their anticancer biological property. For instance, Silva *et al.* [18] used fucoidan to coat magnetite NP in order to study its influence on NP stabilization and magnetic properties and they reported that fucoidan prevented NP agglomeration due to the reduction of NP interactions. Also the magnitude of magnetization was higher after the NP coating with fucoidan. The same group also investigated the anticancer property of fucoidan. In this study they tested the anticancer property of fucoidan-coated NPs in Sarcoma 180 and they observed a reduction of the tumor size [19]. However, only the resulting magnetic properties and the anticancer activity of fucoidan were investigated. The authors did not address the application of these particles on MHT.

The biological activity of fucoidan makes it an agent with great potential in the treatment of cancer and especially in the coating of magnetite NP, thus producing multifunctional nanoparticles to be used in MHT with the association of the anticancer property of fucoidan.

1.2 Magnetic Hyperthermia Therapy

Hyperthermia is characterized by an increase of the body temperature above normal physiological temperature [2]. In this therapy, the tissue/region or organ of the body being treated is exposed to temperatures in the range of 41 to 46 °C, promoting cells apoptosis [1] and to reduce the chemo- and radio-resistant of tumor cells [2]. Three types of hyperthermia therapy (HT) can be distinguish depending on the extent of the treated region: i) whole body hyperthermia (to treat metastatic cancer, using infrared radiators for example); ii) partial/regional hyperthermia (to treat advanced stage cancers using microwaves antennas); and iii) local hyperthermia for tumors that are localized superficially or deep seated (using antennas that emits microwaves, ultrasounds or radio waves) [7]. Figure 1.2 shows the first hyperthermia device (Heckel HT 3000) for the whole body that was introduced in Portugal [20].

Figure 1.2: Application of Whole Body Hyperthermia with water-filtered IR-A- radiation (wIRA) equipment (Heckel HT 3000) [20].

Currently, hyperthermia is approved as treatment therapy for cancer and it has been used along with RT or CT for the treatment of various advanced stage tumors (e.g. prostate cancer, neck and head, breast, etc.) [21]. However, the use of external heat sources to generate the heat (like microwave or radiofrequency) in the tumor tissue creates a temperature gradient. The temperature decreases with the increase of the distance to the heat source. Therefore, there is a heterogeneous heating of tumor, and also healthy tissues are affected [22]. In this way, the conventional HT entails some disadvantages arising from the heterogeneous heating, with the reduction of the treatment effectiveness. It has also side effects such as blisters and skin burns and it cannot be used in deep-seed tumors (due to the inability to prevent overheating) [8]. In order to overcome these issues MHT has arisen.

MHT also comprises heat generation but using MNP as heat mediators in response to an externally applied alternating current magnetic field (AMF). This MNP are dispersed in a liquid media such water, known as magnetic fluid (colloidal suspension of MNP) that can be injected locally or through the intravascular region (Figure 1.3) [9]. After its positioning, an alternating magnetic field is applied. The particles convert the energy of the alternating magnetic field into heat through physical mechanisms (Néel and Brownian relaxation mechanisms explored further ahead in the subchapter 1.3.2) that are dissipated in the tumor tissue [22]. Thus, these MNP can be dispersed into the tumor site to generate a homogenous heating, thereby preventing the lack of heating homogeneity provided by conventional HT [8, 23].

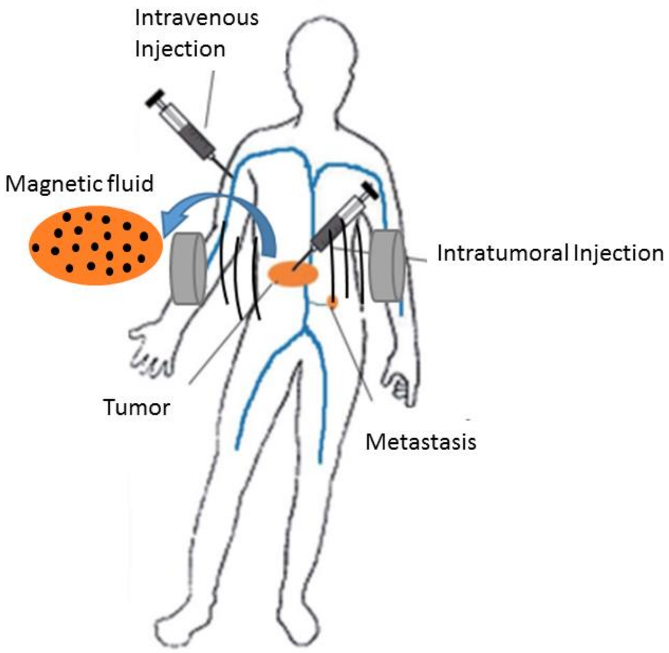

Figure 1.3: Representative illustration of intravenous and intratumoral administration of magnetic fluid for MHT. Adapted from Hervault et al. [7].

The most desirable administration of the magnetic fluid route is through intravenous injection, especially in deep-seated tumors with metastases. As MNP are responsive to an external magnetic field, they can be guided and positioned into the tumor using permanent magnets [7].

MHT has already shown its therapeutic efficacy in clinical trials mostly as a combinatorial approach with other conventional therapies like RT or CT [24, 25]. The first clinical study on magnetic hyperthermia was started in March 2003, in which 14 patients with glioblastoma multiforme were submitted to this therapy combined with RT [24]. It has been demonstrated that the MHT can be safely applied and the side effects have been reduced, increasing the median survival rate of the patients. The treatment included an intracranial injection of iron oxide nanoparticles (diameter of 15 nm) coated with aminosilane, dispersed in water and with an iron concentration of 112 mg/mL (Nanotherm®, MagForce Nanotechnologies AG, Berlin, Germany) [24, 26].

Another clinical study to verify the viability of the MHT was performed in 2005 with 10 patients with locally recurrent prostate carcinoma. The material (Nanotherm®) was retained in the prostate by 6 weeks, which meant that no further application was required in the course of the interval treatment. The results presented a reduction in PSA levels in 8 of the 10 patients and no systemic toxicity was observed during the 17.5 months of follow-up [25].

1.2.1 Temperature effect on cells

The use of hyperthermia arise from the existence of a distinct response to heat effect, between healthy and tumor cells [7]. The cytotoxic effect of hyperthermia is mainly associated with the fact that an increase in temperature have a physiological impact, provoking a denaturation of cytoplasmic proteins, influencing the cell growth and differentiation which in turn can induce apoptosis [7, 23].

The tumor selective effect of hyperthermia is due to physiological differences between the healthy (normal) and the tumor tissue, since there is a distinct architecture of the vasculature (disposition of blood vessels), visualized in Figure 1.4 [7, 21]. In normal tissue, the vasculature has efficient networks of arteries, veins and capillaries, capable of supplying tissue necessities, while the vasculature of tumor tissue is characterized by being inefficient and disorganized (heterogeneous distributions of vascularization) [7, 21, 27].

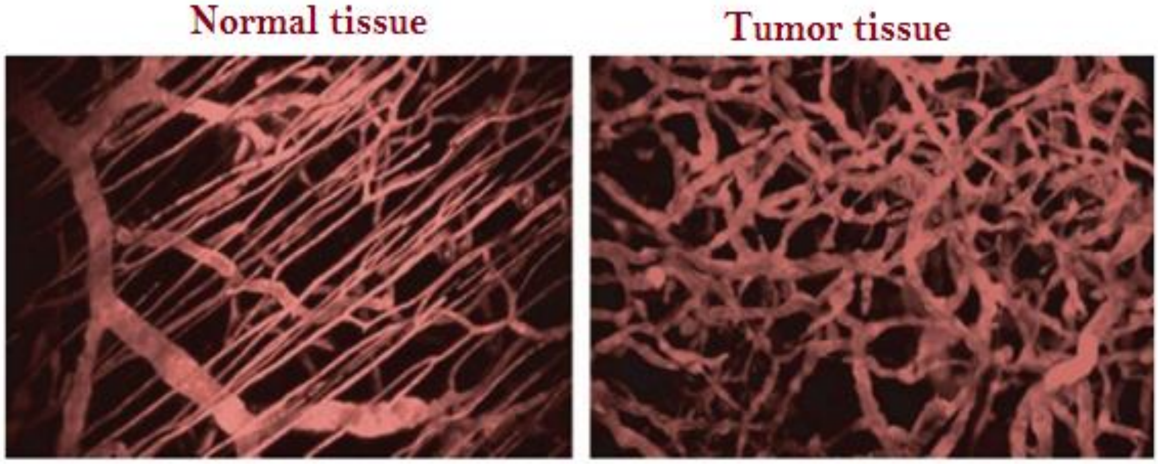

Figure 1.4: Vasculature of normal and tumor tissue. Adapted from Forster et al. [27].

In normal tissues, the heat induces a fast response, which includes an increase of the blood flow, accompanied by vessel dilatation and an increase of the vascular wall permeability, while in the tumor, the vascular network is less efficient namely in exchanging heat and, consequently, it is more likely to be damaged when treated by hyperthermia therapy. For instance, when tumor tissue is subjected to temperatures above 42 °C, the blood flow tends to decrease, while it increases in normal tissues. The decrease in blood flow leads to a lower rate of heat dissipation (lacking an efficient heat exchange system) and therefore the temperature in the tumor will increase more rapidly than in normal tissue. Such difficulty in dissipating heat can cause tumor cells undergo to apoptosis, whereas in normal tissue the physiological temperatures are more easily preserved and maintained since is capable of efficiently dissipate heat [7].

Hyperthermia may induce an increase or a decrease in the tumor oxygenation, depending on the exposed temperature. When this therapy is applied at temperatures below 42 ºC, it is more probable to lead to an increase in blood flow to the tumor, allowing a higher tissue oxygenation. Based on this effect, the cells become more sensitive to RT, since the effect of this treatment is favored in an environment with good oxygenation and are usually resistant to radiation due to the hypoxic environment. Additionally, there is also a synergistic effect of hyperthermia with chemotherapy due to the blood flow increase (below 42 °C) caused by hyperthermia treatment, which allows an increase in the concentration of drugs in the tumor tissue (increase of drug absorption) [7]. Furthermore, it has been demonstrated *in vitro* and *in vivo* that hyperthermia enhances the cytotoxic effect of various antineoplastic drugs (Cisplatin, Doxorubicin, Bleomycin, etc.) [28]. For these reasons, hyperthermia is often used as adjunctive therapy with RT and CT because it has a cooperative effect [7].

1.3 Magnetic Nanoparticles

MNP are extremely promising for a wide range of biomedical applications, such as drug delivery, magnetic resonance imaging (MRI), hyperthermia, among others [29, 30]. They possess physicochemical and magnetic properties that can be tailored for different applications [30].

The fundamentals interactions between materials and an external magnetic field are important to support the understanding of the magnetic behavior required to MNP for MHT application. With this purpose, the next subchapter will focus on some important magnetic concepts. The superparamagnetism behavior will be presented and it will be also introduced the physical phenomena that allows the production of heat by the MNP.

1.3.1 Magnetic properties of materials and the effect of size reduction

The materials exhibit a behavior, when exposed to an external magnetic field (H), that can be classified in relation to the type of magnetism as: diamagnetic, paramagnetic, ferromagnetic, ferrimagnetic and antiferromagnetic [31].

In a crystal, the magnetization (M) results from the interaction between the magnetic moments of the atoms. The M is therefore the magnetic dipole density, and is defined as the atomic magnetic dipole moment density (μ_{at}) per unit volume (V), where N is the number of atoms (Equation 1) [32]:

$$M = \frac{1}{V}\sum_{i}^{N} \mu_{at} \qquad \text{[Equation 1]}$$

Magnetite is an iron oxide type, with the chemical formula Fe_3O_4, and it is one of the most widely used forms in the field of magnetic hyperthermia research, being classified as ferrimagnetic. Their magnetic domains tend to be oriented in the same direction as an applied magnetic field (H). Magnetic saturation (Ms) is achieved when the spins are aligned in the same direction. When the magnetic field is removed, the magnetization does not return to zero, resulting in a remnant magnetization (R). The magnetization returns to zero when is applied a magnetic field (-Hc) in the opposite direction to the one previously applied. The magnitude of this applied field to eliminate the remaining magnetization of the material is known as coercivity or coercive field (Hc) [32-34]. Those characteristics of the ferrimagnetic materials can be visualized in a graph of the M versus H (magnetization curve) representing the magnetic hysteresis cycle (Figure 1.5) [34].

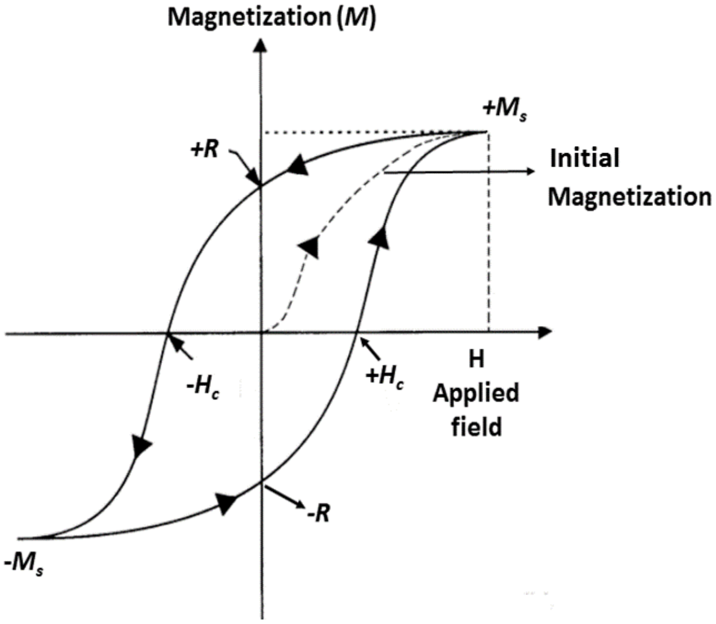

Figure 1.5: Magnetization curve of a ferrimagnetic material. Adapted from Callister et al. [34].

At the nanoscale materials may exhibit magnetic properties different from those of bulk materials. The ferrimagnetic materials in their bulk form are polycrystalline and comprise several magnetic moments that are separated by regions known as magnetic domain walls (normally with hundreds of nanometers of width) [35]. A domain is defined as a region of the material within the spins of the atoms have the same magnetic alignment. Additionally, as a consequence of size reduction, the energy for the formation of multidomains increases favoring the establishment of a single monodomain. The energy needed to divide into magnetic domains is greater than the energy required to remain as a single magnetic domain. When the size of single-domain particles decreases below a certain diameter (Ds), the coercivity becomes zero and the particles acquire a different magnetic behavior, known as superparamagnetic [13, 36].

Small magnetic particle may present a magnetic anisotropy which is the existence of a favored crystallographic direction, i.e. the direction along which the electron spins are more easily aligned/magnetized [33]. For instance, in the case of cubic ferrites as magnetite, the direction along the [111] plane is the direction of easy axis. In addition, it is required a certain energy to rotate the magnetization away from the easy direction, which is termed magnetic anisotropy energy [36]. This energy is given by Equation 2 :

$$E_A = K \times V \times sin^2\theta \qquad \text{[Equation 2]}$$

Where K is the anisotropy constant, V is the volume of the spherical particle and θ is the formed angle between the particle magnetization and the easy magnetization axis that depends on the magnetic anisotropy of the material [36]. Analyzing the Equation 2 it can be noted that the magnetic anisotropy energy decreases when the volume of the particle also decreases [36]. In particles bellow a certain size (Ds), the thermal activation energy ($E_{thermal} = K_B \times T$) is sufficient for the magnetic moments to misalign. The anisotropy energy becomes comparable or even lower than the thermal energy, i.e. the remanent magnetization is no longer fixed in the direction dictated by particle shape or crystal anisotropy; ambient thermal energy may be high enough to cause the magnetic moment to jump between two different stable orientations of magnetization (Figure 1.6). This disorder (molecular motions are random), in the absence of an external magnetic field, originates a zero magnetization value [33, 36]. Magnetic moments have two possible equilibrium positions at 0° and 180° (minimum energy orientations, or easy axes where the anisotropy energy is equal to zero at these angles) and a barrier (anisotropy energy) between them as shown in Figure 1.6. This anisotropy energy has a maximum value at 90° (difficult axis) [36].

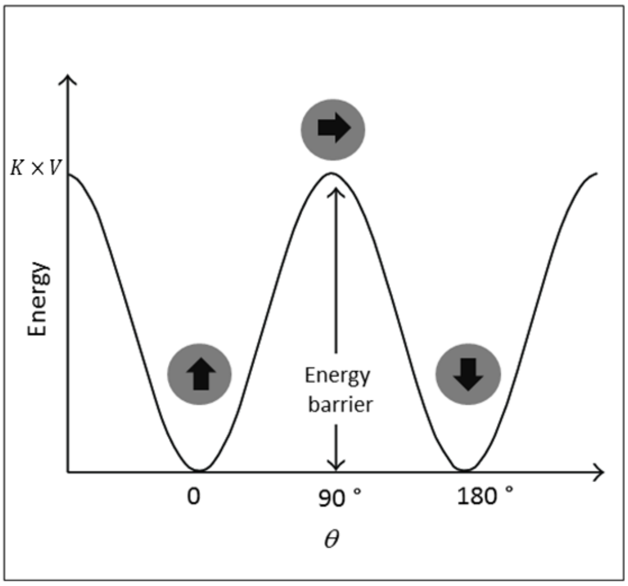

Figure 1.6: a) Angle between the easy axis. Adapted from Laurent et al. [37]*; b) Anisotropy energy barrier for reversing the magnetization. Adapted from Kafrouni et al.* [36].

Superparamagnetism behavior can be as well identified through magnetization curves (Figure 1.7). These superparamagnetic nanoparticles (SPION) have zero coercivity, there is no remnant magnetization and do not show a hysteresis curve when the magnetic field is removed [7]. The relationship between NP size and magnetic domain structures is shown in Figure 1.8. The superparamagnetic properties of the MNP are thus highly dependent on their size [38]. For instance, the behavior of an iron oxide particle changes from ferrimagnetic to superparamagnetic behavior when the particle size decrease to a diameter smaller than 20-30 nm [39].

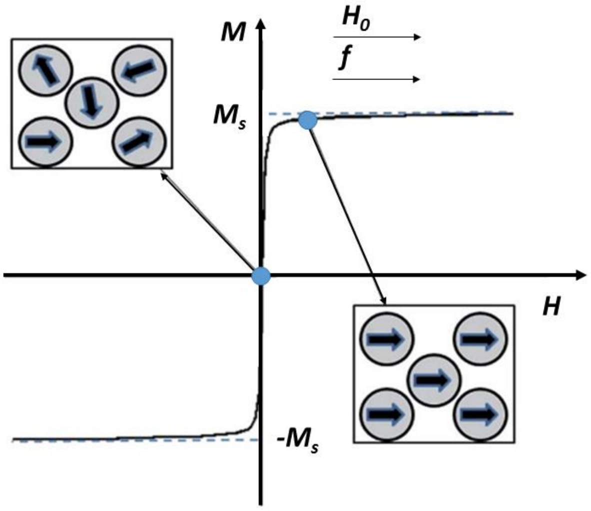

Figure 1.7: Magnetization curve of a superparamagnetic material demonstrating the absence of hysteresis, coercivity and remanence magnetization after removing the external magnetic field (H_0). Adapted from Hervault et al. [7].

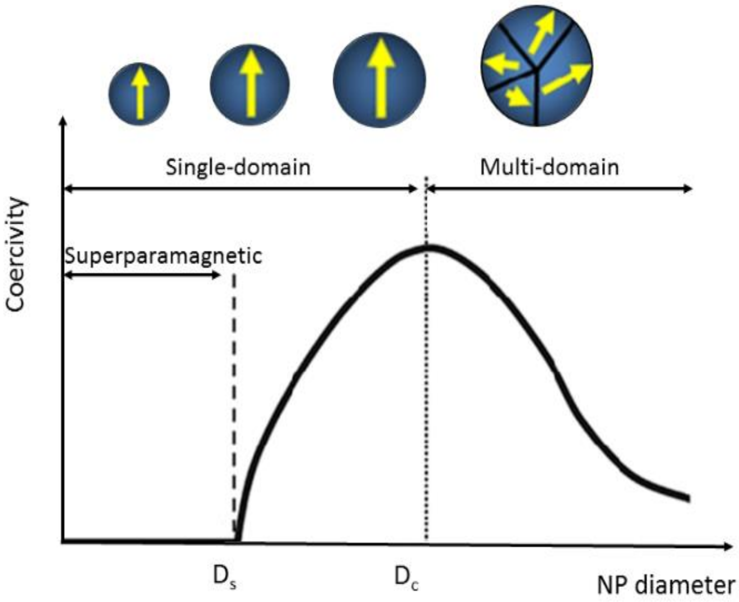

Figure 1.8: Relationship between spherical NP diameter and magnetic domain structures. Ds and Dc are the "superparamagnetism" and "critical" size limits, respectively. Adapted from Akbarzadeh et al. [38].

1.3.2 Mechanism of heat

Superparamagnetic NP dissipate heating through the reorientation of magnetic moment (demagnetization process) to overcome the energy barrier and by the resistive response of the magnetic particle rotation. Two physical mechanisms are involved which include Néel (spin rotation) and Brownian (particle rotation) relaxation (Figure 1.9) [7, 36].

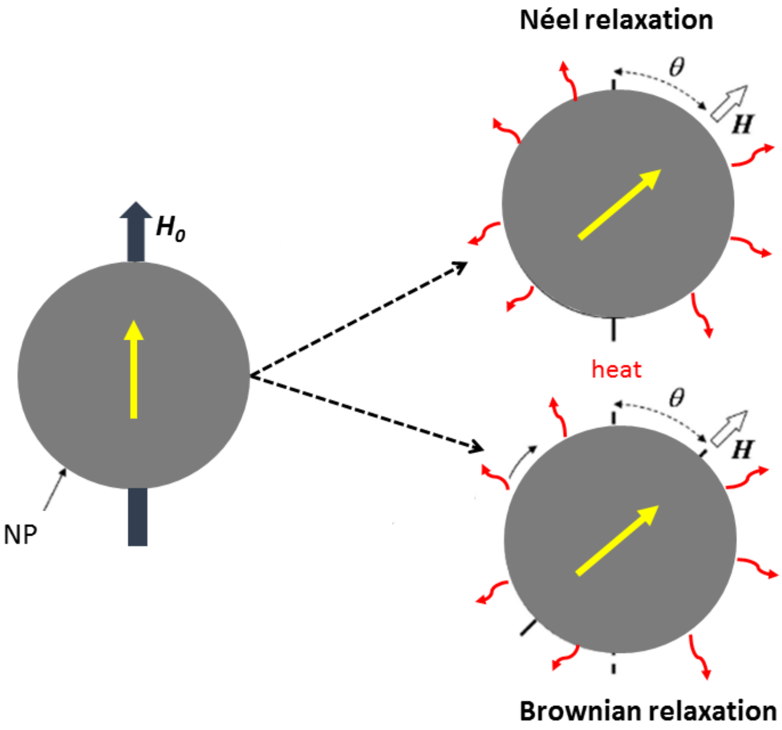

Figure 1.9:Physical mechanisms of relaxation in the production of heat by superparamagnetic nanoparticles. Adapted from Jeyadevan et al. [40].

In the mechanism of Néel, the thermal dissipation results from the rotation of the magnetic moments inside the particles, without moving physically. This process is characterized by a specific relaxation time that can be determined through the Equation 3 [7].

$$\tau_N = \tau_o \exp\left(\frac{KV}{K_B T}\right) \qquad \text{[Equation 3]}$$

In which $\tau_o = 10^{-9}$s, K is the anisotropic constant, V is the particle volume, K_B is the Boltzmann constant and T is the temperature. Once again, this mechanism depends on the NP size/volume. The small particles require less energy for the rotation of its magnetic moment (Equation 2) [7]. Relatively to the Brownian mechanism, the reorganization of the magnetic moments is accompanied by the physical rotation of the particle, and the releasing energy results from the friction of the same with the medium. The Brownian relaxation time can likewise be calculated using Equation 4:

$$\tau_B = \left(\frac{3\eta V_H}{K_B T}\right) \qquad \text{[Equation 4]}$$

Where η is the viscosity of the transport liquid, V_H is the hydrodynamic volume of the particle (size of the particle in suspension), K_B is the Boltzmann constant and T is the temperature. The Brownian relaxation mechanism is also dependent on particle size and medium viscosity. Higher viscosity of the liquid medium will decrease the rotation of the NP, and then it will be more difficult to reverse its magnetization [7].

The total relaxation time that results from those physical mechanisms can be determined through the Equation 5 [7].

$$\tau = \frac{\tau_B \tau_N}{\tau_B + \tau_N} \qquad \text{[Equation 5]}$$

If the MNP are subjected to an AMF with a faster oscillation than relaxation time of those MNP, the heat is dissipated [37]. The heat dissipation (P) can be determined by the Equation 6:

$$P = \chi_0 \, (H_0)^2 \, \mu_0 \pi \frac{2\pi f^2 \tau}{1+(2\pi f \tau)^2} \qquad \text{[Equation 6]}$$

Where χ_0 is the magnetic susceptibility of nanoparticles, H_0 is the amplitude of the applied magnetic field, μ_0 is the permeability of free space(vacuum), f is the frequency of the magnetic field and τ is the total magnetic relaxation time determined by Equation 5 [41].

Furthermore, the Specific Absorption Rate (SAR, also known as Specific Loss Power, SLP) is commonly used as a reference to characterize the performance of NP and it is expressed in W.g^{-1}. SAR can be determined through the Equation 7:

$$SAR = \pi {\mu_0}^2 \left(\frac{\varphi {M_s}^2 \times V}{1000 K_B T}\right) \times H_0^2 f \times \left(\frac{2\pi f \tau}{1 + (2\pi f \tau)^2}\right) \qquad \text{[Equation 7]}$$

Where μ_0 is the permeability of the free space, φ is the volume fraction of superparamagnetic MNP, M_s is the saturation magnetization, V is the volume calculated for a particle with a radius r, K_B is the Boltzmann constant, T is the temperature of the sample, H_0 and f are the intensity and frequency of the applied magnetic field respectively and τ is the total relaxation time [36].

Through Equation 7, it can be verified that the SAR is highly dependent on several parameters as M_s value, which in turn is dependent on physical parameters that includes the degree of crystallinity, size, size distribution, shape, surface modification and composition [41]. This parameters can be tailored to improve the efficiency of the MNP in the heat production. For MHT, it is desirable a high SAR, leading to a greater treatment efficiency, and on another hand allows the reduction of the MNP concentration that need to be introduced into the tumor [36]. In the subchapter 1.4.2, it will be introduced the influence of some of those parameters on NP thermal efficiency.

It also can be noted through the Equation 7 that the capability of MNP to generate heat depends also on the strength (H_0) and frequency (f) of the AMF [29]. Related to the electromagnetic radiation exposure, it was reported that for a safe MHT, the $H_0 f$ factor should not exceed a limit equal to 5×10^8 A $m^{-1}s^{-1}$ in the case of whole-body treatment, and for small regions this limit is 2×10^9 A $m^{-1}s^{-1}$ [1]. Nonetheless, other authors suggested $5\times10^9 Am^{-1}s^{-1}$ as the threshold [9, 42]. These limits, also called as "Brezovich limit" [1], are required in order to avoid excessive heating in the patients, since that induced current in non-magnetic tissues will lead to necrosis or carbonization of healthy tissues which is not desirable [1, 43]. Regarding to the radio-frequency thresholds, they assume values between several kHz and 1 MHz [44].

1.4 Magnetic nanoparticles for hyperthermia therapy

In general, in order to allow the use of NP in the biomedical field is necessary that they possess several requirements or properties: biocompatible, non-toxic, a narrow size distribution, high crystallinity, and stability (in a physiological environment) which requires the control of the NP composition, size and also the coating properties [9, 41]. The stability depends largely on the size of the NP to avoid their precipitation due to gravitational force. Depends also on the charge, and on the chemical surface of the particles, which leads to steric and coulombic repulsions [38].

NP must have a suitable magnetic behavior to be used as heat mediators in MHT, which means that the NP should exhibit a superparamagnetic behavior, not having remaining magnetization when are not subject to a magnetic field [29]. This behavior is essential, in order to avoid the interaction between the particles which will lead to their agglomeration, with the creation of larger particles, and thus preventing a potential embolism [45].

Various types of MNP have been studied developed and used as magnetic mediators and the superparamagnetic iron oxide NP (SPION) are the most successful type that has been widely investigated [37].

1.4.1 Magnetite

Magnetite is a magnetic iron oxide that contains both Fe^{2+} and Fe^{3+}, which means that is composed of iron ions in two different oxidation states. Its chemical formula is Fe_3O_4, more accurately written as $FeO.Fe_2O_3$ ($Fe^{2+}(Fe_2^{3+}O_4^{\ 2-})$), also represented as $Fe_{3-x}O_4$, and have a black colour. It has an inverse spinel-like structure (with a Fd3m space group and 8.397Å as lattice parameter) where each unit cell contains 56 atoms, including 32 oxygen atoms, 16 Fe^{3+} ions and 8 Fe^{2+} ions that are located at two different crystallographic sites: octahedral (site B) and tetrahedral (site A). In the inverse spinel the Fe^{3+} ions are distributed between both the tetrahedral and the octahedral sites. Oxygen ions form a cubic face centered lattice (FCC) along [111] plane (easy axis) and occupy four of the vertices of each of the 8 small cubes which make up the unit cell (Figure 1.10) [33].

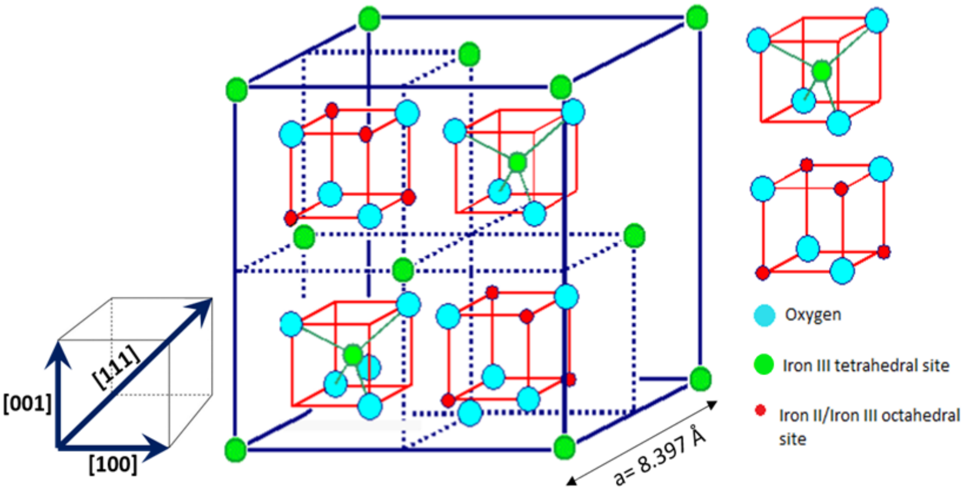

Figure 1.10: The inverse spinel structure of magnetite is grounded on a fcc arrangement of O^{2-} ions in which Fe^{3+} cations occupy 1/2 of the tetrahedral interstices, and a 50:50 combination of Fe^{3+} and Fe^{2+} cations occupy 1/8 of the octahedral interstices. Adapted from Issa et al. [46].

The ferrimagnetic magnetic behavior of magnetite arises from the fact that below a certain temperature, the Curie Temperature (Tc), the spins on the A and B sites are antiparallel, and have different magnitudes originating a residual magnetization [12, 33]. If temperature rise and reaches Tc, the thermal fluctuations destroy the alignments of the magnetic moments, and above the Tc they exhibit a superparamagnetic behavior [47]. In Figure 1.11, the configurations of the magnetic spins moments of the Fe^{2+} and Fe^{3+} constituents of the magnetite can be visualized [34].

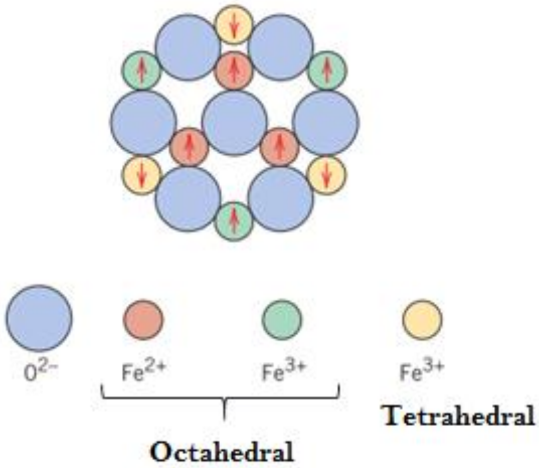

Figure 1.11:Schematic diagram representing the different configurations of the magnetic spins of Fe ions in the two oxidation states (Fe^{2+} and Fe^{3+}). Adapted from Callister et al. [34].

Magnetite particles are highly susceptible to environmental conditions, and easily suffer oxidation to the maghemite phase (metastable), which is represented by γ- Fe_2O_3 and exhibits red-brown color. In its turn, the maghemite becomes hematite (α-Fe_2O_3) for temperatures between 370 and 600 ºC and exhibits red color. The two iron oxides (magnetite and maghemite) differ from each other in terms of their spinel structure. In magnetite, iron occupies positions in both octahedral and tetrahedral sites, while maghemite has cationic vacancies in the octahedral position (cation deficient sites) [33]. The difference in the crystal structure between magnetite and maghemite results in a different net spontaneous magnetization of the iron particles at 300 K, which is 92 emu/g for bulk magnetite and 78 emu/g for bulk maghemite, presenting a slight decrease in the Ms value [48]. Consequently, the modification of the magnetite phase in another phase, in particular in maghemite, will result in an undesirable reduction of the heating capacity of the NP in magnetic hyperthermia application.

The next sections will be focused on the influence of parameters such as particle size, size distribution, shape and chemical composition on the heating efficiency.

1.4.2 Parameters affecting heat efficiency

1.4.2.1 Size

The use of NP in MHT is facilitated considering their nanometric size, which make easy their passage through the physiological barrier, namely the endothelial barrier through the continuous capillaries of the tissues. The NP need to be small enough to overcome this barrier, though it will generate a heterogeneous heat in the tumor zone, since the internal cells of the tumor will not undergo to an efficient heating (soft thermal effect), and thus, the desired effect will not be accomplished. On the other hand, if the size is small enough, they will be able to access the entire tumor zone even the most core area and therefore producing a homogeneous heating which enhance the treatment effectiveness [44]. Their size also plays a role in its permanence time in the tumor zone, avoiding the process of opsonization. This is a process in which a foreign particle is coated with plasma proteins (opsonins) to facilitate the attachment and internalization of the particle by a phagocytic cell (macrophage) to be digested/eliminated. For example, NP of size greater than 200 nm are sequestered by phagocytotic cells of the spleen, whereas particles below 5.5 nm are quickly removed by renal clearance [49]. Additionally, the size of nanoparticles has a high impact on the heating efficiency [41]. The increase of NP size lead to an increase of the saturation magnetization (Ms) value [50]. However, this increase happens until a threshold value, and when this value is attained, the Ms is constant and close to the value of the bulk form [50]. The reason for this to happen is because the NP possess a spin-canted surface layer around 0.5–0.9 nm depth (Figure 1.12a). Since this layer is not dependent on the NP size, the proportion of the magnetically disordered surface reduces as the NP size increases (Figure 1.12b) [50].

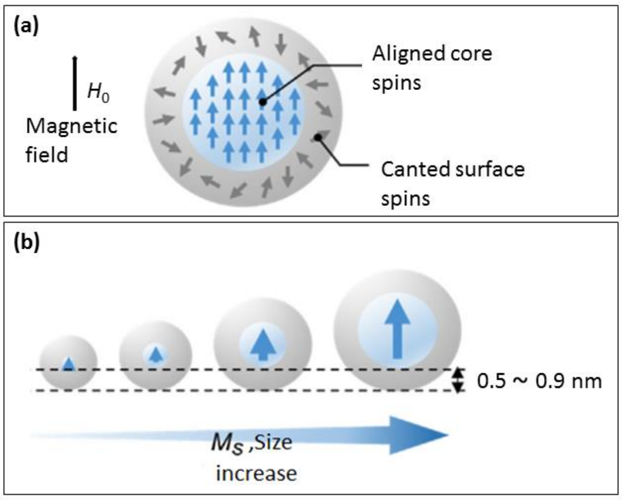

Figure 1.12: Illustration of the magnetic spins: (a) representation of canted surface spins and the core spins aligned with the magnetic field (H_0); (b) representation of the spin-canted surface layer thickness. Adapted from Noh et al. [50].

In addition, it was reported for magnetite NP that reduction of the particle size generates a greater curvature of the surface when compared with large particles, which gives rise to a disordered orientation of the crystal in its surface and consequently leads to a reduction of the Ms value [29]. In this way, the NP must be small enough to facilitate the passage through the physiological barrier, but need to have a sufficient size to be efficient as heat mediators to allow their use on MHT [44].

Furthermore, the relaxation mechanisms that are responsible for the heat dissipation are dependent of the NP volume, then even small changes in this parameter will have a pronounced influence on the SAR value [41]. For instance, experimental values obtained for magnetite are between 30–50 emu/g in the case of NP and 90 emu/g for bulk magnetite [11, 33].

Magnetite NP with size ranging from 10 nm to 40 nm have been proposed as suitable for application in MHT [40], whereas in the case of magnetite at room temperature, it typically acquire a superparamagnetic behavior for sizes less than 25 nm [51]. However, other studies indicate that their size should be less than 20 nm to exhibit this magnetic behavior [52]. Moreover, it is reported that NP sizes between 8 and 20 nm has further advantages such as their greater stability and their easy administration in the patient body [1].

1.4.2.2 Particle Size Distribution

The application of MNP in MHT required the use of a narrowest particle size distributions as possible to achieve uniform physicochemical properties of the NP [41]. For instance, a broad size distribution will lead to a potentially different efficiency in terms of heat/calorific power with distinct values of Ms [1, 41].

It was reported that in general a polydisperse (with non-uniform sizes) sample will lead to a decrease in maximum SAR. On the other hand, monodisperse samples enhance SAR value [41].

1.4.2.3 Shape

MNP shape also influence the Ms value that can be attained. Particles with cubic shape have less defects in their surface than spherical particles. The highest defect content origins a reduction on Ms value [41]. Round shaped NP have larger surface canting effects than the cubic ones and this is due to the curvature [50].

Studies have been done to analyze the effect of the NP shape on the magnetic properties, however different results have been obtained. For example, Zhen *et al*. [53] using magnetite NP reported higher Ms values for cubic-shaped particles (Ms = 40 emu/g) than for spherical-shaped NP (Ms = 31 emu/g), whereas another study performed by Montferrand *et al*. [54] shows lower Ms values for the cubic NP (40 emu/g) than for the spherical NP (80 emu/g), starting from particles with the same size. It was mentioned that this result could be due to the polydispersity of the cubic NP.

In addition, when comparing two NP with the same diameter and composition, the $V_{nanocube} > V_{nanosphere}$ and, as already saw in the Equation 7 (subchapter 1.3.2), SAR value is higher for a higher NP volume.

1.4.2.4 Chemical Composition

Magnetite particles easily suffer oxidation to the maghemite phase. As said before magnetite has higher values of Ms when compared to maghemite (92 emu/g versus 78 emu/g respectively) [48]. As higher values of SAR are desirable for MHT, the proportion between both phases in the sample has an influence on the final magnetic properties and consequently on the calorific power [41].

1.5 Co-Precipitation method in the synthesis of magnetite NP

There are several methods of MNP synthesis including chemical, physical and biological methods. The most commonly used methods are chemical, and the co-precipitation technique is the most used [55] and since has been used in this thesis, it will be described here in further detail.

Co-precipitation method is based on a precipitation reaction, starting from a solution containing metal precursors (salts) which are dissolved in a common solvent, such as water, with a precipitating agent [35]. This synthesis pathway has several advantages, such as the possibility of producing a large number of NP and is relatively simple and fast when compared to other methods [2, 35]. In addition, as it is a synthesis in solution, allows in a relatively simple way to functionalize the NP (during or post-synthesis) through the surface coating [35].

Conventionally, the magnetite is prepared by the addition of a base such as NaOH to an aqueous stoichiometric mixture of Fe^{2+} and Fe^{3+} chloride, usually in a 1:2 stoichiometric ratio [55]. This ratio is supported by studies evaluating the influence on particle size and uniformity. It was observed that a Fe^{2+} / Fe^{3+} ratio of less than 0.3 led to the formation of another phase, goethite. It was also found that a ratio of 0.3 to 0.5, two phases occurred with the formation of small particles around 4 nm and also large particles. For a ratio of 0.5 which corresponds to magnetite stoichiometry, it was obtained NP with a desirable homogeneous composition. Thus, it is suggested that the ratio should be between 0.4 and 0.6, enhancing the synthesis of NP with monodisperse size which is a requirement to MHT [56].

The chemical reaction of Fe_3O_4 precipitation is given in Equations 8 [33]:

$$Fe^{2+} + 2Fe^{3+} + 8OH^{-} = Fe_3O_4 + 4H_2O \qquad \text{[Equation 8]}$$

This method should be carried out in an environment without the presence of oxygen (anaerobic) with an inert gas (e.g. nitrogen) usually being introduced. The maintenance of a non-oxidizing environment is fundamental considering the lack of stability and easy oxidation of magnetite to form an oxidized surface layer, with the conversion of magnetite into maghemite (γ -Fe_2O_3) or ferric hydroxide ($Fe(OH)_3$) according to the following [55]:

$$4Fe_3O_4 + O_2 = 6\gamma - Fe_2O_3 \qquad \text{[Equation 9]}$$

$$Fe_3O_4 + O_2 + H_2O = 3Fe(OH)_3 \qquad \text{[Equation 10]}$$

The main limitations of the co-precipitation method are the difficulties in controlling the size and shape of the nanoparticles. NP resulting from this method are usually characterized by low crystallinity, some polydispersibility and agglomeration with the formation of clusters [12, 56].

Iron oxide NP synthesized by the conventional co-precipitation route as described above have a typical size of around 10 nm in diameter [57, 58]. However, the particle size can be tailored.

Regarding the size control of NP, there are some parameters that have an influence on this property. The reaction temperature [11] and the presence of nitrogen during the synthesis are factors affecting the size of the NP [55]. An increase of temperature (above 50 °C) will increase NP size [59] which is due to an increasing of the nucleation rate (supplement of activation energy). Bubbling the solution during synthesis with nitrogen prevent the oxidation of the magnetite NP to maghemite and have also an influence on their size with a size reduction when compared to other methods with no oxygen removal [29, 55].

Others parameters such as the type of salts (chlorides, sulfates, nitrates, perchlorates, etc.), the Fe^{2+} and Fe^{3+} ratio, pH, ionic strength of medium, type of precipitating agent and the concentration of the base have as well influence in the NP size and shape [29, 30, 55]. For instance, the concentration of the metal salts in the solution has a high impact on the size of the NP. Low concentrations lead to low particles growth, while they are normally more uniform (monodisperse). The opposite happens if there is an increase on the salts concentration, with an increase of NP size but polydisperse particles may be obtained [35].

Furthermore, other approaches may be carried out in order to increase the NP size. For instance, it is reported that the hydrothermal treatment after co-precipitation synthesis allows the increase of the NP size [1].

1.6 Surface Coating

Pristine magnetite NP (in the absence of any type of coating) in aqueous medium (e.g. water) have hydroxyl groups on their surface, as shown in Figure 1.13. Since these functional groups are amphoteric, they can react with both acids and bases, positively or negatively loading the surface of the NP (by protonation and deprotonation reaction of Fe-OH sites on NP surface) as a function of the pH of the solution. Therefore, at pH lower than the isoelectric point the surface charge is positive, and at pH above the surface charge is negative.

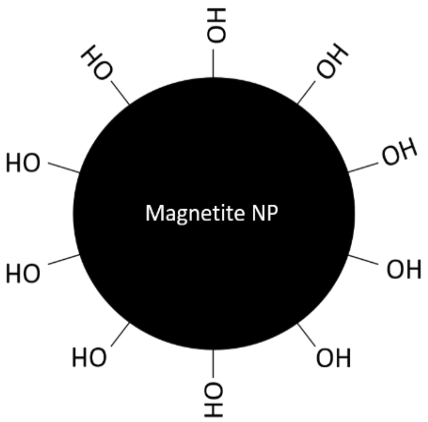

Figure 1.13: Surface structure of magnetite nanoparticles. In the absence of any coating these NP have hydroxyl groups on their surface.

For synthetic magnetite the isoelectric point value is 6.3 in average [60]. The large surface area relatively to the volume and the hydrophobic surface, lead to the aggregation of the particles into clusters to reduce the surface free energy [29, 35, 36, 55]. In turn, the clusters exhibit a strong magnetic attraction dipole-dipole between them, further potentiating the clustering between groups of clusters. The clusters exhibit strong magnetic dipole-dipole attractions between them and show ferromagnetic behavior rather than the fundamental and required superparamagnetic behavior [29]. The phenomenon of particle agglomeration may occur during the NP synthesis, drying or even in the post-processing [35].

For biological applications, stable suspensions at pH around 7.35–7.45 (respective to human blood) are required [2, 29]. For this, it is necessary that the zeta potential value (indicator of NP stability) of the NP suspension is usually greater than 25 mV in module [58] so that there is a sufficient repulsion force to compensate the attraction forces (such as *Van Der Waals* forces and magnetic dipole interactions) between the NP, and thus avoiding their agglomeration when dispersed into high ionic strength solvents such as biological media. Consequently, it is imperative to use biocompatible and non-toxic coatings [29], which can be chemically bound or physically adsorbed, and applicable under physiological conditions. With those purposes, typically the produced Fe_3O_4 nanoparticles are coated with organic or inorganic molecules during (*in situ*) or after the synthesis [10, 13]. Normally, the application of coatings *in situ* are complex, but offer greater stabilization and better magnetic properties [13]. This stabilization is due to the reduction of the NP agglomeration since the coating is accomplished during the synthesis [49].

Organic coatings comprise natural (e.g. dextran, chitosan, gelatin etc.) and synthetic polymers (e.g. PEG(poly(ethy leneglycol), PVA(poly(vinyl alcohol), PLLA (poly(lactic-co-glycolic acid), etc.), surfactants (e.g. oleic acid, stearic acid, lauric acid, etc.), and biological molecules (e.g. proteins, biotins, antibodies, etc.) [13]. Different types of functional groups such as phosphates or sulfates are able to bind to the surface of iron oxides [11, 33]. Inorganic coating includes metallic (e.g. gold, silver, copper, platinum, palladium, and iron) and ceramic (e.g. carbon, silica, etc.) [13]. In the case of polymers, their use in the magnetite NP coating creates repulsive forces (steric stabilization provided by the adsorption or grafting of polymers with passive surface atoms) to balance the magnetic attraction and *Van der Waals* forces, and thus the magnetic particles are stabilized preventing their agglomeration [12]. Although the polymer coatings have an decrease effect on the MNP agglomeration, it can also affect their magnetic properties, taking into account that non-magnetic materials may decrease Ms value [29]. Thus, the modification of the NP surface through the coating is an important parameter that must be taken into account, since it may have an impact on the heat dissipation capacity.

1.7 Fucoidan

The search for new sources of raw compounds to be used in the biomedical field has led to the discovery of several sulphated polysaccharides from marine algae that contain biological properties of interest for biomedical application [16].

Fucoidan is a natural anionic (negatively charged) [61] sulfated polysaccharide soluble in water, that is the main constituent of brown algae [16, 62] but can also be obtained through marine echinoderms [14]. It can be found in large quantities [63] and it has a relatively easy way of extraction, using hot water or acidic solutions [17].

1.7.1 Composition and Structure

Fucoidan presents a complex structure due to the existence of different monosaccharides and their linkages, as well as the distribution of the sulfate groups [16, 62]. Its structure also varies among the different species of brown algae [62, 64]. Overall, the fucoidan is constituted mainly by fucose and sulfate. In addition, may also have other monosaccharides such as galactose, mannose, xylose, glucose, and uronic acids [16, 17, 62].

Many reports describe that sulfated fucoidan has two types of homofucose backbone chains (Figure 1.14). The first, type I, is organized in repeating (α1–3)-L-fucopyranose with one or two sulfate groups in C2 and/or C4, whereas type II chains contains alternating (α1–3)- and (α1–4)-L-fucopyranose disaccharide with one sulfate group in C2 or C4 [64].

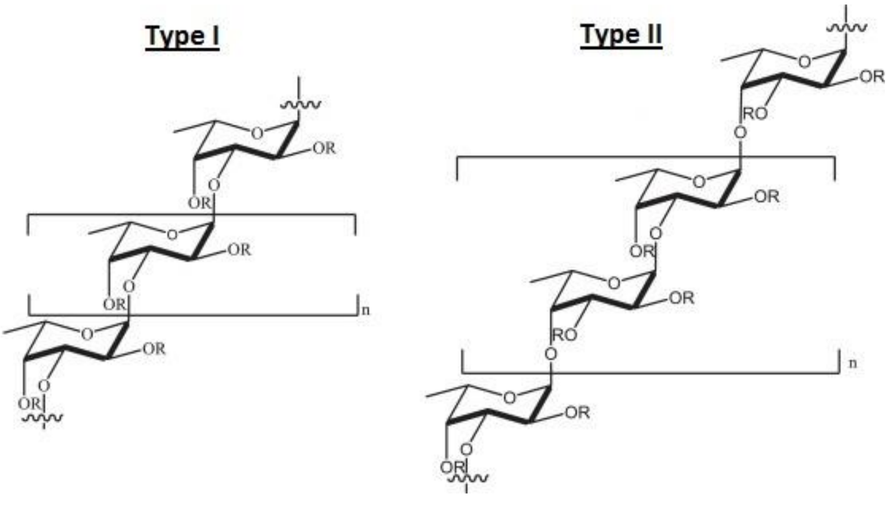

Figure 1.14: Two different types (type I and type II) of homofucose backbone chains in fucoidans extracted from brown seaweed. The R sites can be α-L-fucopyranose and sulfate groups. Adapted from Wu et al. [64].

Recent studies reported that those backbone structures may have further substitutions and may contain for example acetyl groups and sugar compositions and at different positions. For instance, the backbone may contain alternating mannose and uronic acid (also known as glucuronic acid) residues, uronic acid and galactose residues, etc. In the Figure 1.15 it is illustrated some examples of possible structural characteristics of fucose containing sulfated polysaccharides (FCSP) [65].

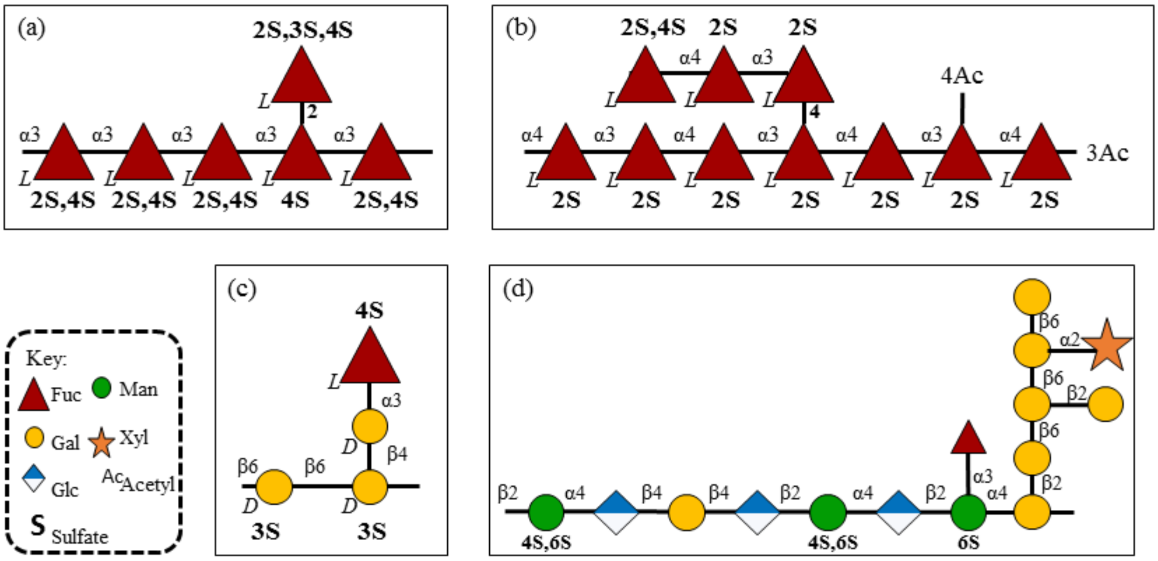

Figure 1.15: Possible structural characteristics found on different FCSP: (a) fucan structure found in species of Laminariales like Saccharina latissima; (b) fucan structure found in species of Fucales in Fucus serratus; (c) fucogalactan found in the Laminariales S. latissima; (d):found in the Fucales S. fusiforme. Adapted from Deniaud-Bouët et al. [65].

1.7.2 Biological properties

The biological properties of fucoidan vary according to the source of brown algae, compound purity, distribution and charge density, compositional and structural traits [17]. It has several biological properties that allows its application in several biological mechanisms such as anticoagulant, anti-adhesive, immunomodulatory, anti-inflammatory, antioxidant, anti-proliferative, anti-thrombotic, anti-platelet aggregation, anti-viral, and antitumor properties [62].

Although the antitumor effects are not yet fully understood, it may directly induce the mechanism of apoptosis in tumor cells [17]. This action includes the arresting of the cell cycle mainly in the G1 phase, which induces the death of tumor cells. It can also indirectly cause the apoptosis of tumor cells by increasing the body's immunity [64].

Sulfate groups are considered an important constituent because of the inhibition of the growth of cancer cells by binding with cationic proteins (proteins contained with lysosomes of neutrophils) presented on surface of the cell, and in turn prevent the vascular endothelial growth factor ($VEGF_{165}$) to bind with its cell surface receptor, inhibiting the tumor angiogenesis (growth of new vessels) [66].

In vitro and *in vivo* studies have demonstrated the anticancer properties of fucoidan in several types of cancers (breast, lung, prostate, colon, and melanoma) [5, 67] which makes it a very promising compound in cancer therapy. In addition, FCSP has low toxicity [17] and is biocompatible [63] being adapted for application in the biomedical field. It has been reported in terms of quantities that a fucoidan concentration of 10–200 µg/mL can induce cell apoptosis in an effective way [68].

Furthermore, in a combined phase I and II study on humans with 10 participants, 100 mg (5 participants) or 1000 mg (5 participants) of fucoidan dose was tested. The results showed that seaweed containing fucoidan extracts were safe during a period of 4 weeks at both doses [69].

1.7.3 Current and potential uses of Fucoidan as NP coating agent

Different studies have been arisen using the synergetic combination of fucoidan with MNP in the biomedical field [18, 19, 7-72].

Besides their anticancer properties, fucoidan can also act as NP stabilizer (including magnetite, silver, zinc oxide and cobalt ferrite) [15]. Additionally, fucoidan NP avoid their aggregation during blood circulation since reduces their interaction with serum proteins which in turns avoid their elimination [61].

For instance, in a study conducted by *Silva et al.* [18] agglomeration of magnetite NP (with sizes around 10 nm) was prevented through the fucoidan coating (reducing the dipole-dipole interactions). Furthermore, the use of fucoidan-coated magnetite NP on *in vivo* studies with Sarcoma 180 revealed a reduction in the tumor size, not observed in treatments using NP without fucoidan coating [19].

The coating of the NP with fucoidan also allows the addition of drugs using their functional groups, which may have the potential of enhance the efficiency of the treatment with these NP. The potential for drug introduction enables a simultaneous treatment using magnetic hyperthermia and chemotherapy known as thermo-chemotherapy. Studies *in vitro* have already demonstrated the synergistic effect of those combinatorial treatment [7].

For instance, Balasubramanian *et al.* [70] in a study using magnetite MNP encapsulated in poly (D, L- lactic-co-glycolic acid) loaded with anti-cancer drugs like curcumin, demonstrated the improvement on treatment efficacy allied to the multifunctionality (as heat-mediators and drug carriers).

Jang *et al.* [71], have coated gold NP with fucoidan and introduced doxorubicin. They reported the cooperative anticancer effect of the fucoidan associated with the anticancer drug. The anticancer effect was enhanced by the synergetic combination and it was also showed the fucoidan NP stabilization effect.

In a study realized by Moorthy *et al.* [72], magnetite NP were coated with silica functionalized with doxorubicin and fucoidan. These NP were synthesized to be used in chemotherapy, as drug carriers, and in magnetic hyperthermia. Fucoidan was introduced as drug protective agent, which was present in the pores of silica, to prevent it from being released prematurely. In addition, this polysaccharide showed a response to pH *stimulus* (in acid environment) and to magnetic hyperthermia allowing the release of the drug.

In another *in vitro* and *in vivo* study, it was reported that fucoidan has the potencial to increase the circulatory time of dextran-coated superparamagnetic iron oxide nanoparticles through the temporary inhibition of the immune system components responsible for the clearance of NP, and allowing in this way the enhance of treatment with the SPION [73].

1.8 Aim of the work

In this work is proposed the development of a hybrid multifunctional agent for a combined therapy of cancer based on the conjugation of magnetic hyperthermia with the antitumoral activity of a certain natural compound. Superparamagnetic iron oxide nanoparticles, which generate heat in the presence of a magnetic field, will be synthetized and coated with an antitumor polysaccharide, named fucoidan, to produce a novel anticancer agent. The coating of the NP with fucoidan will also allow the protection of the NP against oxidation in addition to preventing their aggregation.

Specific objectives:

i- Synthesis of magnetite superparamagnetic nanoparticles through the co-precipitation method and hydrothermal synthesis;

ii- Physical-chemical characterization, with the evaluation of their heating efficiency;

   a) Study of the effect of the synthesis conditions on their physical-chemical properties.

iii- Synthesis of NP coated with fucoidan by addition of fucoidan during (*in situ*) or after (post-synthesis) the co-precipitation/hydrothermal synthesis of the NP. Evaluation of coating quality, and analysis of the impact of this coating on the NP properties and also in their heating efficiency:

   a) Influence of NP size on NP functionalization with fucoidan in post-synthesis coating;
   b) Effect of fucoidan at different concentrations in post-synthesis coating;
   c) Influence of a reaction temperature (50 ºC) on NP functionalization with fucoidan in the *in situ* coating;
   d) Effect of different fucoidan concentrations in the *in situ* coating.

Chapter 2 Experimental Procedure

2.1 Fucoidan Characterization

In order to carry out an initial evaluation regarding the composition of fucoidan that was used for NPs coating, a characterization was performed for the determination of the neutral monosaccharides, uronic acids and sulfate content.

2.1.1 Neutral monosaccharides composition

In order to verify the purity of the sample and its sugar constitution the alditol acetates method was performed [74]. This was achieved through the polysaccharide hydrolysis to monosaccharides followed by a reduction and acetylation into alditol acetates and analysis by gas chromatography with a flame ionization detector (GC-FID).

For hydrolysis the procedure was as follows: 1-2 mg of sample was weighted into a culture tube (≈10 mL), then 200 µL of H_2SO_4 72% was added and incubated at room temperature for 3 h to dissolve the sample (shaken 2 to 3 times). Afterward, a volume of 2.2 mL of distilled water was added to the culture tube and hydrolyzed at 100 ºC in a heating block for 2.5 h (after 1 h the sample was cooled down, through an ice bath and 0.5 mL was removed to be used in uronic acid analysis, the hydrolysis was proceeded for another 1.5 h). Then, the tubes were cooled down in an ice bath.

For the step of reduction and acetylation, the procedure was as follows: first, to each culture tube 200 µL of an internal standard (2-deoxy-D-glucose 1 mg/mL) were added. Then, 1.0 mL of the hydrolyzed sample was transferred to new culture tubes and neutralized with 200 µL of NH_3 25%. Afterward, the reducing agent $NaBH_4$ (15% (w/v) in NH_3 3 M) was added and incubated in the heating block at 30 ºC for 1 h. Subsequently, the tubes were cooled down in an ice bath and, to eliminate the excess of BH_4^-, 2 volumes of 50 µL of glacial acetic acid were added. Then, a volume of 300 µL was transferred to Sovirel tubes with teflon caps to avoid potential contaminations) to which were added, in an ice bath, 450 µL of 1-methylimidazole and 3 mL of acetic anhydride, and were incubated in the heating block at 30 ºC for 30 min. After, in an ice bath, 3.0 mL of distilled water (to decompose the excess of acetic anhydride) and 2.5 mL of dichloromethane were added, stirred energetically to extract alditol acetates, then centrifuged at 3000 rpm for 30 s (to separate the phases). The aqueous phase was then removed by suction. Once more 3.0 mL of distilled water and 2.5 mL of dichloromethane were added, stirred and centrifuged and the aqueous phase removed by suction. The organic phase was washed again with 3 mL of distilled water, stirred, centrifuged at 3000 rpm for 30 s and the aqueous phase was removed. The organic phase was transferred to speedvac tubes and the dichloromethane was evaporated at reduced pressure. After, 1 mL of anhydrous acetone was added and evaporated as previously described. This step was repeated once more.

The alditol acetates were dissolved in 50 µL of anhydrous acetone and analyzed by GC-FID (Perkin Elmer – Clarus 400 chromatograph) using a capillary column DB-225 (30 m long, 0.25 mm of diameter and 0.15 µm of thickness). For this analysis, the volume of injection was 2 µL, the injector and detector temperature were at 220 °C and 230°C respectively. The temperature program was set with an initial temperature of 200 °C, was increased to 220 °C at 40°C/min, being maintained at this temperature for a period of 7 min, followed by an increase to 230 °C at 20 °C/min, at which was maintained for 1 min. The analysis of neutral sugars was carried out in duplicate. The sugars were identified by retention time in comparison with standards.

2.1.2 Uronic acids determination

Uronic acids were determined by the *m*-phenylphenol colorimetric method [75]. First, the previously hydrolyzed sample (that was obtained in the hydrolysis process for sugar analysis) (0.5 mL) was diluted with 3 mL of distilled water. Then, galacturonic acid standard (0.5 mL) with a concentration from 0 to 80 µg/mL (four standard solutions) was added to the sample (3.5 mL), in triplicate (2 replicas, 1 blank). After, in an ice bath it was added to each tube 3 mL of sodium borate 50 mM in concentrated H_2SO_4. After 60 s of mixing each sample, they were incubated at 100 ºC for 10 min. Afterwards, in the dark, 100 µL of MFF (m-phenylphenol 0.15% (w/v) in 0.5% (w/v) NaOH) were added to the sample tube (2 of the 3). The tubes were one more time shaked for 60 s and kept in the dark for 30 min. Subsequently, the samples were transferred to a microplate and the absorbance was read at 520 nm. The determination of uronic acids concentration was calculated by comparison with the calibration curve.

2.1.3 Elemental analysis

To complement the fucoidan composition characterization, elemental analysis was also executed in Department of Chemistry of University of Aveiro by Dr. Manuela Marques. The analysis of C (carbon), H (hydrogen), N (nitrogen) and S (sulfur) content was carried out using Truspec Micro 630-200-200 equipment. Two replicates were measured.

2.2 Magnetite Nanoparticles Synthesis

The co-precipitation method was used to synthetize magnetite NP, through the addition of a base (NH_4OH) to a stoichiometric aqueous solution of Fe^{2+} ($FeSO_4.\ 7H_2O$) and Fe^{3+} ($FeCl_3$) (Figure 2.1), in a molar ratio of 1:2 according to Equation 10. The stoichiometric quantities were used, in order to enhance the production of monodisperse NP [56].

$$2FeCl_3 + 1FeSO_4.7H_2O + 8NH_4OH = \boldsymbol{Fe_3O_4} + 6NH_4Cl + (NH_4\,)_2SO_4 + 11H_2O \text{ [Equation 10]}$$

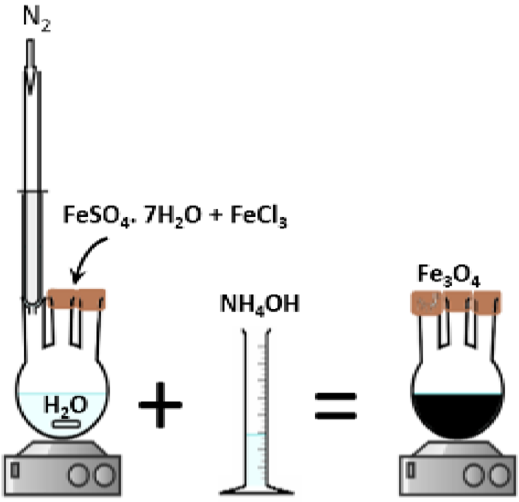

Figure 2.1: Schematic illustration of co-precipitation synthesis to produce magnetite NP.

The protocol employed in the magnetite NP synthesis was adapted from literature [58]. First, 25 mL of distilled water was added in a 3 necked flask along with a magnet (to magnetically stir the solution at 800 rpm). After, this flask was placed on a magnetic stirrer where degassing took place for 30 min under a nitrogen atmosphere to avoid oxidation of the ferrous ions. Then, 0.0076 mol of iron(III) chloride ($FeCl_3$, 97%, Merck) and 0.0038 mol of ferrous(II) sulfate heptahydrate ($FeSO_4.\ 7H_2O$, 99.5 %, Merck) were mixed with magnetic stirring (800 rpm) until the dissolution of the reactants was visible (approximately 20 min). This stirring speed was chosen according to the study performed by Mahdavi *et al.* [76]. Subsequently, 3.33 mL of ammonium hydroxide (NH_4OH, 25 %, Sigma-Aldrich) was added and magnetic stirring was maintained for 15 min producing magnetite NP. Some of the particles were aged at room temperature for 1 hour. Then, the NP were washed several times with distilled water to remove excess NH_3 and until pH 7 was attained. The pH value of 7 was chosen according to literature, as being the most adequate to achieve the fucoidan coating on iron oxide nanoparticles [77].

2.2.1 Hydrothermal treatment

In order to analyze the effect of the use of hydrothermal treatment on the magnetite NP properties, syntheses were carried out at different time/temperatures conditions: (1) the solutions of NP were submitted at 150 °C for 1, 2, and 3 h; (2) the solutions of NP was treated at 200 °C for 1, 2, and 3 h. The hydrothermal treatment with 150 and 200 °C was performed after the magnetite synthesis, using a Teflon-lined stain steel autoclave and kept in a lab oven at the established temperature during the defined time. After cooling at room temperature, the supernatant was removed from NP solutions using a permanent magnet. Then, the NP were washed several times with distilled water until pH of 7 was obtained. Between the washes the supernatant was removed using a pipette.

Magnetite NP were left in deionized water to be further characterized by the different techniques (subchapter 2.4) and to be coated (only 2 solutions. The obtained NP though co-precipitation and through hydrothermal synthesis were designated as: M_hour_temperature, as described in the Table 2.1.

Table 2.1: Sample label according to time and temperature conditions used for the synthesis.

Sample label	Time (hour)	Temperature (°C)
M_1_25	1	25
M_1_150	1	150
M_2_150	2	150
M_3_150	3	150
M_1_200	1	200
M_2_200	2	200
M_3_200	3	200

2.3 Nanoparticles Coating

The NP were coated by one-pot (*in situ*) or by post-synthesis methods. The efficiency of the methodologies was evaluated in terms of colloidal stabilization, the coating quality (coating of individualize NP instead of clusters), and SAR value.

2.3.1 Post-synthesis coating

The post-synthesis coating was accomplished by the adsorption method and was based on the work of Silva *et al*. [18]. Some variations were performed in terms of fucoidan concentration, maintaining a proportion of 2:1 relatively to the magnetite NP and fucoidan quantity. For the coating, the NP selected were M_1_25 and M_2_200. A fucoidan solutions were prepared with different concentrations (2, 4, 6 and 50 mg/mL) and were added to the solutions constituted by the previously obtained magnetite NP (containing 300 mg of magnetite) and was maintained at room temperature under stirring for 16 h (Figure 2.2). Then, the supernatant was removed from the solution using a permanent magnet and the NP were washed several times with distilled water and left in deionized water to be further characterized. The pH value of the fucoidan was measured before its use to evaluate if the pH of magnetite NP would be altered by the coating agent. It was not necessary to adjust the pH value as fucoidan has a pH between 7 and 8. The resulting samples obtained after coating were labeled as M_hour_temperature_F# where F denote fucoidan and # is the respective concentration in mg/mL. The sample M_1_25 was just coated with a fucoidan concentration of 2 mg/mL and the sample M_2_200 was coated with 2, 4, 6 and 50 mg/mL. All the samples are presented in the Table 2.2.

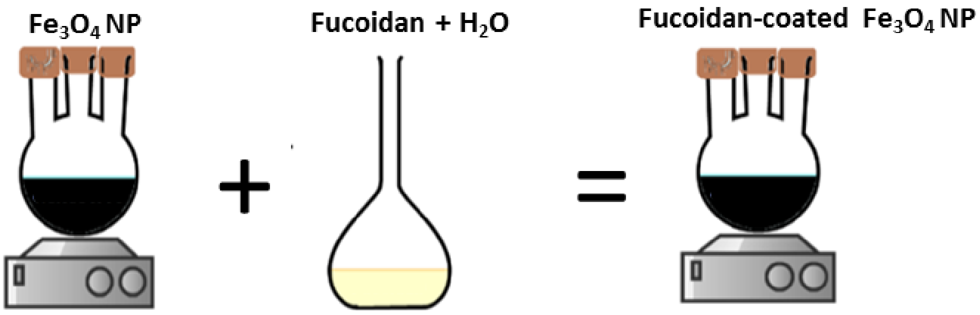

Figure 2.2:Schematic illustration of post-synthesis coating. .

Table 2.2: Sample label for the coated NP at different concentrations.

Uncoated sample	Fucoidan concentration (mg/mL)	Coated sample
M_1_25	2	M_1_25_F2
M_2_200	2	M_2_200_F2
	4	M_2_200_F4
	6	M_2_200_F6
	50	M_2_200_F50

2.3.2 *In situ* coating

The *in situ* coating method was performed in a single step, according to an adaptation of the methodology described by Yew *et al*. [78] The reactants and their quantities for the formation of magnetite NP were maintained, in relation to the above syntheses to produce pristine magnetite NP (subchapter 2.2).

For these experiences, a solution of iron salts II and III were mixed with a solution of fucoidan, followed by the addition of a base to produce fucoidan-coated magnetite NP (Figure 2.3).

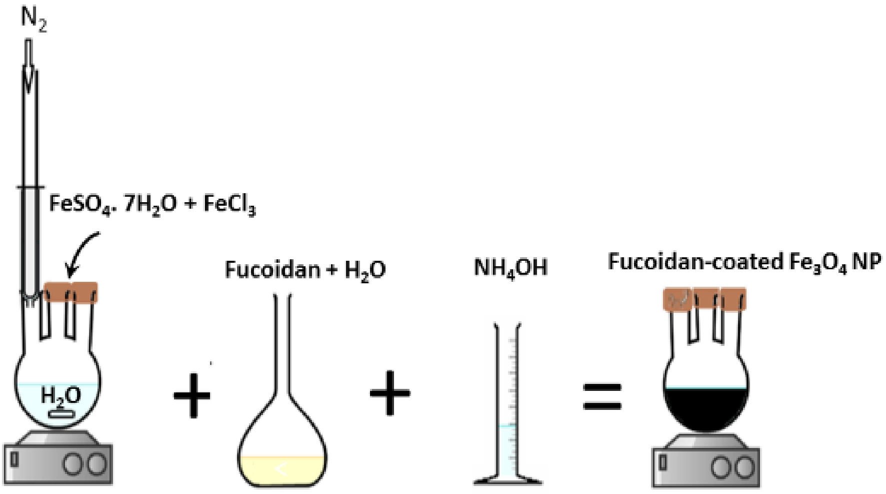

Figure 2.3: Schematic illustration of the in situ magnetite NP coating.

The synthesis was performed at room temperature, with a fucoidan concentration of 2 mg/mL. Then, 3 new syntheses were carried out, in which the temperature of reaction was 50 °C and different fucoidan concentrations (2,4 and 6 mg/mL) were used.

Distilled water (15 mL) was degassed for 30 min in a 3 necked flask with magnetic stirring (800 rpm). Then, 0.0076 mol of iron (III) chloride and 0.0038 mol of ferrous (II) sulfate heptahydrate were added until the dissolution of the reactants was visible (approximately 20 min). Afterwards, a solution of fucoidan (2 mg/mL) and ammonium hydroxide (3.33 mL) were added and magnetic stirring was maintained for 1 h. Then, the supernatant was removed from the solution using a permanent magnet and NP were washed several times with distilled water until a pH of 7 was obtained. The other syntheses were performed following the same protocol, but with a higher temperature (50 °C) during the synthesis, and varying fucoidan concentration (2,4 and 6 mg/mL).

The NP were kept in solution to be further characterized. The resulted samples were labeled as MF#_T, in which M comes from magnetite, F# from fucoidan and respective concentration in mg/mL, and T is the reaction temperature (25 or 50 °C). From all these syntheses the obtained samples can be seen in the Table 2.3.

Table 2.3:Sample label for the in-situ *magnetite NP coating.*

Reaction temperature	**Fucoidan concentration (mg/mL)**	**Sample label**
25 °C	2	MF2_25
50 °C	2	MF2_50
	4	MF4_50
	6	MF6_50

2.4 NP characterization techniques

Different characterization techniques were used to evaluate and study the NP properties. A brief description of the techniques and conditions applied, and their respective purposes are described in this subchapter.

2.4.1 X-Ray Diffraction (XRD)

X-ray diffraction (XRD) analysis was carried out in Department of Chemistry of University of Aveiro by Dr. Rosário Alves, and was performed to evaluate the crystal structure (to confirm the phase), the crystallinity and crystallite size of the NP. As the distances among the atoms in a crystal structure are comparable to the X-ray wavelengths, crystals diffract the X-ray beams. The diffraction pattern allows to determine the crystal structure and thus, the type of iron oxide [33].

The X-ray diffractograms were obtained with the Philips Analytical PW 3050/60 X' Pert PRO (θ / 2θ) diffractometer, with Cu-Kα radiation (λ = 1.54060 Å). The diffractograms were obtained by scanning in the 2θ range from 20 to 80° with a step of 0.02º and a scan step time of 96.4 s, at room temperature. In the case of the fucoidan-coated NP diffractograms were obtained by scanning in a 2θ range from 20 to 70°. In order to identify the crystallographic phase, it was used the database of *Powder Diffraction Files* (PDF) from the *International Centre of Data Diffraction* (ICDD) [79]. Through the broadening of the X-ray diffraction peaks and taking into account the instrumental correction, the crystallite size was determined using the Debye–Scherrer Equation [80], and assuming the spherical shape of the particles and

$$D = \frac{0.89\lambda}{(\beta \times \cos\theta)} \qquad \text{[Equation 11]}$$

Where λ is the wavelength of Cu-K_α radiation and β is the full width at half maximum of the peak (FWHM), and θ is the diffraction angle.

Peak (311) with the respective 2θ value for each sample (around 35º) was selected for the application of the Scherrer's equation as it is a single peak with the highest intensity.

2.4.2 Specific Surface Area (A_{BET})

Brunauer-Emmett-Teller (BET) was carried out in the Department of Materials Engineering and Ceramics of University of Aveiro by Eng. Célia Miranda, and was used to determine the specific surface area of NP [81]. The equipment used was *Micromeritics® – Gemini 2380 V2.00*. The samples were degassed overnight at 150 ºC to remove physically adsorbed water which would interfere with the surface area results. Before analysis, the samples were cooled down using liquid nitrogen to -196 °C. The specific surface area of the materials was determined from nitrogen gas adsorption–desorption.

2.4.3 Transmission Electron Microscopy (TEM)

TEM analysis was performed to evaluate the NP morphology, shape and size. TEM micrographs were obtained in two different equipment.

TEM images of samples M_1_25, M_2_200, M_1_25_F2, M_2_200_F2 and MF2_25 were obtained using the equipment JEOL 2200FS with an acceleration potential of 200 kV. To prepare the samples, some particles were transferred to an Eppendorf containing ethanol, then a droplet of suspension was deposited onto a lacey carbon coated copper grid from Agar Scientific® and left to evaporate at 35 ºC in a lab oven for 1 hour. These TEM images was obtained by Eng. Marta Ferro from the Department of Materials Engineering and Ceramics of University of Aveiro.

The TEM micrographs for the samples M_1_25, M_2_200, M_1_25_F2, M_2_200_F2, M_2_200_F6, MF2_50 and MF6_50 were carried out in a double corrected equipment JEOL cold FEG Grand ARM 300 and was operated at 300 kV and at 80 kV. The column was equipped with JEOL spherical aberration correctors which were tuned before every observation assuring a point resolution of 0.7 Å at 300 kV. The microscope was also equipped with a JEOL EDX spectrometer and a Gatan Quantum Energy Filter. For the samples preparation the suspensions were sonicated over several minutes to disperse the NP, then few drops of the suspensions were placed onto holey carbon copper microgrids. These TEM images was obtained by DR. Alvaro Mayoral and DR. Qing Zhang from School of Physical Science and Technology in Shanghai.

The ImageJ® program [82] was used to estimate the mean size of the NP, and also the particle-size distributions (a minimum of 100 particles was used for each sample, measuring the size of each particle). The histograms were fitted assuming a Log-Normal distribution of the NP diameters, and the particle size distribution of the samples was determined statistically.

2.4.4 Fourier Transform Infrared spectroscopy (FT-IR)

To study the functionalization of the magnetite nanoparticles with fucoidan (surface coating), FT-IR spectroscopy was performed. FT-IR spectra were recorded over the range of 4000 - 500 cm^{-1} with Perkin Elmer Spectrum BX, and with a resolution of 4 cm^{-1} and 64 scans per sample. For each sample 5 replicates were measured.

2.4.5 Zeta Potential

To evaluate the colloidal stability of the solutions, measurements of the zeta potential as a function of pH were performed following the procedure used by Bini *et al*. [83]. Zeta potential was measured using a Zetasizer Nano ZS from Malvern Instruments.

2.4.6 Magnetic hyperthermia

The evaluation of the nanoparticles SAR under AC magnetic field was carried out using an Easy Heat 0224 device (Ambrell), with a two-turn Helmholtz solenoid of around 6 cm diameter and working at 276 kHz frequency with an AC field amplitude of 14.7 kA m^{-1} (below “Brezovich limit”).

These measurements were performed by Prof. Margarida Cruz and Prof. Liliana Ferreira from the Physics Department of Faculty of Sciences of the University of Lisbon. The experimental setup and the protocol used to determine the Specific Absorption Rate of the samples are reported on the work performed by Cruz *et al.* [1].

Chapter 3 Results and discussion

3.1 Fucoidan analysis

The fucoidan used in this work was characterized concerning the neutral monosaccharides, uronic acids and sulphate groups content. The results obtained can be observed in Table 3.1. Fucoidan is mainly constituted by fucose (418 µg/mg$_{\text{fucoidan}}$), galactose (230 µg/mg$_{\text{fucoidan}}$) and mannose (51 µg/mg$_{\text{fucoidan}}$). Since this fucoidan contains less than 90 % of fucose, according to IUPAC (International Union of Pure and Applied Chemistry), it can be considered fucoidan and not fucan [84]. Comparing the fucose content of this fucoidan with the commercially available fucoidan from Sigma Chemical Co, obtained from *Fucus vesiculosus*, it can be said that is slightly lower (commercial is composed by 44% w/w) [14]. This fucoidan has a higher amount of galactose than the commercial one, as it was extracted from green algae [85]. However, galactose is part of the composition of many brown algae such as *Laminariales S. latissima* and in the *Fucales S. fusiforme* as already shown in Figure 1.15 (subchapter 1.7.1). In addition, Duarte *et al.* [86] performed structural studies on fucoidans from the *Sargassum stenophyllum*, which is a brown seaweed, and they likewise reported not only fucose but also galactose as major components.

Table 3.1: Fucoidan monosaccharide composition and sulfate (µg/mg).

Monosaccharide composition (µg/mg fucoidan)							***Sulfate content (µg/mg fucoidan)***	***Total (µg/mg fucoidan)***
Fuc	Glc	Man	Xyl	Gal	Rha	Uronic acids		
418.1	24.8	**51.1**	17.6	**229.6**	21.5	75.9	**104.5**	943.2

Fuc: Fucose; Glc: Glucose; Man: Mannose; Xyl: Xylose; Gal: Galactose; Rha: Rhamnose

By the elemental analysis results (Table 3.2) it was possible to see the sulfur content of the fucoidan. Using the obtained 3.38% value, it was calculated the percentage of 10.1% in sulfate ester as constituent of fucoidan. This calculation was performed considering the known ratio between sulfur atom and sulfate ester masses which is 2.99. Then, a sulfate content value of 104.5 µg/mg$_{\text{fucoidan}}$ was calculated (Table 3.1).

The content of sulfate is within the range when compared with fucoidan extracted from *Ascophyllum nodosum, Sargassum kjellmanianum, Sargassum thunbergii*, that presents a percentage of sulfate content between 8 and 25% [62]. As already mentioned in subchapter 1.7.2, sulfate groups are considered an important constituent because of the inhibition of the growth of cancer cells. Thus it is very important the presence of this element on fucoidan composition [66].

In addition, fucoidan has also traces of nitrogen content (%N) which may be associated with the existence of some compounds containing amino groups (e.g., protein or amino sugars) [87].

Table 3.2: Elemental analysis results of fucoidan.

Element content (%)			
% C	**% H**	**% N**	**% S**
22.57	4.59	0.37	3.38

3.2 NP syntheses

3.2.1 Effect of the synthesis method on crystallinity and crystallite size

The NP were synthetized by co-precipitation at room temperature and hydrothermal methods. In the case of the hydrothermal syntheses, different temperatures (150 and 200 ºC) and reaction times (1,2 and 3 h) were used. In order to evaluate the influence of the synthesis conditions on the NP crystallinity and crystallite size, the NP were analyzed by X-ray diffraction (Figure 3.1).

In order to confirm the phase, the obtained diffractograms patterns of all samples are display together with the reference pattern of magnetite (magnetite, card no. 04-002-3668). The characteristic peaks (220), (311), (400), (422), (511), and (440) can be observed, which are in accordance with the inverse cubic spinel phase of Fe_3O_4.

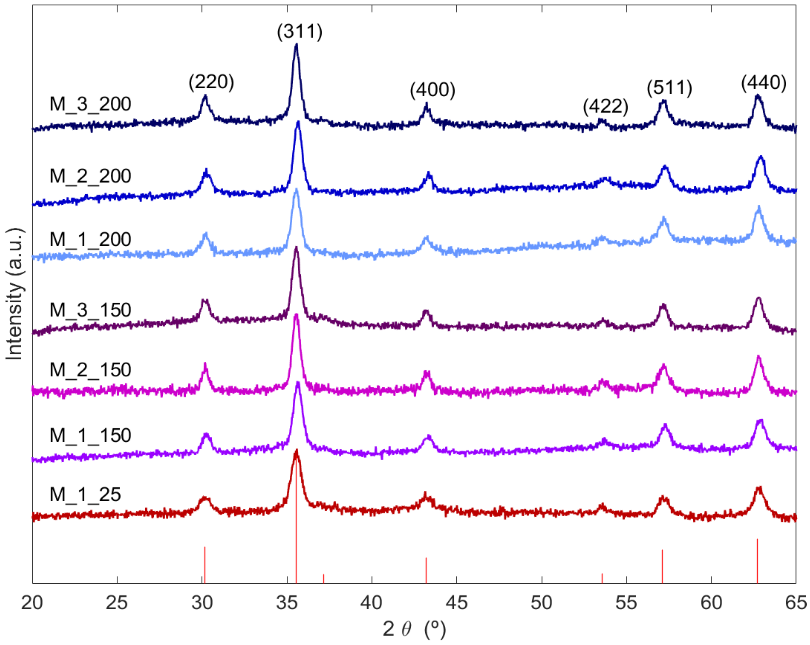

Figure 3.1: Normalized XRD patterns obtained for the different samples: M_1_25; M_1_150, M_2_150; M_3_150; M_1_200; M_2_200; and M_3_200. The red lines represent the peaks of the magnetite phase card no. 04-002-3668.

According to the diffractograms it can be seen that the increase in time and temperature was reflected in an increase in the peaks intensity of the samples, that may be due to a higher crystallinity or to a higher NP size. In this way, the sample with no hydrothermal treatment exhibited a pattern with broad and less intense peaks. The samples with a hydrothermal treatment at 200 °C, show patterns with more intense and narrow peaks. Increasing the duration of the synthesis also results in narrow and more intense peaks.

Based on the diffractograms, the sample labeled as M_2_200 (2 h at 200 °C) was selected to be further characterized and coated with fucoidan. The sample M_3_200 was not selected since there was no great difference in the diffractogram when compared to the sample M_2_200. In addition, to verify the impact of the hydrothermal treatment on the final MNPs properties namely in the heat efficiency, the sample M_1_25 was also used for comparison. After this selection, the remaining characterization was performed, namely in terms of morphology, size and size distribution, as well as heating efficiency.

TEM micrographs of the sample prepared by co-precipitation at room temperature (M_1_25) can be seen in the Figures 3.2 and 3.3. The NP presents some polydispersivity and agglomeration due to the high surface-to-volume ratio and the dipole-dipole magnetic interactions between NP. Regarding the morphology, the nanoparticles are quasi-spherical. Additionally, in Figure 3.3 (top panel) the image of the lattice fringes is given and is coherent with (110) plan of the cubic structure of magnetite.

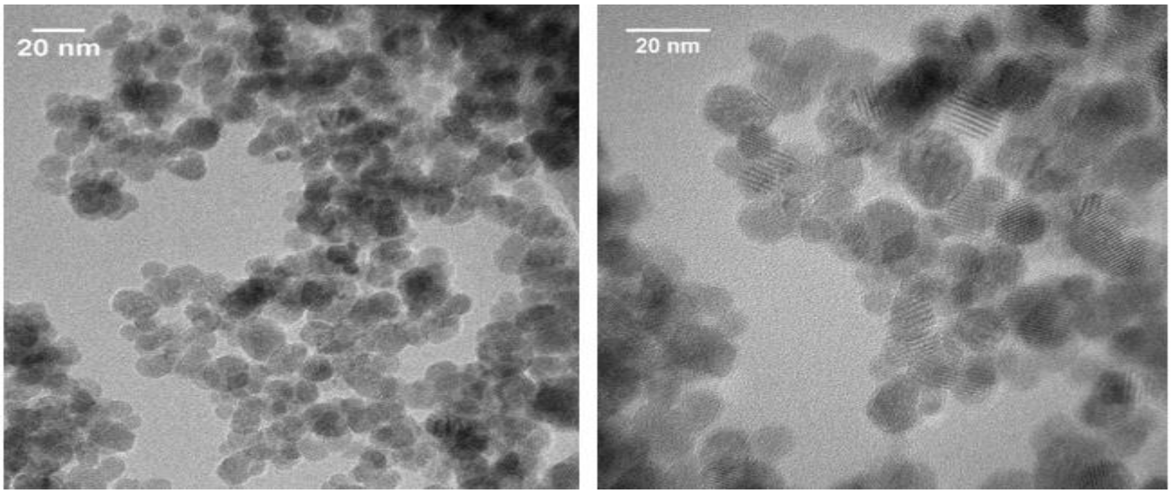

Figure 3.2:TEM micrographs of the magnetite NP sample M_1_25 (acquired with JEOL 2200FS with an acceleration potential of 200 kV).

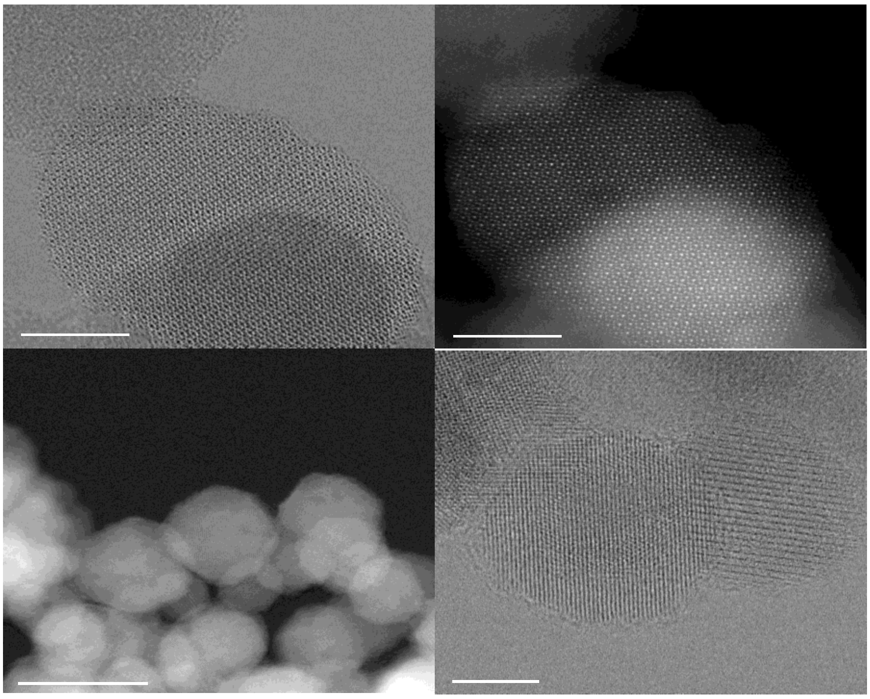

Figure 3.3: High resolution TEM images of the sample M_1_25 (acquired with JEOL cold FEG Grand ARM 300 equipment at 300 kV).

A medium particle size of 10.2 ± 3.3 nm (resulting from the measurement of ca. 100 particles in the TEM images) was obtained for the M_25_1 sample (Figure 3.4), which is a value in accordance to the reported value for particles prepared by precipitation method [57, 58, 88]. In addition, according to the literature, this size is in the proposed range for application on MHT [1, 40, 52].

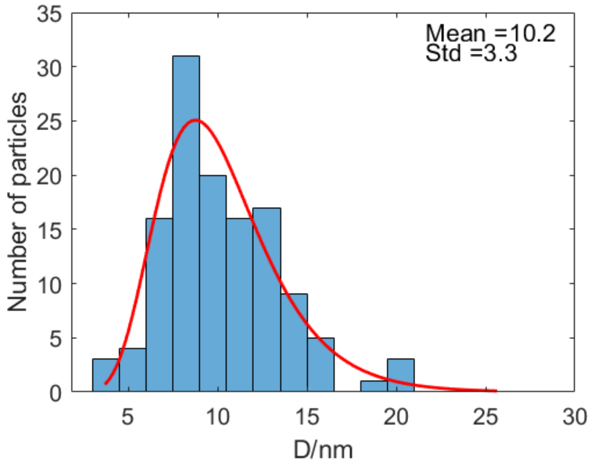

Figure 3.4: Particle size distribution of the sample M_1_25.

Regarding to the sample subjected to a hydrothermal treatment (M_2_200), TEM micrographs can be seen in Figures 3.5 and 3.6. The NP are not completely spherical in shape and also exhibits some agglomeration as the M_25_1 sample. The average particle size is 15.8 ± 3.6 nm, which is higher than those obtained for the co-precipitation sample at room temperature. This confirms the increasing of the NPs size with a hydrothermal treatment after co-precipitation synthesis, as already reported in the literature [1, 57]. In the study performed by this research group, a hydrothermal treatment in an autoclave at 150 °C for 1 h and 6 h was realized after the NP precipitation synthesis, the results showed an increase on the NP size. For instance, in the case of 1 h there was an increase on the NP size around 5 nm (estimated by the Scherrer equation) [57].

This raise may be explained through the coarsening of the NP, phenome also known as Ostwald ripening, in which small particles dissolve due to the energy supplied by the hydrothermal treatment, and reform onto larger particles [56]. Although these NP are larger than the previous ones, they are still within the recommended size for MHT [1, 40, 52]. It must be noted that this NP can be tailored to a higher size, preferable not above 20 nm, in order to enhance the magnetic properties without compromising the superparamagnetic behavior.

By analyzing and comparing Figure 3.5 with Figure 3.2 relatives to NP synthesized by the co-precipitation method, a minor agglomeration can be observed. This is due to the fact that smaller

NPs possess a large surface area relatively to the volume, and in order to reduce the surface energy, they have a greater tendency for agglomeration [29, 35, 36, 55]. Additionally, in Figure 3.6 it can be seen the lattice fringes corresponding to the (211) and (111) plans of magnetite and the representation of the oxygen and iron atoms.

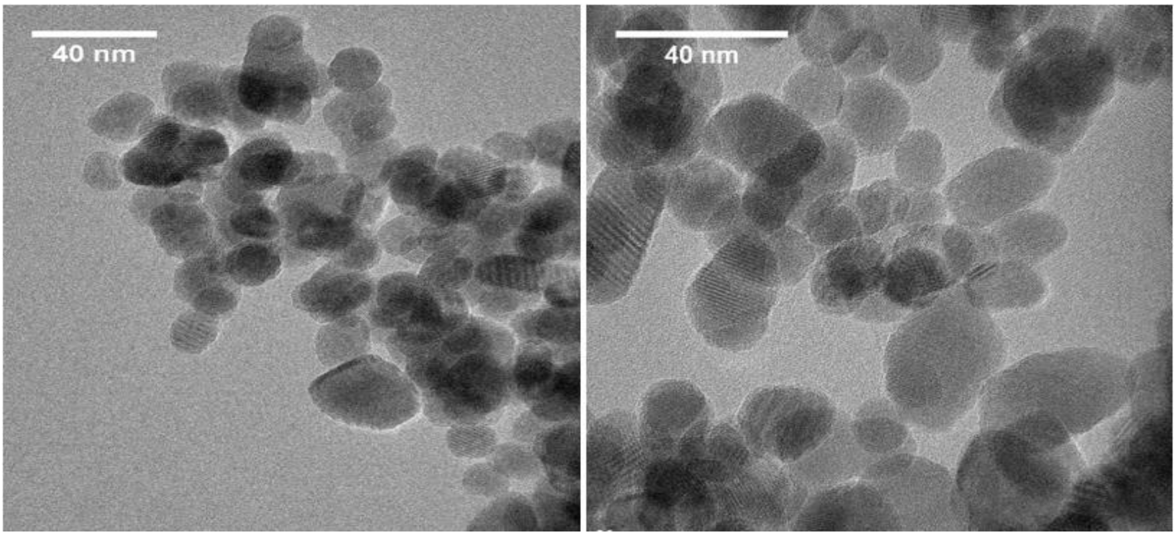

Figure 3.5: TEM micrographs of the sample M_2_200 (acquired with JEOL 2200FS with an acceleration potential of 200 kV).

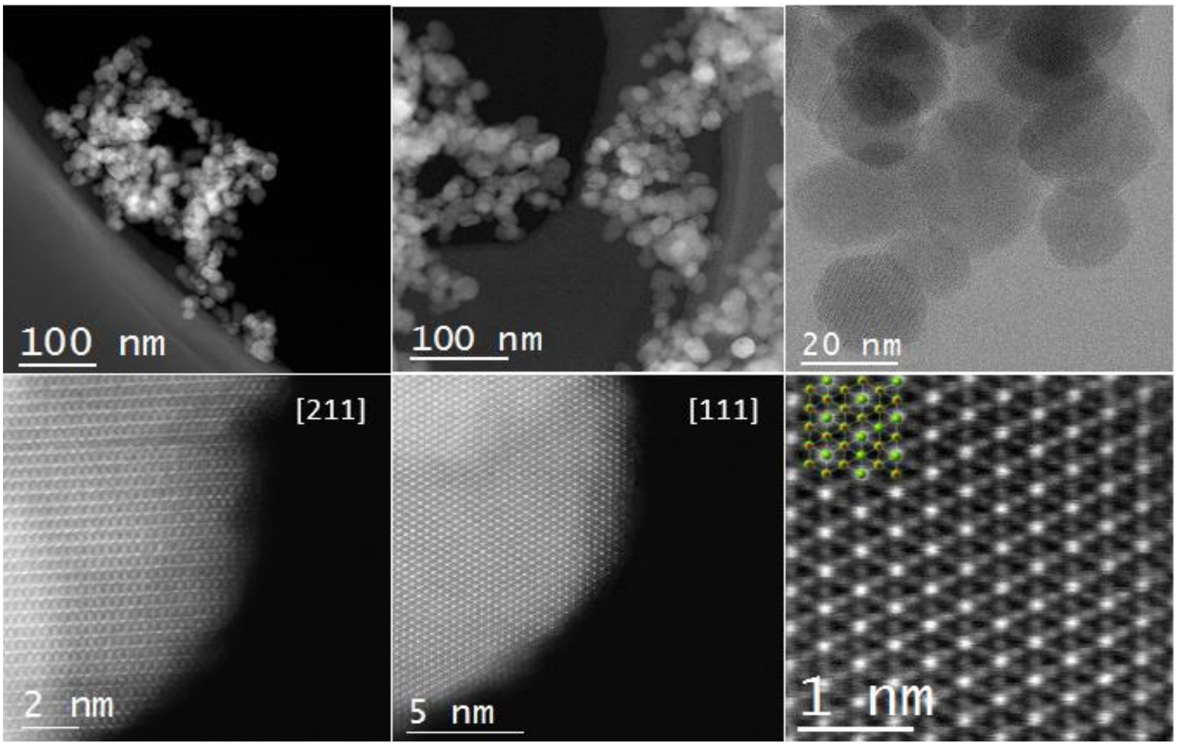

Figure 3.6: High resolution TEM images of the sample M_2_200 (acquired with JEOL cold FEG Grand ARM 300 equipment at 300 kV).

It can also be noted that M_2_200 sample its more polydisperse (Figure 3.7) than the obtained with co-precipitation synthesis at room temperature. This increase of polydispersivity was already observed in the literature by Carvalho *et al.* [57], since they also observed an increase in the distributions size when subjected the NPs to a hydrothermal treatment of 150 °C for 1 h or 6 h.

In addition, it is reported that with the increase of particle growth there is a loss of uniformity in terms of size [35]. It is crucial to produce monodisperse NP, since narrow distributions of size enhance SAR value [41] which translates in a higher thermal efficiency. Moreover, a high SAR is desirable in MHT, which means that a lower dose may be administered in the patient [36].

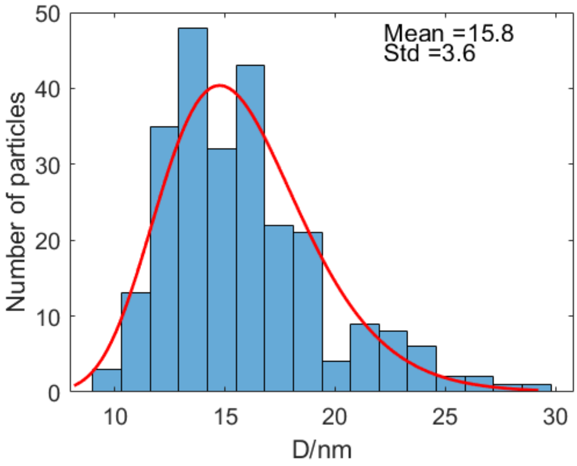

Figure 3.7: Particle size distribution of the sample M_2_200 prepared with hydrothermal treatment.

NP size was also evaluated using XRD patterns and the Scherrer Equation. The sample M_1_25 obtained a mean crystallite size of 12.6 nm, while the sample M_2_200 had a higher value of 16.8 nm. These values are also closed to the ones obtained through TEM analysis and confirm once more the increase of NP size with the thermal treatment under pressure.

Relative to the NP specific surface area, determined by Brunauer-Emmett-Teller (BET), the highest A_{BET} was obtained for the NP M_1_25 (96 m²/g), which is consistent with the smaller particle size. The A_{BET} of sample M_2_200 was determined to be 58 m²/g. Moreover, the adsorption and desorption isotherms of those samples can be visualized in the Figure 3.8.

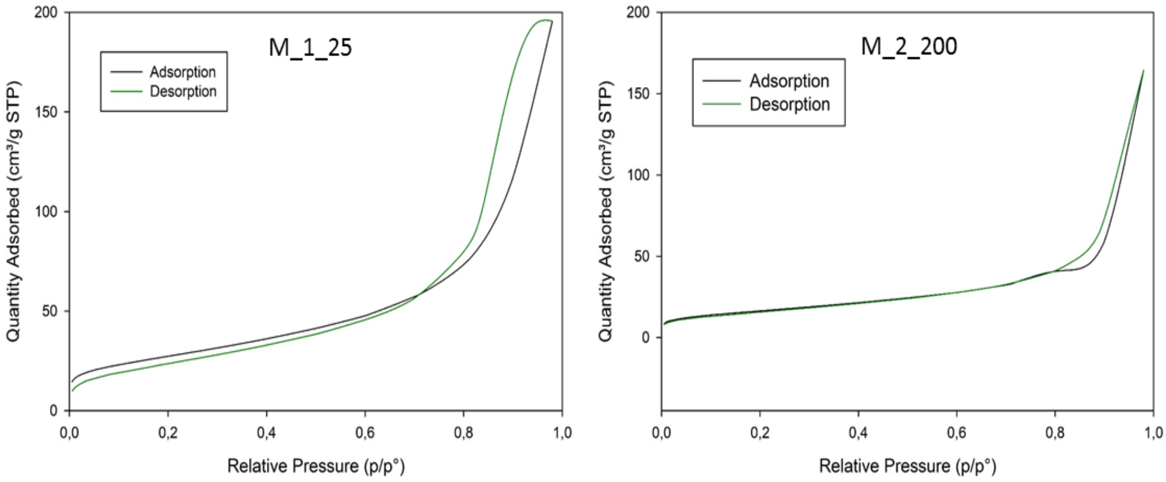

Figure 3.8: -196 °C N_2 adsorption and desorption isotherms for samples M_1_25 and M_2_200.

According to the IUPAC, the M_1_25 sample displays a type II isotherm characteristic of non-porous materials [89] supporting that the highest specific surface area results mainly from the low particle size of the sample. It is noteworthy that both samples exhibited a narrow hysteresis loop at high values of relative pressures ($P/P_0 = 0.80 – 0.98$). This effect is due to the mesopores formed between nanoparticles (interparticles porosity) due to the agglomeration and not because of the existence of pores in the NP. Mascolo *et al.* [88] also reported the existence of the hysteresis loop at higher pressures due the existence of mesopores originated by the NP agglomeration.

In general, this result is expected since magnetite NP are assumed as a non-porous material [33, 47].

3.3 Nanoparticles Coating

This subchapter is subdivided into the analysis and characterization of NP coated after their syntheses and coated *in situ* during the NP synthesis. First, it will be presented the results obtained by the two coating methods and the different characterizations techniques to evaluate: functionalization with fucoidan, phase purity, morphology, size and size distribution, and colloidal stabilization. In addition, the results in terms of thermal efficiency will be also presented and discussed for the samples coated by the 2 methods, in order to compare the results which in turn arises from the different properties previously characterized and discussed.

3.3.1 Coating with fucoidan

The post-synthesis coating was performed on the sample synthetized by co-precipitation at room temperature (M_1_25) and on the sample with hydrothermal treatment (M_2_200) with the same fucoidan concentration (2 mg/mL). Considering that the NP submitted to a hydrothermal treatment showed a higher crystallinity, different concentrations of fucoidan (4, 6 and 50 mg/mL) were also used. The objective was to increase the quantity of fucoidan on the NP surface and to study the influence on the NP stabilization and in their properties, namely the heat efficiency.

3.3.1.1 Functionalization of magnetite NP with Fucoidan

In Figure 3.9, FT-IR spectra of the samples M_1_25 and M_2_200 and the respective coated samples (M_1_25_F2 and M_2_200_F2) with the same fucoidan concentration (2 mg/mL) are exhibited. In Figure 3.10 are presented the FT-IR spectra of the samples that resulted from the coating of the M_2_200 NP with different fucoidan concentrations (2, 4, 6 and 50 mg/mL, samples M_2_200_F2, M_2_200_F4, M_2_200_F6 and M_2_200_F50 respectively), in order to analyze if the increasing concentration in fucoidan results in the increase of the vibration bands associated to fucoidan functional groups.

The magnetite spectrum has the representative peak around 564 cm^{-1}, which corresponds to the stretching vibrations of metal at the tetrahedral site, characteristics of Fe-O band, and proves the existence of the Fe_3O_4 nanoparticle core.

Analyzing the spectrum of the M_2_200 sample before and after coating with a fucoidan concentration of 2 mg/mL, it can be seen that there is the appearance of the peaks around 842, 1030 and 1628 cm $^{-1}$, attributed to the C-O-S, C_O_SO_3, and C=O vibration groups, respectively. Additionally, the peak around 3366 cm^{-1}, due to -OH vibration, becomes more evident after the coating, and this change arise from fucoidan contribution.

Relatively to the coating of the M_1_25 NP, with a mean particle size of 10.2 nm ± 3.3, the peaks around 842, 1030, 1224, 1628 cm^{-1} are exhibited (Figure 3.9). The peak around 3366 cm^{-1} appears after NP coating. These results from the FT-IR allow to confirm the presence of fucoidan on the NP surface.

In general, analyzing the impact of NP size on the fucoidan coating efficiency, it is verified that although the observed peaks are not very expressive with the respective coatings at the same concentration, the spectrum relative to the coating of the lower-size NP exhibited more peaks attributed to fucoidan when compared to the spectra relative to the coating of the larger size NP. This result may be associated to the fact that NP with smaller size have a larger specific surface area, which in turn provides a larger area for the coating to be performed more efficiently.

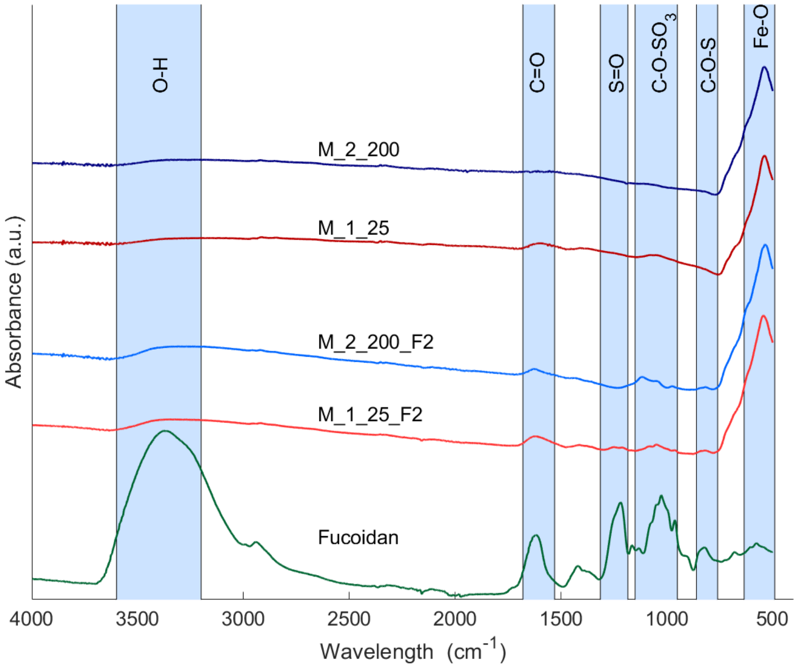

Figure 3.9: Normalized FT-IR spectra of the samples M_1_25 and M_2_200 and the respective coated samples (M_1_25_F2 and M_2_200_F2) with the same fucoidan concentration (2 mg/mL). The fucoidan spectra are also presented.

The comparison between the different fucoidan concentrations on the NP functionalization, can be observed in the Figure 3.10. It can be seen in all the spectra the presence of Fe-O band (564 cm^{-1}) and the peaks referred to fucoidan as previously described. As the concentration of fucoidan increased from 2 to 4, 6 and 50 mg/mL, there was no significant increase in their peaks that easily allow to distinguish the different concentrations coatings.

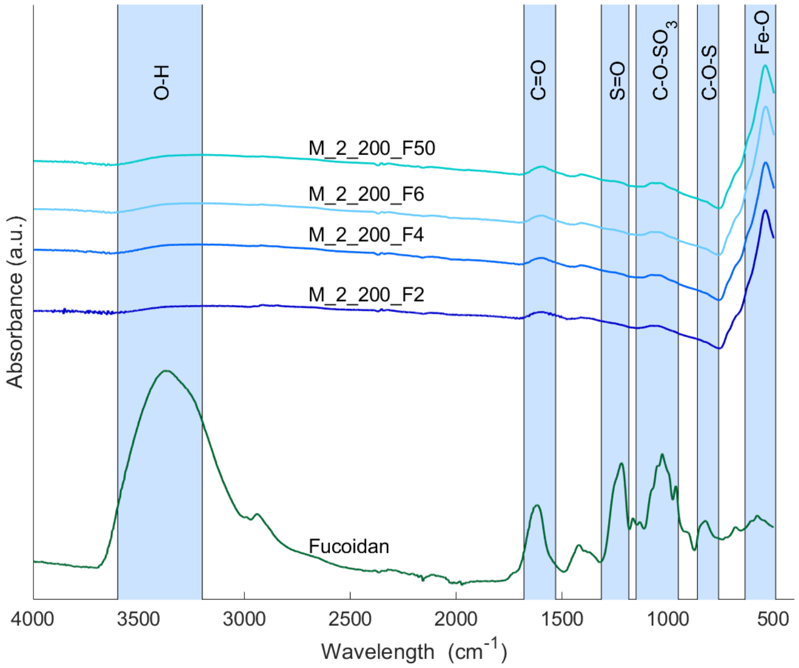

Figure 3.10: Normalized FT-IR spectra of the samples that resulted from the coating of the M_2_200 NP and with different fucoidan concentrations (2, 4, 6 and 50 mg/mL, samples M_2_200_F2, M_2_200_F4, M_2_200_F6 and M_2_200_F50 respectively) and of fucoidan.

The diffractograms obtained from the coating of M_1_25 (M_1_25_F2) and M_2_200 (M_2_200_F2, M_2_200_F4, M_2_200_F6 and M_2_200_F50) with different fucoidan concentrations can be observed in the Figure 3.11 and 3.12, respectively. In order to confirm the maintenance of phase after the coating, the obtained diffractograms patterns of the samples coated with fucoidan are display together with the reference pattern of magnetite.

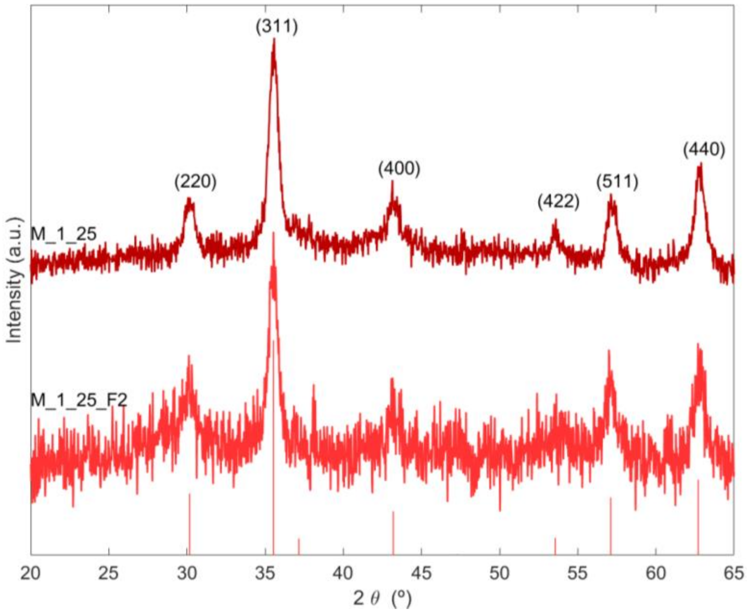

Figure 3.11: Normalized XRD diffractogram of magnetite M_1_25 NP before and after coating with fucoidan with a concentration of 2 mg/mL (M_1_25_F2). The red lines represent the peaks of the magnetite phase card no. 04-002-3668.

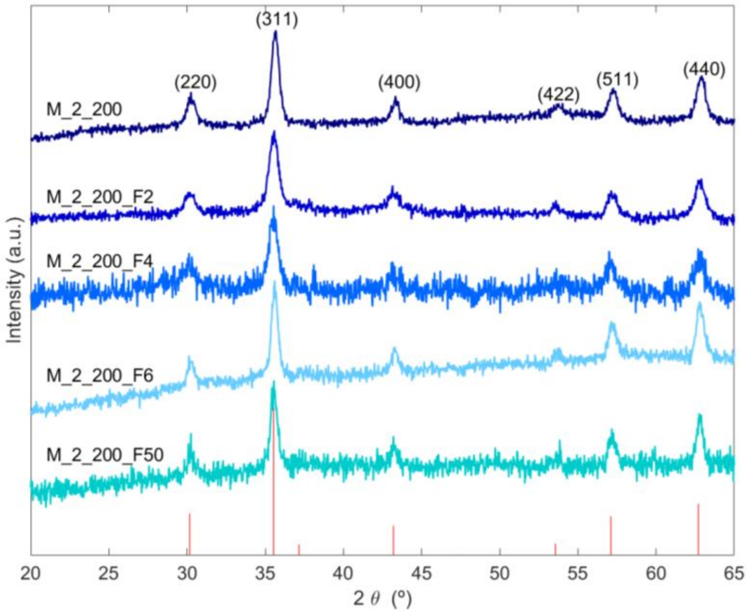

Figure 3.12: Normalized XRD diffractograms of magnetite NP with hydrothermal treatment (M_2_200) and their coated counterparts (M_2_200_F2, M_2_200_F4, M_2_200_F6 and M_2_200_F50 respectively). The red lines represent the peaks of the magnetite phase card no. 04-002-3668.

In general, there is clear a reduction of the intensity of the diffraction peaks as the concentration of fucoidan increases, which should not be assigned to a reduction of the crystallinity but to a dilution effect of the magnetite signals due to the increase of the fucoidan layer on the samples. Therefore, the sample M_2_200_F50 exhibited the pattern with the lowest intensity which is an indication of the presence of a larger amount of fucoidan at the magnetite surface. Nevertheless, the characteristics peaks of magnetite are present in all the samples, demonstrating that the coating did not affect the NP core as already reported by Silva *et al.* [18, 19]. This intensity reduction effect is predictable as it is being added to the material another phase which reduce the volume of the particles analyzed. Moreover, no extra diffraction peaks appear on the pattern because fucoidan is amorphous as it can be seen in the Figure 3.13. The decrease of intensity observed in the diffractograms and originated by the coating with fucoidan was also previously observed by Silva *et al.* [18, 19] and Moorthy *et al.* [72].

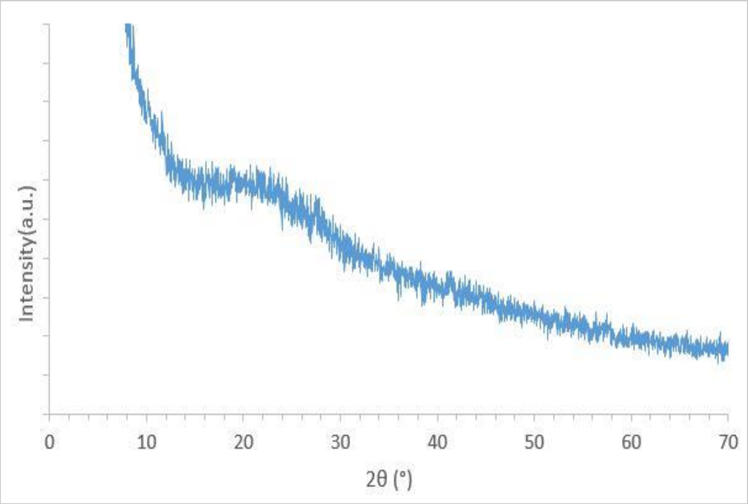

Figure 3.13: XRD diffractogram of fucoidan.

TEM images of the samples M_1_25_F2, M_2_200_F2 and M_2_200_F6 and their particle size distributions are presented in Figures 3.14, 3.15, 3.16, 3.17, 3.18, 3.19, 3.20 and 3.21. TEM analysis was performed in these samples since they showed higher intensity peaks on XRD diffractograms (Figure 3.12).

The TEM micrographs of NP without hydrothermal treatment (M_1_25) and coated with fucoidan (2 mg/mL, M_1_25_F2) can be visualized in the Figures 3.14 and 3.15. In the images is observed some agglomeration of the NP, as was already been verified for uncoated NP. Thus, the coating in agglomerated zones is more around groups of particles instead of in individualized NP.

Through the TEM images it is not perceptible if the coating provided higher NP dispersion according to their stabilizing effect reported in the literature [15]. For instance, in the study of Silva *et al.* [18, 19] they observed a higher NP dispersion after the coating with fucoidan. In the Figure 3.15 it can be seen the image of the lattice fringe referred to (100) plan of magnetite.

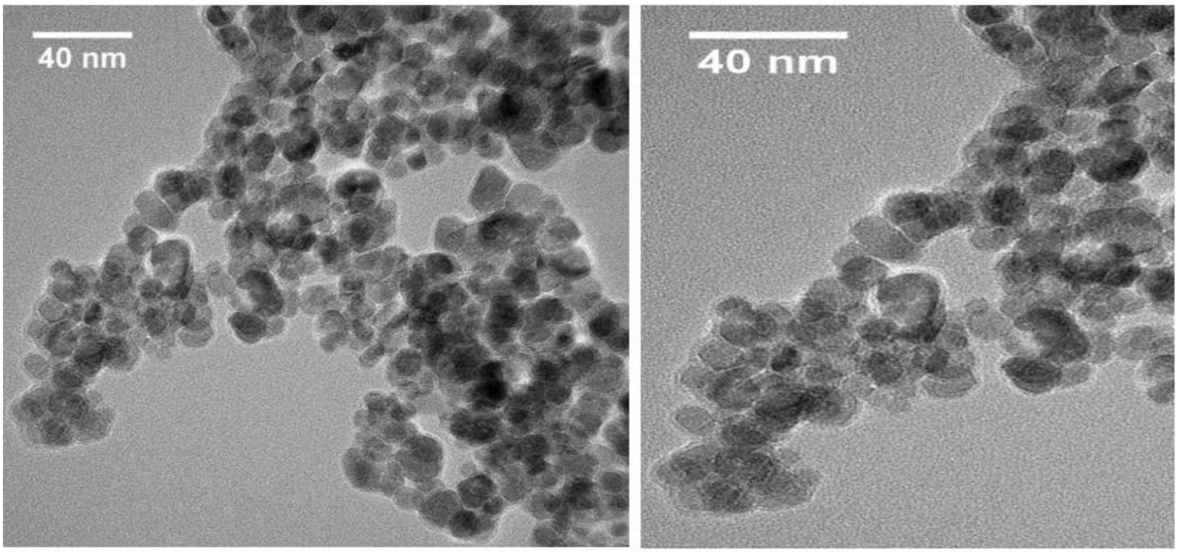

Figure 3.14:TEM images of magnetite NP synthetized by co-precipitation and coated with a fucoidan concentration of 2 mg/mL: M_1_25_F2 (acquired with JEOL 2200FS with an acceleration potential of 200 kV.

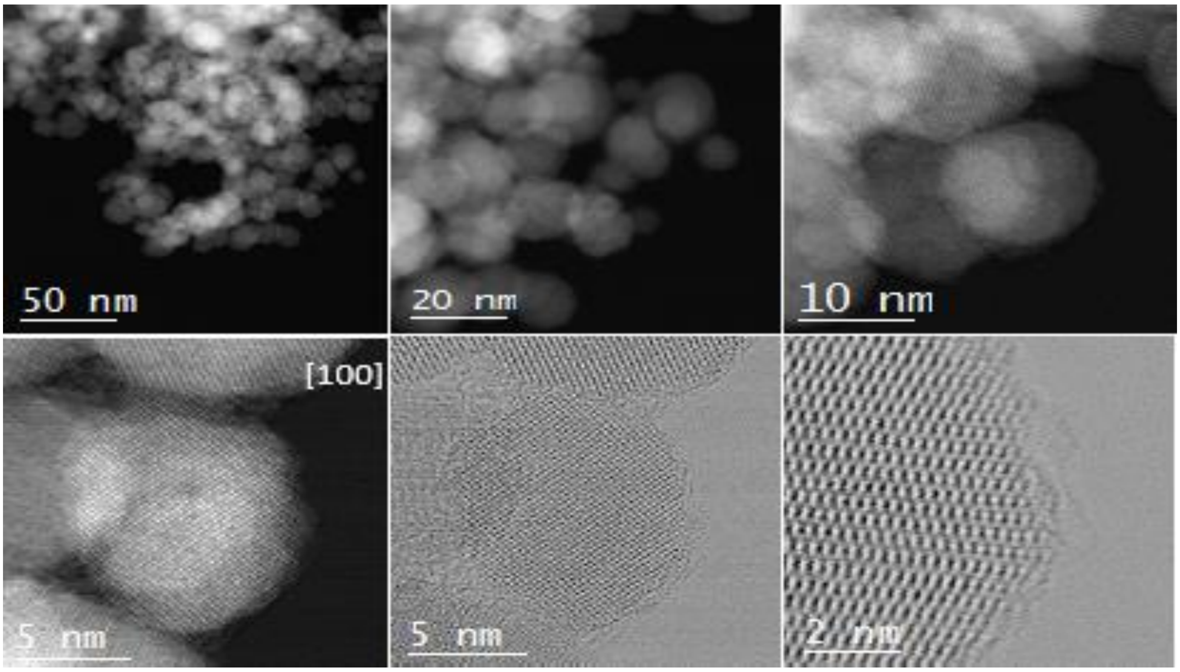

Figure 3.15:High resolution TEM images of magnetite NP synthetized by co-precipitation and coated with a fucoidan concentration of 2 mg/mL: M_1_25_F2 (acquired with JEOL cold FEG Grand ARM 300 equipment at 300 kV).

The medium size of the sample M_1_25_F2 was 11.7 nm ± 3.1, higher than the obtained for the NP without coating (10.2 nm ± 3.3). The size distribution of the sample M_1_25_F2 can be seen in the Figure 3.16.

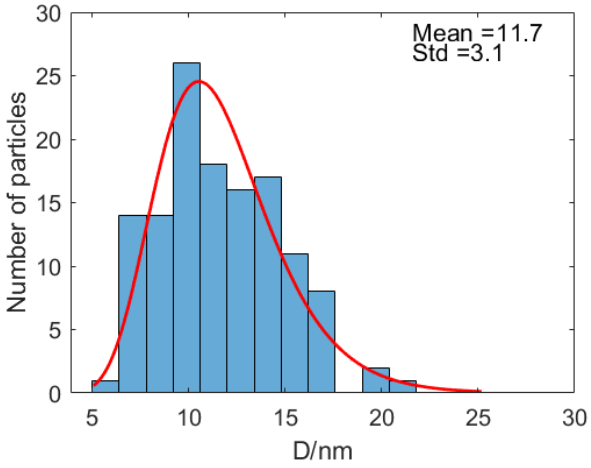

Figure 3.16: Particle size distribution of the sample M_1_25_F2.

The NP synthetized by hydrothermal synthesis and coated with a fucoidan concentration of 2 mg/mL (M_2_200_F2) can be visualized in Figures 3.17 and 3.18. It can be noted through the Figure 3.17 that in the agglomerated zones the coating is also around the group of particles as already saw in the previous TEM micrographs (Figures 3.14 and 3.15). In addition, it also can be seen that in individualize NP the coating is around the particle. In this way, the coating may be accomplishing with a higher efficiency if there was a higher NP dispersion.

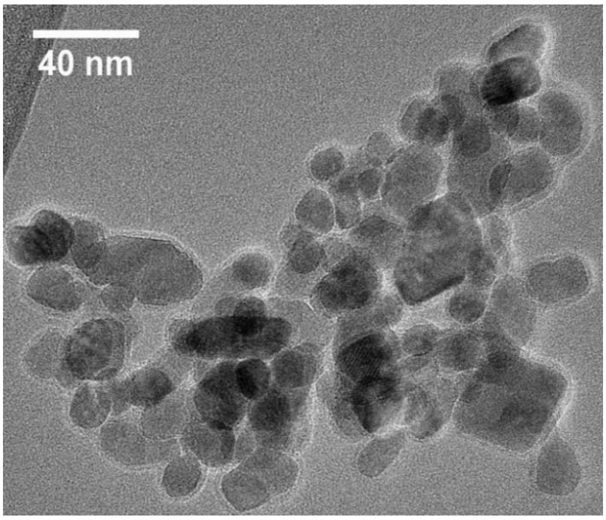

Figure 3.17: TEM images of magnetite NP synthetized by hydrothermal synthesis and coated with a fucoidan concentration of 2 mg/mL: M_2_200_F2 (acquired with JEOL 2200FS with an acceleration potential of 200 kV).

In Figure 3.18, it can be visualized the lattice fringe of the magnetite through the (111) plan. Oxygen and iron atoms represented by red and green spheres, respectively, are also represented in the bottom panel (right image).

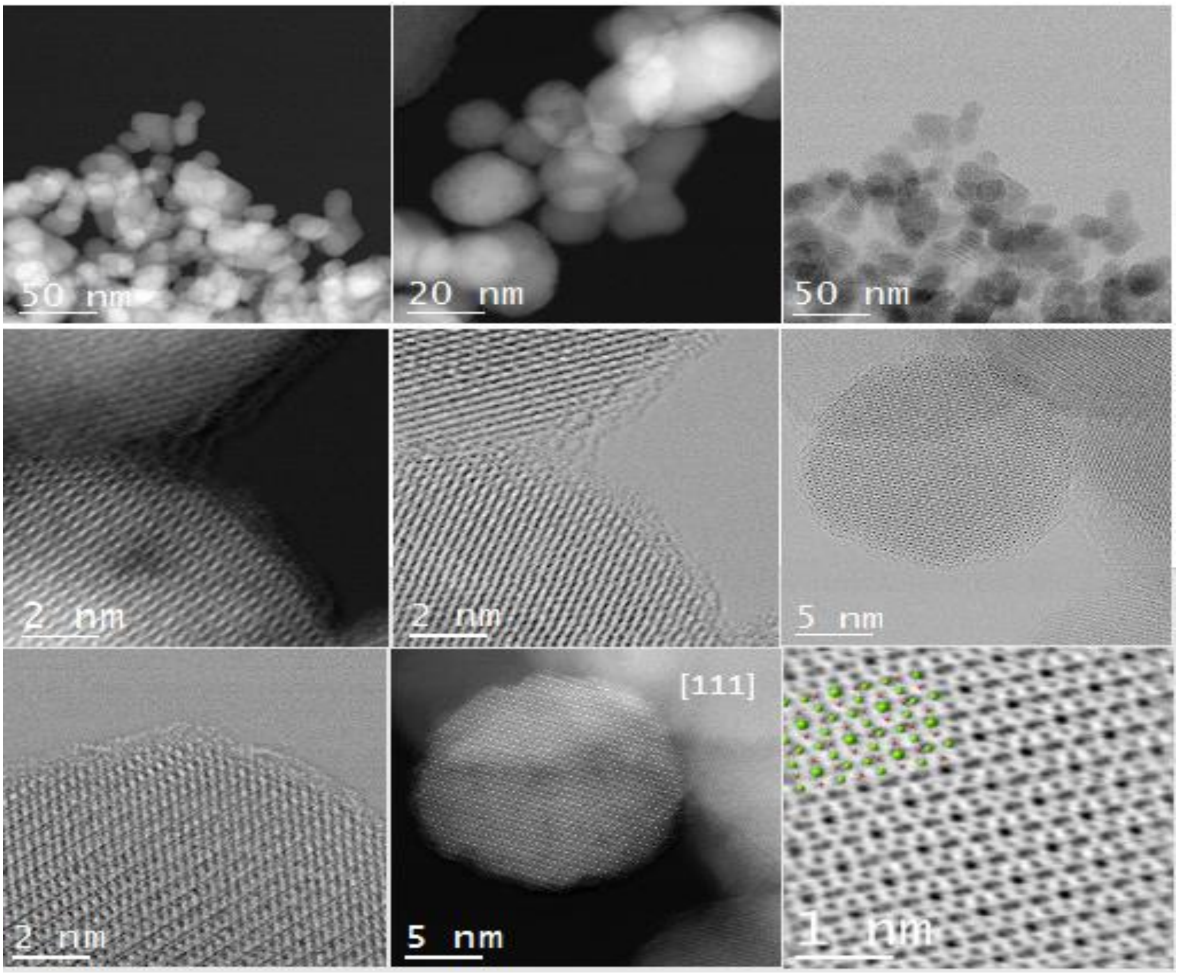

Figure 3.18: High resolution TEM images of magnetite NP synthetized by hydrothermal synthesis and coated with a fucoidan concentration of 2 mg/mL (M_2_200_F2) (acquired with JEOL cold FEG Grand ARM 300 equipment at 300 kV).

The size distribution of this sample can be seen in the Figure 3.19. The medium size of NP was 18.2 ± 5.3 nm which is higher than the NP without coating (15.8 ± 3.6 nm). This size is higher than that obtained by Silva *et al.* [18] that reported around 10 nm of size before and after coating (with a higher fucoidan concentration, 50 mg/mL) determined from the XRD pattern using the Scherrer formula.

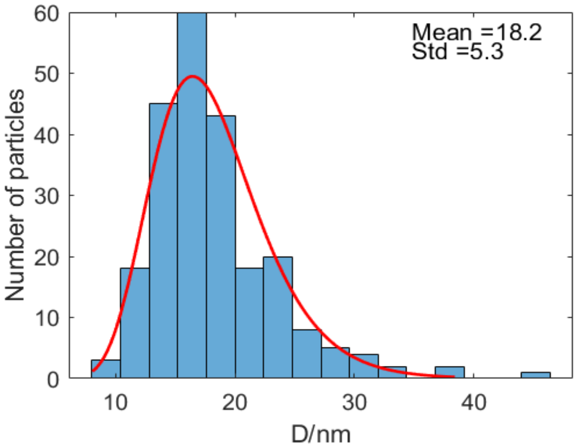

Figure 3.19: Particle size distribution of the sample M_2_200_F2.

TEM images of the sample coated with a fucoidan concentration of 6 mg/mL(M_2_200_F6) are exhibited in the Figure 3.20. When comparing with the TEM images of the sample with a fucoidan concentration of 2 mg/mL (M_2_200_F2) there is no significant changes which are in accordance with FT-IR analysis since there was no significant changes between the samples (Figure 3.10). For this sample a medium size of 19 ± 3.6 nm was obtained (Figure 3.21), which is not significantly higher than the obtained for the coating with a fucoidan concentration of 2 mg/mL (18.2 ± 5.3 nm).

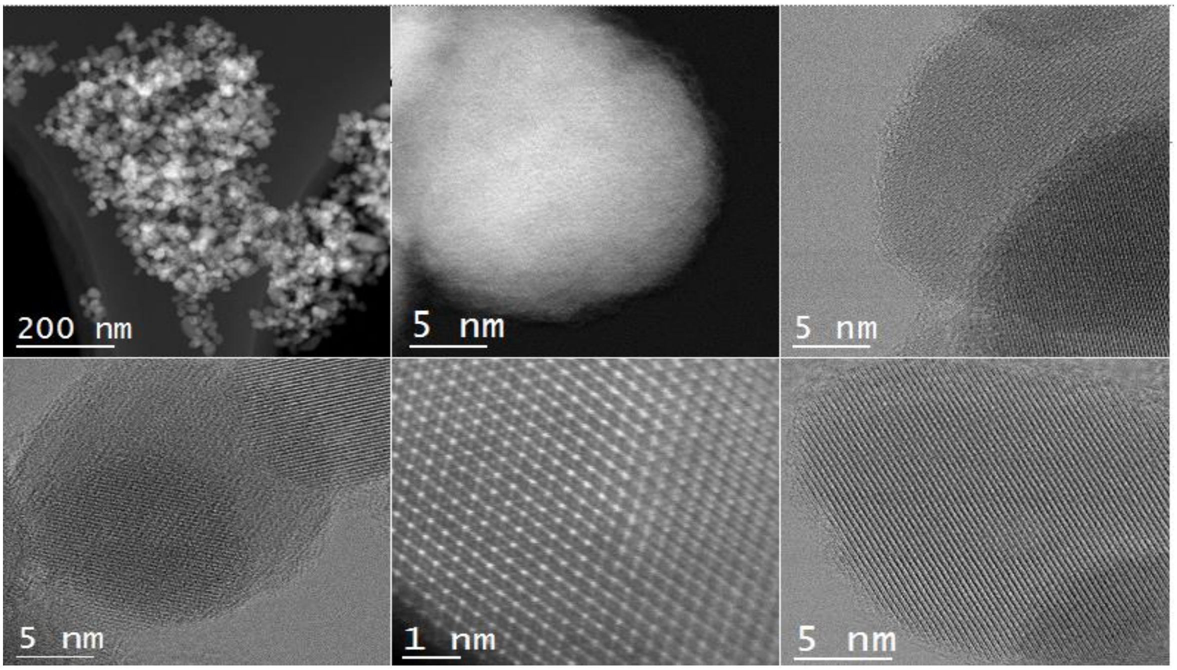

Figure 3.20: High resolution TEM images magnetite NP synthetized by hydrothermal synthesis and coated with a fucoidan concentration of 6 mg/mL (M_2_200_F6) (acquired with JEOL cold FEG Grand ARM 300 equipment at 300 kV).

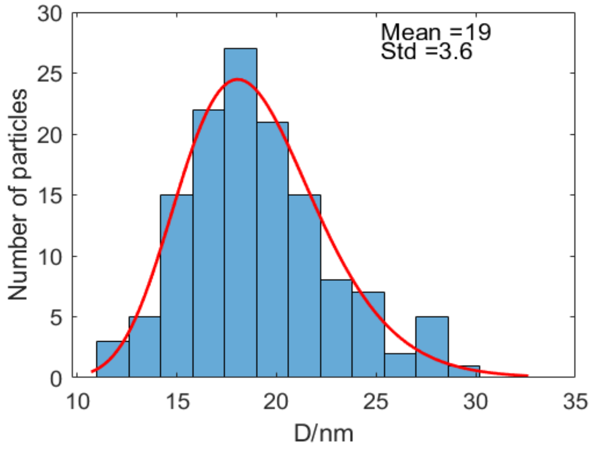

Figure 3.21: Particle size distribution obtained from the ImageJ® program [82] *for the sample M_2_200_F6.*

Table 3.3 resumes the average crystallite sizes obtained using the X-ray diffractogram; the average crystal sizes resulting from the measurement of at least 100 particles in the TEM image, and the specific surface area of all the samples. The specific surface area of the coated NP decreases with the increasing of the size (D_{TEM}) for the M_1_25_F2 sample.

For the coated sample M_2_200_F2, it was observed a similar behavior with a decrease of the A_{BET} with the increasing particle size. For the sample M_2_200_F50 there was no significant change in relation with the sample without coating (M_2_200).

Table 3.3: Average crystal sizes measured in TEM image using at least 100 particles(D_{TEM}) and standard deviation (σ) obtained from fitting Log-Normal distributions to histograms; average crystallite sizes obtained via X-ray (D_{XRD}); and specific surface area (A_{BET}) of the samples.

Sample	**D_{TEM}(nm)***	**σ (D_{TEM})**	**D_{XRD}(nm)**	**A_{BET} (m^2/g)**
M_1_25	10.2	3.3	12.6	96.3
M_1_25_F2	11.7	3.1	13.8	91.3
M_2_200	15.8	3.6	16.8	57.7
M_2_200_F2	18.2	5.3	15.8	51.6
M_2_200_F4	-[a]	-[a]	15.9	52.2
M_2_200_F6	19	3.6	18.5	54.0
M_2_200_F50	-[a]	-[a]	15.0	57.8

* Measured with ImageJ®; [a] The sample was not measured due to the level of crystallinity relatively to the other coated samples.

The isotherms of the post-synthesis coated samples have the same shape than the samples without coating. As an example, the isotherms of samples M_1_25 and M_1_25_F2 are shown in Figure 3.22. The isotherm is type II corresponding to the IUPAC classification for non-porous materials. A small hysteresis occurs due to the pores formed between nanoparticles. The samples obtained by co-precipitation are the one presenting the smallest particle size and then the one presenting the highest specific surface area. After coating a decrease on the specific surface area is observed mainly assigned to increase of the overall size of the particles (10.2 to 11.7 nm). In addition, as some particles are coated together, it may happen a decrease of the area due to the blockage of inter-particles areas. This surface area reduction due to particle agglomeration has already been reported in the literature by Mascolo *et al.* [88].

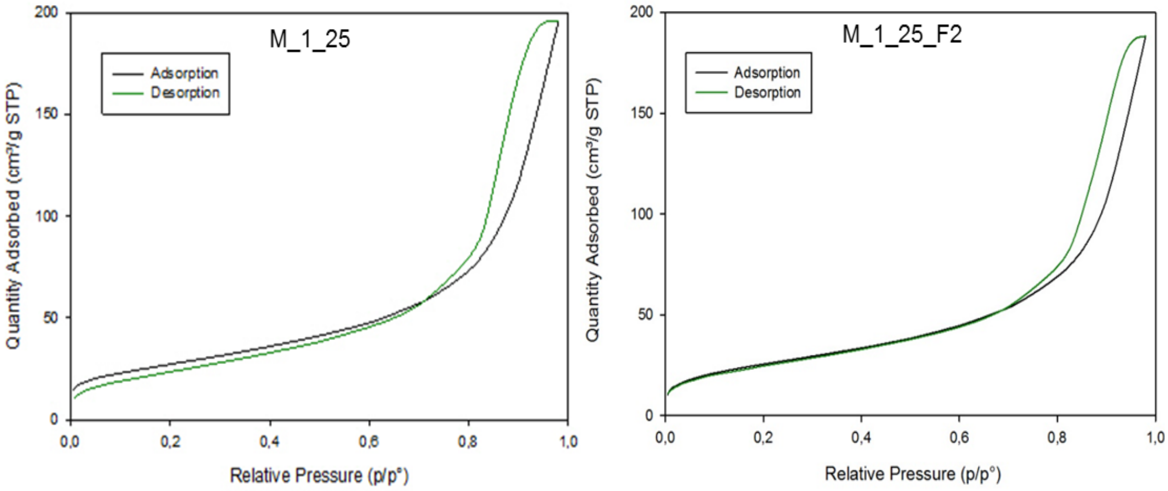

Figure 3.22: -196 °C N_2 *adsorption and desorption isotherms of the sample synthetized by co-precipitation and coated with a fucoidan concentration of 2 mg/mL: M_1_25 and M_1_25_F2 respectively.*

4.3.1.2 Colloidal stabilization

To evaluate the stability of the samples required to the MHT application and to compare the impact or influence of the coating on this stabilization, the zeta potential curves of the samples prepared by co-precipitation (M_1_25) and by hydrothermal synthesis (M_2_200) and their respective coatings (M_1_25_F2, M_2_200_F2, M_2_200_F4, M_2_200_F6 and M_2_200_F50) can be observed in Figures 3.23 and 3.24. Additionally, Table 3.4 summarize the zeta potential values obtained at pH 7.

Observing the curves of the samples M_1_25 (Figure 3.23) and M_2_200 (Figure 3.24) is verified that isoelectric point is approximately 4.4 and 4.7 respectively, which is lower than the reported for synthetic magnetite (pH 6.3). However, different values have been obtained from different authors [60]. Based on these values, synthetized NP has a positive charge at pH below 4.4 and 4.7 for the NP produced by co-precipitation and by hydrothermal synthesis respectively. In this work, the adsorption of fucoidan was carried out near pH 7 grounded on the literature [77], taking into account the isoelectric points mentioned above, this pH was not suitable to obtain the maximum chemisorption of the fucoidan. This condition does not favor the adsorption of the sulfates groups of fucoidan because of the charge repulsion. However, pH 7 is the required pH to be applied in biological environment. Regarding the coating of M_1_25 NP there was a reduction of the isoelectric point, being more stable at alkaline pH values.

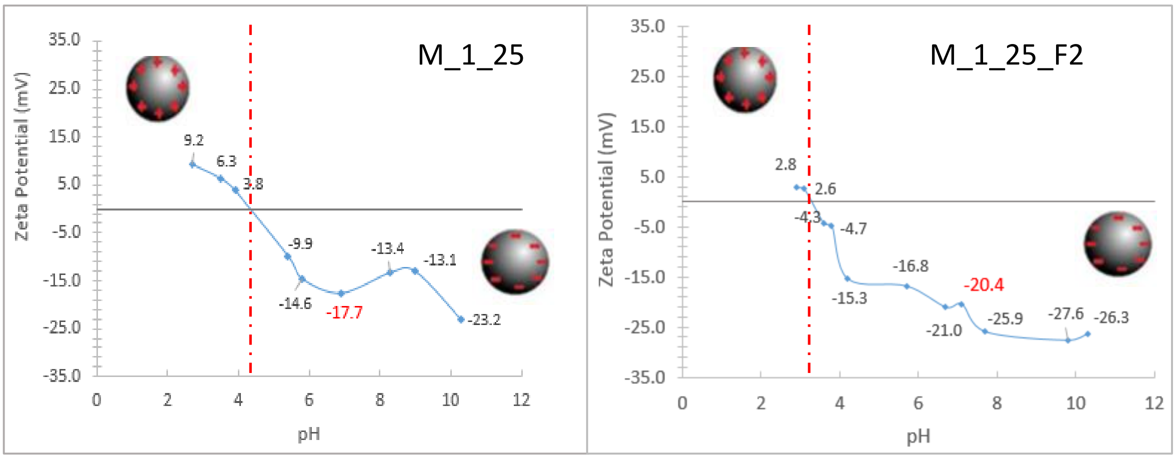

Figure 3.23: Zeta potential variation with pH value for the sample M_1_25 and their coating with fucoidan with a concentration of 2 mg/mL (M_1_25_F2).

It is reported that commercial ferrofluids are usually stable at pH values below 5 or above 8 [11]. The reduction of the isoelectric point value can be explained as a consequence of the coating with the fucoidan as already observed by Moorthy *et al.* [72]. It is noteworthy that there was an increase of zeta potential value from -17.7 to -20.4 mV with the coating, that can be also explained by the presence of fucoidan sulfate groups on the NP surface, since fucoidan is an anionic (negative charge) [61] sulfated polysaccharide. Though, these values are lower than the desired (above ± 25 mV) [58]. Additionally, negative zeta potential values are in accordance with other reports for NP coated with fucoidan [73, 90, 91]. For example, Amorim *et al.* [90] coated silver NP with fucoidan, obtaining a negative value of -18 mV for NP with a size of 210 nm.

Relatively to the coating of the sample M_2_200, there is also a reduction of the isoelectric point (from 4.7 to 3.4) when the NP were coated with a concentration of 2 mg/mL (M_2_200_F2). Therefore, the increase of fucoidan concentration lead to NP with negative superficial charge

(M_2_200_F4, M_2_200_F6 and M_2_200_F50, Figure 3.24). Once more, there was a slight increase of zeta potential with the increase of fucoidan concentration that can be explained by the presence of sulfate groups from fucoidan. The NP coated with a fucoidan concentration of 50 mg/mL (M_2_200_F50) showed a higher zeta potential value (-26.2 mV) than the other samples which are in accordance with the literature since the coating had a stabilization effect [15]. The sample coated with a fucoidan concentration of 6 mg/mL (M_2_200_F6) also had a value higher than 25 mV (-26.1 mV). Furthermore, in general the obtained zeta potential values are very consistent among samples, which it is also in accordance with the FT-IR (Figure 3.10) since there was no substantial differences between them.

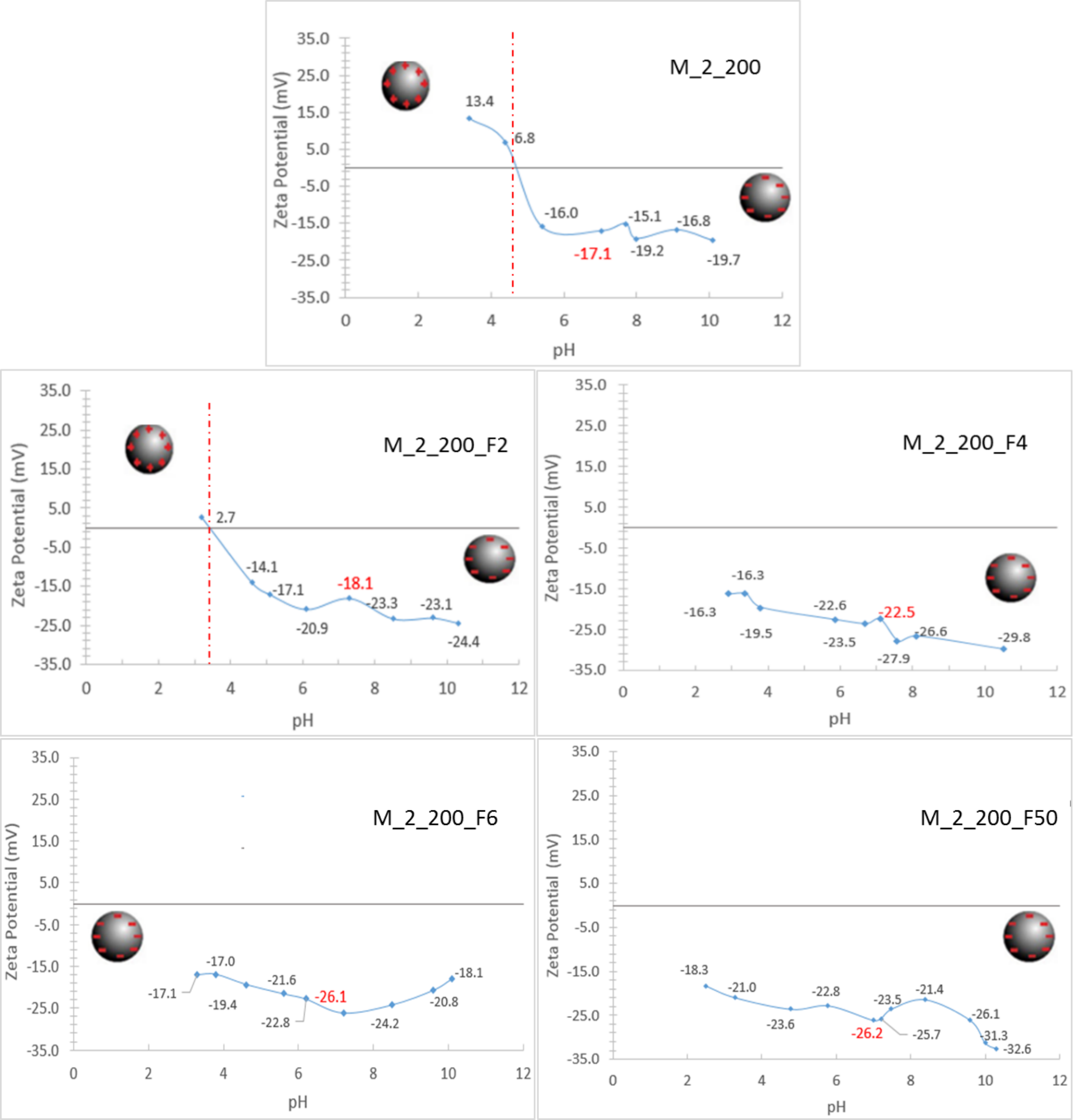

Figure 3.24: Zeta potential variation with pH value for the sample M_2_200 and their respective coatings at different fucoidan concentrations (2,4,6 and 50 mg/mL, samples M_2_200_F2, M_2_200_F4, M_2_200_F6 and M_2_200_F50 respectively).

Table 3.4: Zeta potential results of the pristine samples prepared by co-precipitation and by hydrothermal treatment, and post-synthesis coated samples with different fucoidan concentrations.

		Samples	Fucoidan concentration (mg/mL)	Zeta potential (mV)
Co-precipitation	Pristine	M_1_25	-	-17.7
	Coated	M_1_25_F2	2	-20.4
Hydrothermal synthesis	pristine	M_2_200	-	-17.1
	coated	M_2_200_F2	2	-18.1
		M_2_200_F4	4	-22.5
		M_2_200_F6	6	**-26.1**
		M_2_200_F50	50	**-26.2**

3.3.2 Simultaneous synthesis with fucoidan

3.3.2.1 Functionalization of magnetite NP with Fucoidan

The diffractogram relative to the samples obtained with synthesis and coating in one step ("*in situ*") with a fucoidan concentration of 2 mg/mL at room temperature (MF2_25) and at 50 °C are exhibited in the Figure 3.25.

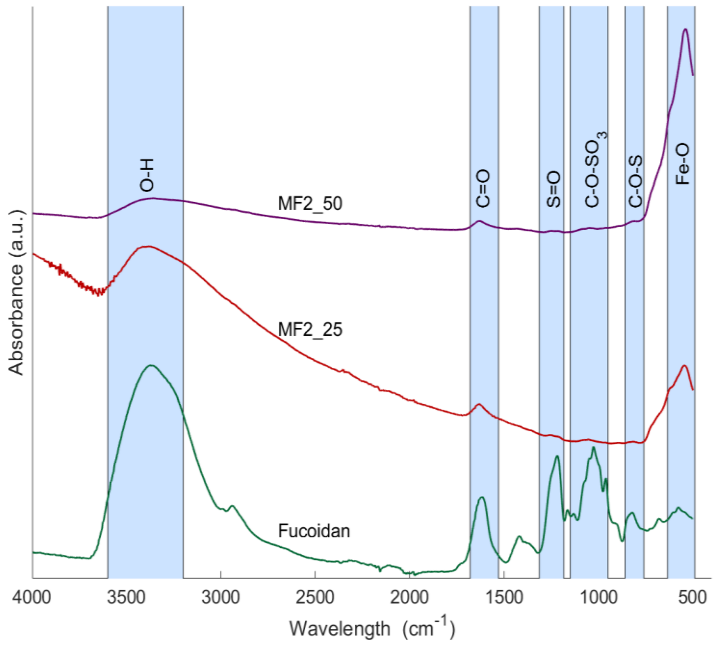

Figure 3.25: Normalized FT-IR spectra of the magnetite NP coated in situ at room temperature (MF2_25) and at 50 °C (MF2_50) with a fucoidan concentration of 2mg/mL are presented. Spectrum of fucoidan is also exhibited.

In the FT-IR spectra, the peak referent to the Fe-O are observed. When comparing the effect of a reaction temperature on NP functionalization, it is not perceptible differences between the samples, although in the both spectra it is observed the peak relative to O-H group and C=O group which may be due to the contribution of the fucoidan groups. The others peaks associated to fucoidan are not easly observed, which is may be a result of an insufficient fucoidan concentration. Thus, it will be necessary a further evaluation, or use a higher fucoidan concentration in order to conclude if the reaction temperature had an effect on NP functionalization with fucoidan.

Comparing the FT-IR spectra of the samples, with the higher reaction temperature and with different fucoidan concentrations, is noted that with the increase of fucoidan concentration the peaks referred to the fucoidan functional groups that were little expressive in the case of a fucoidan concentration of 2 mg/mL (MF2_50) are more intense with a higher content of fucoidan (Figure 3.26). Thus, the spectrum corresponding to the *in situ* coating with a concentration of 6 mg/mL (MF6_50) showed a greater expression of the peaks related to fucoidan (Figure 3.26).

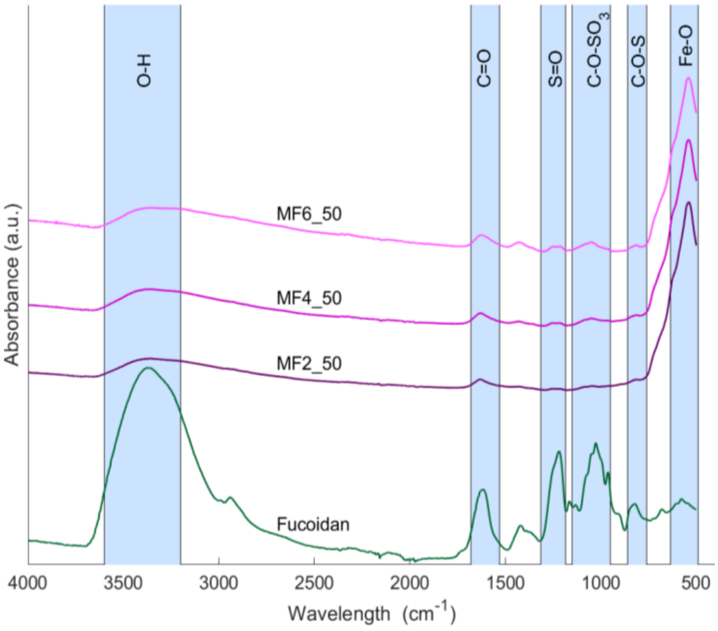

Figure 3.26: Normalized FT-IR spectra of the magnetite NP coated in situ with a reaction temperature and with different fucoidan concentrations: 2, 4 and 6 mg/mL, samples MF2_50, MF4_50 and MF6_50 respectively. Spectrum of fucoidan is also exhibited.

3.3.2.2 Phase purity and crystallinity

All the syntheses of the NP coated *in situ* presented the characteristic peaks respective to the inverse cubic spinel phase of Fe_3O_4, as can be seen in Figures 3.27 and 3.28.

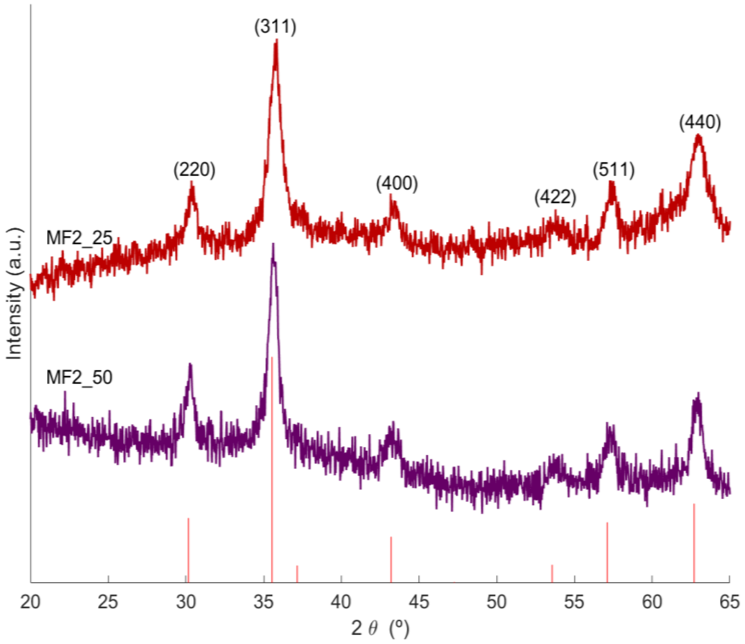

Figure 3.27: Normalized XRD diffractograms of the NP coated in situ without and with a reaction temperature (50 °C) and with a fucoidan concentration of 2 mg/mL: MF2_25 and MF2_50 respectively. The red lines represent the peaks of the magnetite phase card no. 04-002-3668.

The sample MF2_25 presents a greater level of noise ratio diffractogram on the diffractogram than MF2_50, which can be associated to a lower degree of crystallinity or to the existence of smaller particles. Indeed, Mahdavi *et al.* [76] study the effect of the reaction temperature on particle size, and through XRD they reported an increase of NP size from 8.3 nm to 13.2 nm when the temperature increased from 45 to 85 °C, due to the easier growth of the magnetite nucleus when the temperature is higher than 45 °C. On another study, Khan *et al*. [59] showed that an increase on NP size only happens when the reaction temperature is higher than 50 °C.

For the samples synthetized with a higher temperature reaction (Figure 3.28) it can be noted that with the increase of fucoidan concentration to 4 or 6 mg/mL there was a slight decrease of the peaks intensity. This may be associated with the fact that with a higher fucoidan concentration, and since the synthesis and coating is accomplished in just one step, fucoidan interfere in the NP nucleation and growth [11, 49] which in turn gives rise to small particles. This reduction effect was also observed by Lee *et al.* [49] where they syntetized Fe_3O_4 particles in one step-synthesis, trough a precipitation reaction and using poly (vinyl alcohol) (PVA) as the coating agent. Daniel *et al*. [92], using an *in situ* chemical co-precipitation synthesis at 60 °C produced carrageenan-coated magnetite NP, and also observed a reduction in NP size with the increasing of carrageenan concentration.

Therefore, as the fucoidan concentration increase in the medium, it may be adsorbed on the nuclei or may enhance viscosity, decreasing the mobility of species, and inhibiting the growth of the NP, with consequent lower of peaks intensity on the diffractogram.

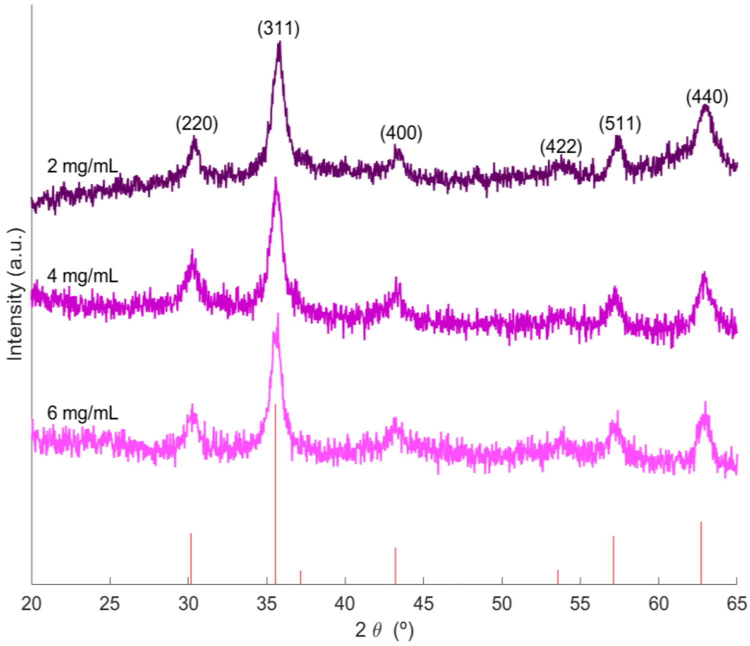

Figure 3.28: Normalized XRD diffractograms of the NP coatings in situ at different fucoidan concentrations (2, 4 and 6 mg/mL) and with a reaction temperature of 50 ºC: MF2_50, MF4_50 and MF6_50 respectively.

3.3.2.3 Morphology, size and size distribution

Relatively to the *in situ* synthesis and coating of NP at room temperature and with a fucoidan concentration of 2 mg/mL (MF2_25), the shape of the obtained NP is more irregular (Figure 3.29) and seems to be more agglomerated than the NP obtained without *in situ* coating. Relatively to the coating, it can be seen that is also more around the group of particles (clusters) than individual particles.

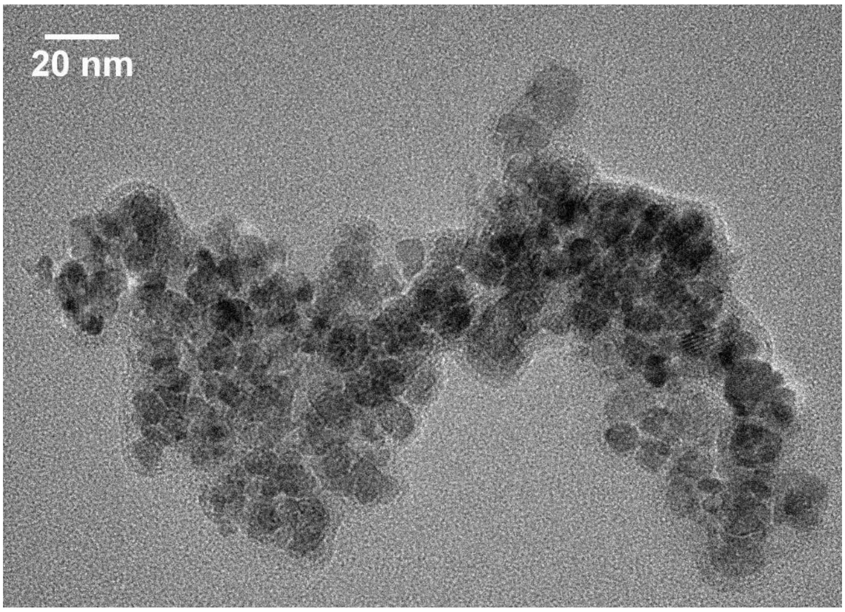

Figure 3.29: TEM images from the magnetite NP coated in situ at room temperature and with an fucoidan concentration of 2 mg/mL (MF2_25) (acquired with JEOL 2200FS with an acceleration potential of 200 kV).

In terms of size, MF2_25 NP are smaller than the other samples already analyzed (M_1_25, M_2_200 and their respective coatings) with a medium size of 6.4 ± 1.6 nm (Figure 3.30), which makes them more unstable due to their high surface-to-volume ratio, justifying a greater agglomeration.

It can be verified that the NP have a much lower polydispersion than the samples obtained with the synthesis and post- synthesis coating, since they are smaller [35].

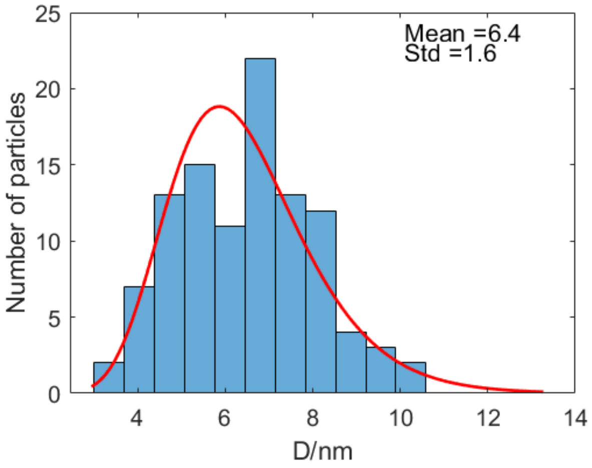

Figure 3.30: Particle size distribution of the sample MF2_25.

TEM micrographs of the samples produced with a higher reaction temperature (50 ºC) and with a fucoidan concentration of 2 mg/mL (MF2_50) and 6 mg/mL (MF6_50) are exhibited in the Figure 3.31 and 3.32, respectively. In general, both samples showed a shape not totally spherical and a smaller size and exhibit a greater agglomeration than those obtained through co-precipitation and hydrothermal synthesis and post-synthesis coating. However, the sample MF6_50 (Figure 3.32) presented a lower agglomeration than the two previous samples, which may be associated with a greater functionalization with fucoidan already showed in FT-IR analysis (Figure 3.26). Regarding the NP sizes, due to the agglomeration state it was not possible to carry out a reliable statistical size distribution through ImageJ® program, and therefore the sizes and the histograms of particle distribution for those samples could not be presented

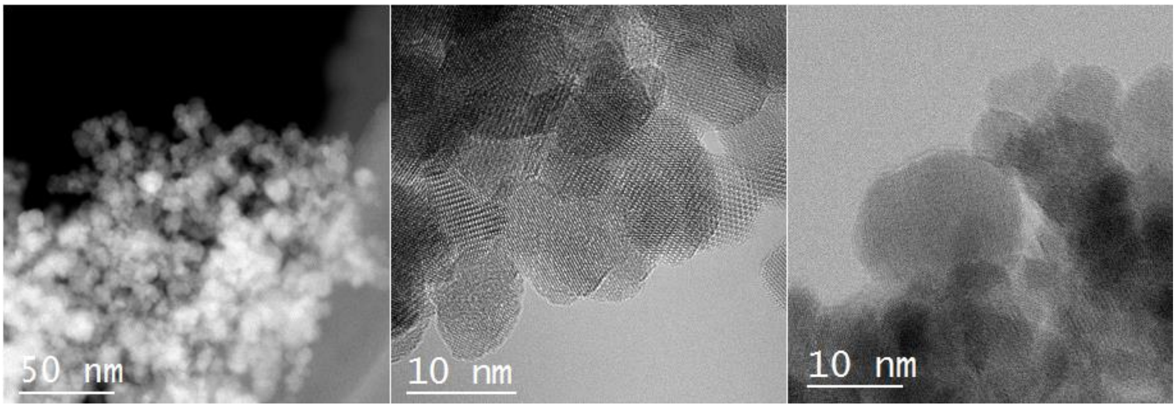

Figure 3.31: High resolution TEM images of sample with in situ coating, with a reaction temperature and with a fucoidan concentration of 2 mg/mL(MF2_50) (acquired with JEOL cold FEG Grand ARM 300 equipment at 300 kV).

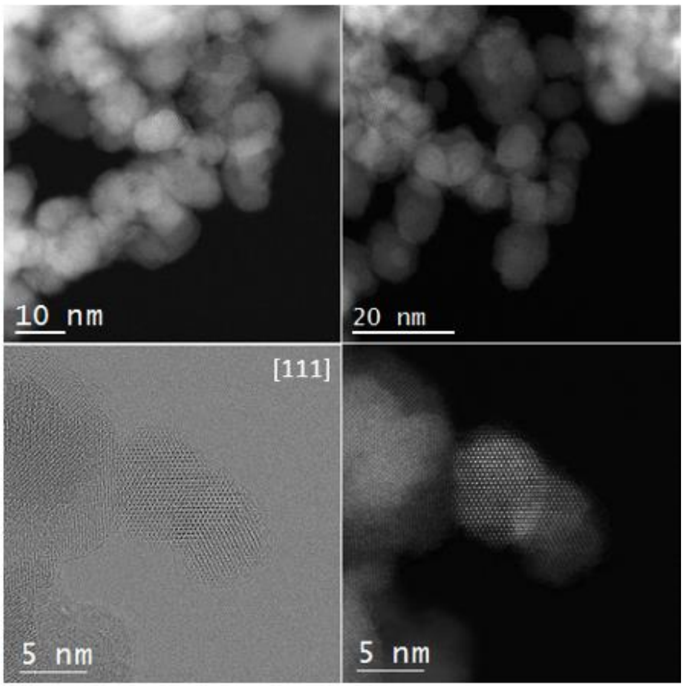

Figure 3.32: High resolution TEM images sample with in situ coating, with a reaction temperature and with a fucoidan concentration of 6 mg/mL (MF6_50) (acquired with JEOL cold FEG Grand ARM 300 equipment at 300 kV).

The BET analysis of the NP obtained by *in situ* method exhibit also type II isotherms (Figure 3.33).

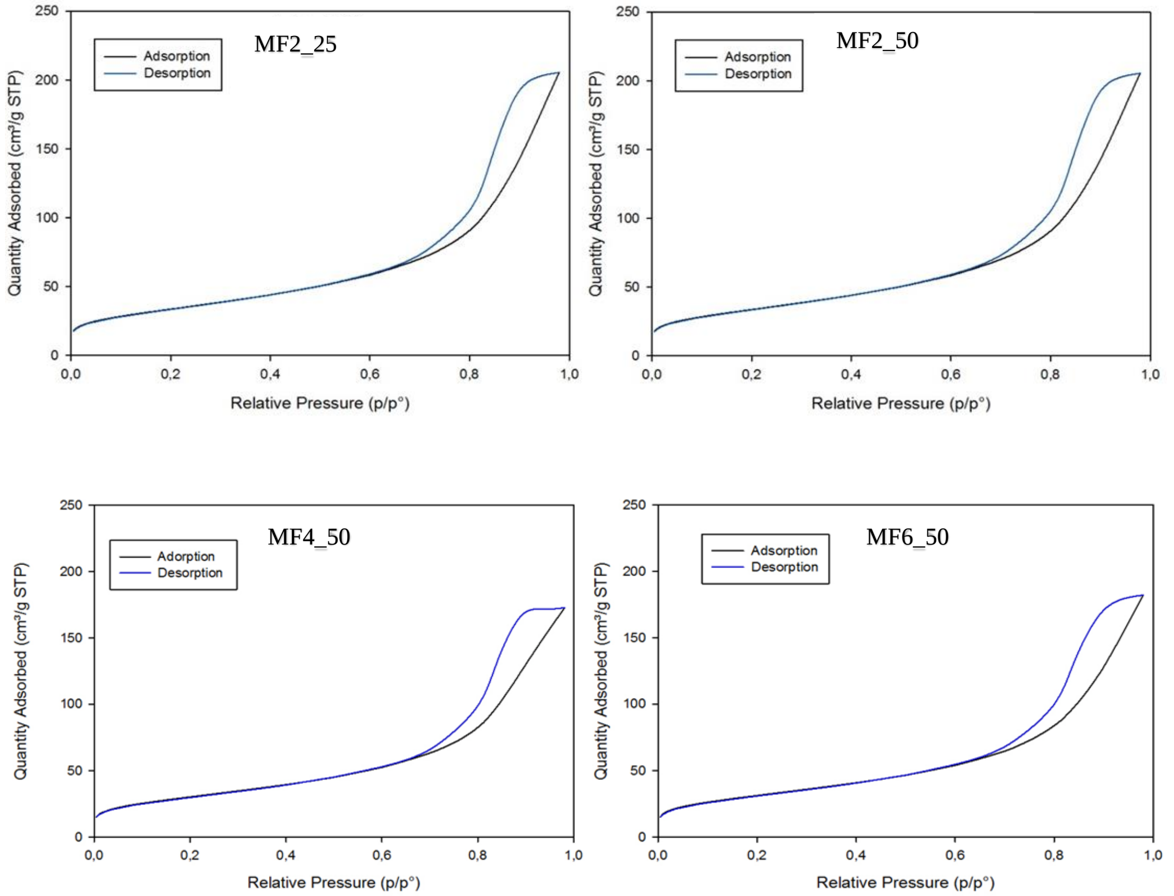

Figure 3.33: -196 °C N_2 adsorption and desorption isotherms for samples MF2_25, MF2_50, MF4_50 and MF6_50.

As a resume, the mean particle size of the different samples coated *in situ* and obtained from different techniques can be seen in the Table 3.5. In terms of specific surface area NP produced by the *in situ* method have a larger area considering that they have a much smaller size than those obtained with the other method. In addition, there is no significant differences on size and surface area between the samples.

Table 3.5: $\langle D_{TEM} \rangle$ Mean particle size determined from TEM data ;$\langle D_{XRD} \rangle$: mean particle size determined from the XRD data; $\langle D_{BET} \rangle$: Specific Surface area obtained from BET analysis.

Label	D_{TEM}(nm)*	σ (D_{TEM})	D_{XRD}(nm)	A_{BET} (m^2/g)
MF2_25	6.4	1.6	11.0	111.8
MF2_50	-	-	10.2	119.2
MF4_50	-	-	10.3	107.2
MF6_50	-	-	11.2	110.9

* Measured with ImageJ®; It was only possible to measure the mean particle size for the sample MF2_25 though the ImageJ® program. The other samples showed a higher agglomeration.

3.3.2.4 Colloidal stabilization

In Figure 3.34 are exhibited the zeta potential curves of the *in situ* samples MF2_25, MF2_50, MF4_50, and MF6_50. Comparing the sample MF2_50 and MF2_25, both coated with 2 mg/mL of fucoidan, the isoelectric point was 6.5 and 5.9 respectively, but in terms of zeta potential value they were similar. This are in accordance with the FT-IR analysis (Figure 3.25) which showed no expressive differences in the fucoidan groups between these samples. The increase of fucoidan concentration to 4 mg/mL (MF4_50), originate the decrease of isoelectric point from 6.5 to 3.5, confirming a high functionalization. In the case of the 6 mg/mL concentration of fucoidan (MF6_50) the surface of magnetite NP coated with fucoidan showed a negative charge. The same trend was observed in terms of the zeta potential value and the increase of fucoidan concentration. As the fucoidan content increases, the zeta potential value also increases.

In addition, according to the values obtained for the sample MF6_50, it was confirmed to be more efficiently coated (confirmed by FT-IR, Figure 3.26), presenting a higher zeta potential value than the other samples synthesized by this method, which resulted in a smaller agglomeration visualized in TEM (Figure 3.32).

In general, the zeta potential values obtained by this method are lower than those obtained with the previous method (coated post-synthesis) which may be due to their high surface-to-volume ratio and the tendency to reduce free surface energy. These results confirm the existence of a greater agglomeration of the NP that had occurred and already observed through the TEM images. Table 3.6 summarize the zeta potential values obtained for the pH at 7.

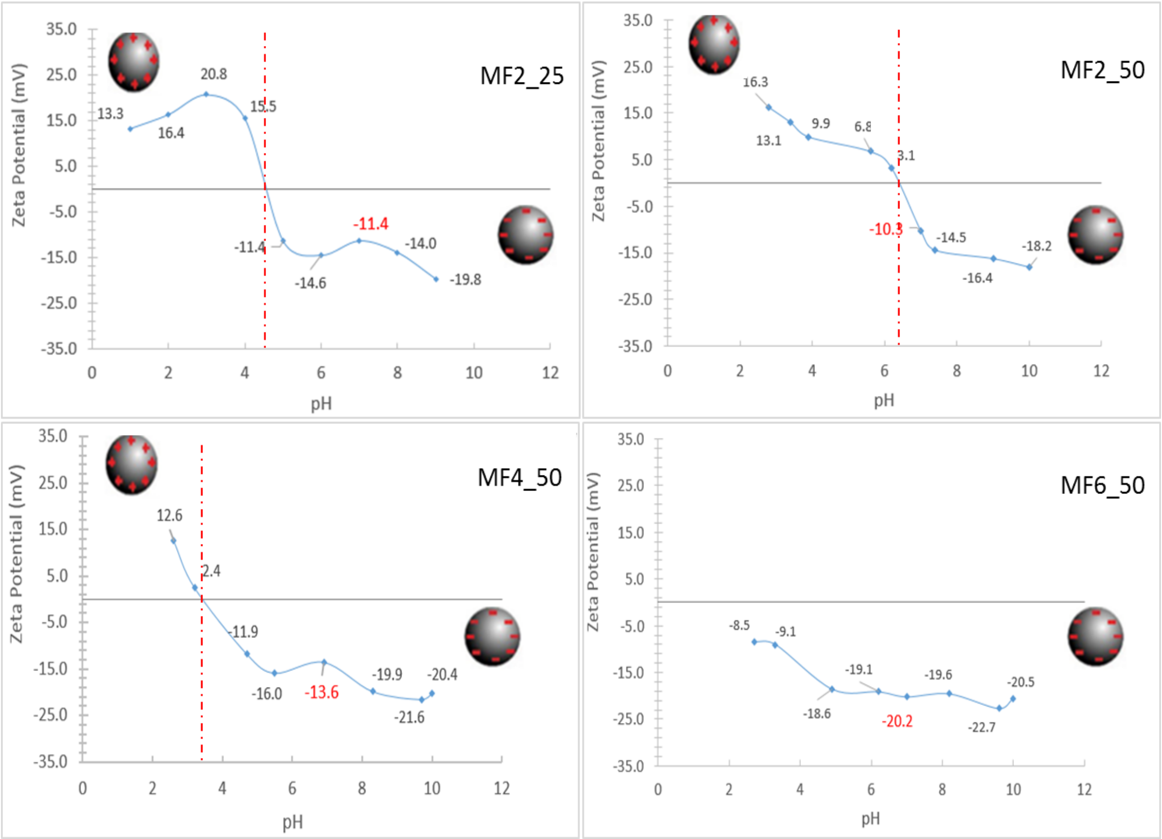

Figure 3.34: Variation of Zeta potential with pH value for the magnetite NP coated in situ at different fucoidan concentrations: MF2_25, MF2_50, MF4_50 and MF6_50.

Table 3.6:Zeta potential results for the samples coated in situ: MF2_25, MF2_50, MF4_50 and MF6_50.

Temperature (°C)	Samples	Fucoidan concentration (mg/mL)	Zeta potential (mV)
25	MF2_25	2	-11.4
50	MF2_50	2	-10.3
	MF4_50	4	-13.6
	MF6_50	6	-20.6

3.3.3 Thermal efficiency of the NP

To assess the NP potential for MHT, the heating efficiency was determined. In Table 3.7 are summarized the SAR values obtained for the different samples with and without coating, at different concentrations of fucoidan coating and obtained by the two methods of synthesis/coating. In the same Table are pointed out some ILP reported values and founded on literature with similar NP sizes. The SAR measurements were carried out for a magnetic field amplitude of 14.7 kA/m and with a frequency of 276 KHz. These values meet the Brezovich limit and, for instance, commercial clinical applications systems (MagForce Nanotechnologies) apply a frequency of 100 kHz and amplitudes up to 15 kA/m (NanoActivator F100) [1] or up to 18 kA/m (MFH® 300F) [25]. To compare the obtained results with the ones reported in the literature, performed at different experimental conditions of amplitude (H) and frequency (*f*) of the magnetic field, the corresponding intrinsic loss power (ILP) values were calculated using Eq. 13 [1, 93] and are also included on Table 3.7:

$$ILP = \frac{SAR}{H^2 \times f} \text{ [Equation 13]}$$

According to the literature, ILP values between 2 and 4 nHm^2/kg have been proposed as suitable for MHT and even lower values close to 1.6 nHm^2/kg have been considered acceptable and sufficient to be thermally efficient [94].

Table 3.7: Hyperthermia values obtained for all the samples.

Samples		Medium size (D_{TEM})(nm)	SAR (W/g)	ILP (nHm^2/kg)
Pristine	M_1_25	10.2	30	0.5
	M_2_200	15.8	15	0.2
Post-synthesis coated	M_1_25_F2	11.7	156	**2.6**
	M_2_200_F2	18.2	0	0
	M_2_200_F4	n.m.	n.m.	n.m.
	M_2_200_F6	n.m.	20	0.3
	M_2_200_F50	n.m.	15	0.2
In situ coating	MF2_25	6.4	100	**1.7**
	MF2_50		31	0.5
	MF4_50	n.m.	n.m.	n.m.
	MF6_50	n.m	62	1

Literature report

Synthesis method	SPION	Medium size (nm)	SAR (W/g)	ILP (nHm^2/kg)	Author/ group
Co-precipitation	Magnetite	10-12	25	0.2	Bahadur *et al.*[96]
	Magnetite	20	38.5	0.2	Ghosh *et al.* [97]
	Magnetite coated with PEG	10	28.3	0.1	Ghosh *et al.* [97]
Thermal decomposition	Magnetite	10.2	63	2.3	Alves *et al.* [58]

n.m.: Data not measured; D_{TEM} was not measured through ImageJ® program since those sample showed a higher agglomeration. In the case of Hyperthermia, a selection was made, and the samples with a fucoidan concentration of 4 mg/mL was excluded since it was not expected a higher difference when compared with the samples with less and higher fucoidan concentration.

In the case of the sample with hydrothermal treatment and coated with the fucoidan concentration of 2 mg/mL (M_2_200_F2) the NP deposited in a few minutes, inhibiting the accurate determination of the SAR value. For the samples prepared in the same way, by co-precipitation at room temperature (M_1_25) or with hydrothermal treatment (M_2_200), SAR values of 29.50 and 14.57 W/g, respectively, were obtained, indicating that the hydrothermal treatment decrease the NP heating efficiency. This was unexpected since the NP of the sample with hydrothermal treatment were larger when compared with the sample without treatment, as confirmed by TEM and XRD analysis, parameter that frequently are associated with an increase of SAR. As mentioned in the subchapter 1.4.2.1 the increase of NP size lead to an increase of the saturation magnetization (Ms) value [50], which in turn increase the SAR value according to Equation 7 (subchapter 1.3.2). The obtained result is explained by polydispersity, since the treated sample was more polydisperse. According to the literature, in general, a polydisperse sample will lead to a decrease in maximum SAR owing to the reduction in the proportion of NP that contribute to the total heat, whereas monodispersed samples enhance SAR value (subchapter 1.4.2 Parameters affecting heat efficiency) [41]. Gonzales-Weimuller *et al.* [95] study the size and distributions size effect on NP thermal efficiency and they showed a decrease in the SAR value for the samples with higher polydispersibility. In addition, they also predicted a decrease of SAR value around 50% when the polydispersity of the sample increased from 0 to 15 %.

In the Literature report (Table 3.7), it is visible that Alves *et al.* [58] through thermal decomposition, synthetize magnetite NP with a medium size of 10.2 nm and obtained a ILP of 2.3 nHm^2/kg which is higher than the obtained with the sample M_2_200 with a higher medium size (15.8 nm). This synthesis method is reported to produce NP with narrow distributions size which may justify this difference [11]. However, thermal decomposition uses relatively high temperatures [11], uses organic solvent and other toxic reagents [1], and the synthesis is more complex than co-precipitation method [11].

Regarding the coating of sample M_2_200 with 6 and 50 mg/mL we were conditioned by the polydispersion exhibited by this sample, thus we did not obtain much difference when compared with the pristine sample. Ghosh *et al.* [97] also obtained a SAR of 38.45 W g^{-1} (ILP = 0.2 nHm^2/kg) for pristine magnetite NP synthetized by co-precipitation with similar size (20 nm), which was lower than the obtained in M_2_200_F6 sample and equal to sample M_2_200_F50. Concerning the coating, for the case of the sample synthetized by co-precipitation at room temperature and coated with a concentration of 2 mg/mL (sample M_1_25_F2, mean size of 11.7 nm), the highest SAR value was obtained (155.72 W/g) corresponding to an ILP value of 2.6 nHm^2/kg. This value is higher than the values reported as sufficient to be thermal effective [94], which is very promising. This value is higher than the one obtained in a previous work by Bahadur *et al.* [96], in which they used also the co-precipitation method to synthetized magnetite NP and the result NP had similar sizes of 10-12 nm, (through TEM micrograph) and ILP of 0.22 nHm^2/kg was obtained. Ghosh *et al.* [97] also through co-precipitation method, obtained for magnetite NP post-synthesis coated with PEG and with a medium size of 10 nm an ILP value of 0.1 nHm^2/kg, which is much lower than the value resulted from M_1_25_ F2.

Regarding the *in situ* coated samples, higher SAR values were generally obtained when compared to post-synthesized NP coating. This result can be explained by the lower polydispersion of these samples relative to the post-synthesized coating samples. Thus, it seems that the influence of distribution size had a higher impact on SAR than the NP size, since that NP obtained by this method were much smaller. The sample with lower reaction temperature and with a fucoidan concentration of 2 mg/mL (MF2_25), exhibited a SAR value of 100.26 W/g (ILP= 1.7 nHm^2/kg), which was higher than the value attained by the other samples, even though they were produced with higher reaction temperature (50 °C) which leaded to NP size increasing. Moreover, this value is higher than the minimum limit to be thermally efficient [94]. According to ILP values reported in the literature and comparing with NP with higher sizes, we attained a ILP value with potential to MHT even with a small NP size which means that if we increase the size of NP without increasing the polydispersion higher ILP values are expected.

In order to compare the response of the samples with higher ILP values (M_1_25_F2 and MF2_25), the temperature variation as a function of time can be seen in the Figure 3.35.

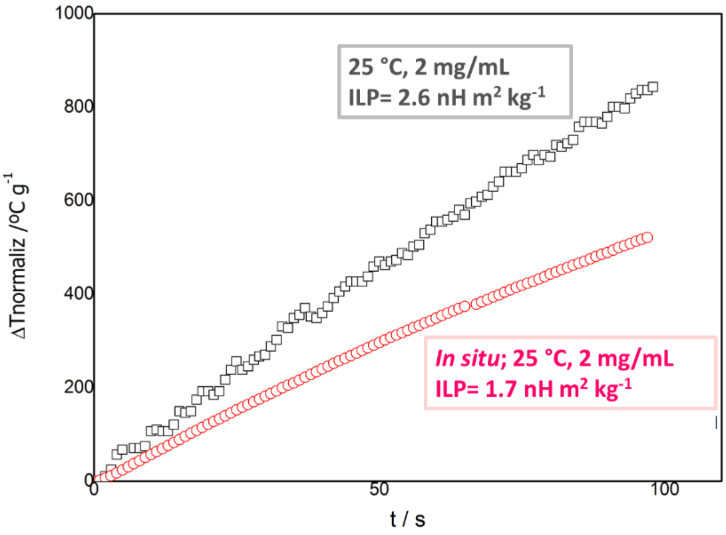

Figure 3.35: Hyperthermia comparison between the samples that obtained higher ILP values (M_1_25_F2 black squares, and MF2_25 – red circles).

As can be verified, the sample M_1_25_F2 shows the highest and the fastest temperature variation with time, showing a higher thermal efficiency expressed by a higher ILP value.

Furthermore, it is reported in the literature that there is a decrease in the Ms value for sizes below 10 nm [29]. The reduction of the particle size enhances the curvature of the surface, which gives rise to a disordered orientation of the crystal in its surface and consequently leads to a reduction of the Ms value [29]. Thus, it is preferable to produce NP with size over 10 nm to avoid this reduction. On the other hand, as described in subchapter 1.3.2, the reduction of the Ms value has a negative impact on the thermal efficiency of NP [41]. Taking this into account, an increase on NP size would favour a high ILP value and thus, syntheses parametes such as salts concentration may be optimize in order to produce higher NP [35]. Nevertheless, a balance must be found in order to avoid a higher polydispersion. For instance, in the study performed by Alves *et al.* [58] the lowest SAR values were obtained for the sample with smallest size (ILP =2.3 nHm^2/kg). Furthermore, Madhavi *et al.* [76] reported higher values of Ms and was reported an increase from 58.60 to 78 $emu.g^{-1}$ with the increase of NP sizes from 7.8 to 9.4 nm.

According to the literature, the application of coatings *in situ* are more complex, but provide greater stabilization and better magnetic properties [13]. However, in this work the NP coated *in situ* presented greater agglomeration and showed lower colloidal stability, with lower zeta potential value. The increase in the SAR value cannot be directly associated with the coating method.

In general, a reduction on SAR value with the fucoidan coating was expected when compared with the bare NP since is a non-magnetic coating and according to the literature this coating would lead to a Ms decrease [3]. However, in this work an increase in the SAR value was observed with the fucoidan coating and we attained ILP values suitable for MHT in both synthesis methods for the samples coated with fucoidan. This can only be explained on light of the better solution dispersion of the NP due to the coating as observed thought Zeta Potential measurements.

Chapter 4 Conclusions and future work

The use of hydrothermal treatment on NP synthesis allowed to increase in NP size. However, the thermal efficiency decreased with the hydrothermal treatment, which should be associated with the fact that these samples had a higher polydispersity than the sample without treatment. The NP without the hydrothermal treatment post-synthesis coated with fucoidan (2 mg/mL) revealed a greater thermal efficiency, colloidal stability, and a suitable size, allowing their use for MHT.

When the NP are synthetized and coated simultaneously (*in situ* preparation) a slight increase on the NP functionalization was observed with the increase of fucoidan concentration. However, these NP presented a higher agglomeration, which may be associated with their larger surface area when compared to the post-synthesis coated samples, reducing the free surface area. The thermal efficiency is higher for NP synthetized with lower temperature, as their size is lower.

The coating with fucoidan contribute to a better colloidal stability, as well as avoids the NP aggregation. Independently of the coating methodology the lowest concentration of fucoidan (2 mg/mL) is the one that leads to the highest thermal efficiency and, consequently, the most promising for MHT. The post-synthesis coated NP showed a 50% higher thermal efficiency comparing to the *in situ* (SAR 100 W/g), which allow to tailor the NP preparation according to the type of MHT treatment required for different cancer.

Both coating methodologies with a fucoidan content of 2 mg/mL allowed to achieve SAR values in general higher than the ones reported in the literature for other magnetite NP non-coated or coated with other polymers. In addition, fucoidan has the advantage of having antitumoral activity, which could enhance the cancer treatment.

Future work

This work allows to select two types of magnetite NP coated with fucoidan with potential for MHT. For further application will be important to:

- Analyse the cytotoxicity of NP coated with fucoidan;
- Study the antitumor effect of NP coated with fucoidan for different tumoral cell lines;
- Assess the hyperthermia property of NP coated with fucoidan for tumor regression;
- Study the possibility of drug introduction using fucoidan functional groups, and its evaluation in terms of antitumor efficiency

References

[1] M. M. Cruz, L. P. Ferreira, A. F. Alves, S. G. Mendo, P. Ferreira, M. Godinho & M. D. Carvalho, “Nanoparticles for Magnetic Hyperthermia,” in *Nanostructures for Cancer Therapy*, vol. 63, Elsevier Inc., 2016, pp. 485–511.

[2] Salunkhe, Khot and Pawar, “Magnetic hyperthermia with magnetic nanoparticles: a status review.,” *Curr. Top. Med. Chem.*, vol. 14, no. 5, pp. 572–94, 2014.

[3] “http://www.who.int/news-room/headlines/03-02-2017-early-cancer-diagnosis-saves-lives-cuts-treatment-costs,” 2018. [Online]. Available: http://www.who.int/mediacentre/factsheets/fs297/en/. [Accessed: 08-Mar-2018].

[4] Direcçao-Geral da Saúde, “Doenças Oncológicas em Números,” Lisboa, 2015.

[5] Atashrazm, Lowenthal, Woods, Holloway and Dickinson, “Fucoidan and cancer: A multifunctional molecule with anti-tumor potential,” *Mar. Drugs*, vol. 13, no. 4, pp. 2327–2346, 2015.

[6] “Liga Portuguesa contra o cancro.” [Online]. Available: https://www.ligacontracancro.pt/metodos-de-tratamento/. [Accessed: 30-May-2018].

[7] Hervault and Thanh, “Magnetic nanoparticle-based therapeutic agents for thermo-chemotherapy treatment of cancer,” *Nanoscale*, vol. 6, no. 20, pp. 11553–11573, 2014.

[8] Shetake, Balla, Kumar and Pandey, “Magnetic hyperthermia therapy: An emerging modality of cancer treatment in combination with radiotherapy,” *J. Radiat. Cancer Res.*, vol. 7, no. 1, p. 13, 2016.

[9] Hedayatnasab, Abnisa and Daud, “Review on magnetic nanoparticles for magnetic nanofluid hyperthermia application,” *Mater. Des.*, vol. 123, pp. 174–196, 2017.

[10] Mohammed, Gomaa, Ragab and Zhu, “Magnetic nanoparticles for environmental and biomedical applications: A review,” *Particuology*, vol. 30, pp. 1–14, 2016.

[11] Lu, Salabas and Schüth, “Magnetic nanoparticles: Synthesis, protection, functionalization, and application,” *Angew. Chemie - Int. Ed.*, vol. 46, no. 8, pp. 1222–1244, 2007.

[12] Majewski and Thierry, “Functionalized Magnetite Nanoparticles - Synthesis, Properties, and Bio-Applications,” *Crit. Rev. Solid State Mater. Sci.*, vol. 32, no. 3, pp. 203–215, 2007.

[13] Ghazanfari, Jaafari and Shams, “Perspective of Fe3O4 Nanoparticles Role in Biomedical Applications,” *Biochem. Res. Int.*, vol. 7, no. 5, pp. 1–32, 2016.

[14] Li, Lu, Wei and Zhao, “Fucoidan: Structure and Bioactivity,” *Molecules*, vol. 13, pp. 1671–1695, 2008.

[15] L. Chollet, P. Saboural, C. Chauvierre, J. N. Villemin, D. Letourneur, F. Chaubet & P. Laurienzo, “Fucoidans in nanomedicine,” *Mar. Drugs*, vol. 14, no. 8, pp. 1–24, 2016.

[16] Sanjeewa, Lee, Kim and Jeon, “The potential of brown-algae polysaccharides for the development of anticancer agents: An update on anticancer effects reported for fucoidan and laminaran,” *Carbohydr. Polym.*, vol. 177, no. June, pp. 451–459, 2017.

[17] Kwak, “Fucoidan as a marine anticancer agent in preclinical development,” *Mar. Drugs*, vol. 12, no. 2, pp. 851–870, 2014.

[18] Silva, Andrade, Silva, Bustamante, De Los Santos Valladares and Albino Aguiar, “Synthesis and characterization of Fe3O4 nanoparticles coated with fucan polysaccharides,” *J. Magn. Magn. Mater.*, vol. 343, pp. 138–143, 2013.

[19] V. A. J. Silva, P. L. Andrade, A. Bustamante, L. de los Santos Valladares, M. Mejia, I. A. Souza, K. P. S. Cavalcanti, M. P. C. Silva & J. A. Aguiar, “Magnetic and Mössbauer studies of fucan-coated magnetite nanoparticles for application on antitumoral activity,” *Hyperfine Interact.*, vol. 224, no. 1–3, pp. 227–238, 2013.

[20] “The new heckel HT3000.” [Online]. Available: http://www.hydrosun.de/en/products/ht3000. [Accessed: 08-Apr-2018].

[21] Mallory, Gogineni, Jones, Greer and Simone, “Therapeutic hyperthermia: The old, the new, and the upcoming,” *Crit. Rev. Oncol. Hematol.*, vol. 97, pp. 56–64, 2016.

[22] J. Beik, Z. Abed, F. S. Ghoreishi, S. Hosseini-Nami, S. Mehrzadi, A. Shakeri-Zadeh & S. K. Kamrava, “Nanotechnology in hyperthermia cancer therapy: From fundamental principles to advanced applications,” *J. Control. Release*, vol. 235, pp. 205–221, 2016.

[23] A. C. Silva, T. R. Oliveira, J. B. Mamani, S. M. F. Malheiros, L. Malavolta, L. F. Pavon, T. T. Sibov, E. Amaro, A. Tannús, E. L. G. Vidoto, M. J. Martins, R. S. Santos & L. F. Gamarra, “Application of hyperthermia induced by superparamagnetic iron oxide nanoparticles in glioma treatment.,” *Int. J. Nanomedicine*, vol. 6, pp. 591–603, 2011.

[24] K. Maier-Hauff, R. Rothe, R. Scholz, U. Gneveckow, P. Wust, B. Thiesen, A. Feussner, A. Deimling, N. Waldoefner, R. Felix & A. Jordan, “Intracranial thermotherapy using magnetic nanoparticles combined with external beam radiotherapy: Results of a feasibility study on patients with glioblastoma multiforme,” *J. Neurooncol.*, vol. 81, no. 1, pp. 53–60, 2007.

[25] Thiesen and Jordan, “Clinical applications of magnetic nanoparticles for hyperthermia,” *Int. J. Hyperth.*, vol. 24, no. 6, pp. 467–474, 2008.

[26] M. Johannsen, U. Gneveckow, K. Taymoorian, B. Thiesen, N. Waldöfner, R. Scholz, K. Jung, A. Jordan, P. Wust & S. A. Loening, “Morbidity and quality of life during thermotherapy using magnetic nanoparticles in locally recurrent prostate cancer: Results of a prospective phase I trial,” *Int. J. Hyperth.*, vol. 23, no. 3, pp. 315–323, 2006.

[27] Forster, Harriss-Phillips, Douglass and Bezak, “A review of the development of tumor vasculature and its effects on the tumor microenvironment.,” *Hypoxia (Auckland, N.Z.)*, vol. 5, pp. 21–32, 2017.

[28] Issels, “Hyperthermia adds to chemotherapy,” *Eur. J. Cancer*, vol. 44, no. 17, pp. 2546–2554, 2008.

[29] Gupta and Gupta, “Synthesis and surface engineering of iron oxide nanoparticles for biomedical applications,” *Biomaterials*, vol. 26, no. 18, pp. 3995–4021, 2004.

[30] Wu, Wu, Yu, Jiang and Kim, “Recent progress on magnetic iron oxide nanoparticles: Synthesis, surface functional strategies and biomedical applications,” *Sci. Technol. Adv. Mater.*, vol. 16, no. 2, p. 23501, 2015.

[31] Cullity and C.D.Graham, *Introduction To Magnetic Materials*, IEEE Press. Wiley, 2009.

[32] O´Handley Robert C., *Modern Magnetic Materials: principles and applications*. John Wiley & Sons, Inc., 2000.

[33] R.M.Cornell and U.Schwertmann, *The Iron Oxides*. WILEY-VCH GmbH& Co.KGaA, 2003.

[34] Callister and Rethwisch, *Materials science and engineering: an introduction*, vol. 94. John Wiley & Sons, Inc., 2007.

[35] Willard, Kurihara, Carpenter, Calvin and Harris, “Chemically prepared magnetic

nanoparticles," *Int. Mater. Rev.*, vol. 49, no. 3–4, pp. 125–170, 2004.

[36] Kafrouni and Savadogo, "Recent progress on magnetic nanoparticles for magnetic hyperthermia," *Prog. Biomater.*, vol. 5, no. 3–4, pp. 147–160, 2016.

[37] Laurent, Dutz, Häfeli and Mahmoudi, "Magnetic fluid hyperthermia: Focus on superparamagnetic iron oxide nanoparticles," *Adv. Colloid Interface Sci.*, vol. 166, no. 1–2, pp. 8–23, 2011.

[38] Akbarzadeh, Samiei and Davaran, "Magnetic nanoparticles: preparation, physical properties, and applications in biomedicine," *Nanoscale Res. Lett.*, vol. 7, no. 1, p. 144, 2012.

[39] Dave and Gao, "Monodisperse magnetic nanoparticles for biodetection , imaging , and drug delivery : a versatile and evolving technology," *Nanomed Nanobiotechnol*, no. December, pp. 583–609, 2009.

[40] Jeyadevan, "Present status and prospects of magnetite nanoparticles-based hyperthermia," *J. Ceram. Soc. Japan*, vol. 118, no. 6, pp. 391–401, 2010.

[41] Salas, Veintemillas-Verdaguer and Morales, "Relationship between physico-chemical properties of magnetic fluids and their heating capacity," *Int. J. Hyperth.*, vol. 29, no. 8, pp. 768–776, 2013.

[42] Obaidat, Issa and Haik, "Magnetic Properties of Magnetic Nanoparticles for Efficient Hyperthermia," *Nanomaterials*, vol. 5, no. 1, pp. 63–89, 2015.

[43] Wu and Wang, "Magnetic hyperthermia performance of magnetite nanoparticle assemblies under different driving fields," *AIP Adv.*, vol. 7, no. 5, 2017.

[44] Banobre-Lopez, Teijeiro and Rivas, "Magnetic nanoparticle-based hyperthermia for cancer treatment," *Reports Pract. Oncol. Radiother.*, vol. 18, no. 6, pp. 397–400, 2013.

[45] Mosayebi, Kiyasatfar and Laurent, *Synthesis, Functionalization, and Design of Magnetic Nanoparticles for Theranostic Applications*, vol. 1700306. 2017.

[46] Issa, Obaidat, Albiss and Haik, "Magnetic nanoparticles: Surface effects and properties related to biomedicine applications," *Int. J. Mol. Sci.*, vol. 14, no. 11, pp. 21266–21305, 2013.

[47] Lee, "Magnetite (Fe3O4): Properties, Synthesis, and Applications," *Lehigh Rev.*, vol. 15, 2007.

[48] Bououdina and Davim, *Handbook of Research on Nanoscience, Nanotechnology, and Advanced Materials*. IGI Global, 2014.

[49] Sun, Lee and Zhang, "Magnetic nanoparticles in MR imaging and drug delivery," *Adv. Drug Deliv. Rev.*, vol. 60, no. 11, pp. 1252–1265, 2008.

[50] Noh, Moon, Shin, Lim and Cheon, "Recent advances of magneto-thermal capabilities of nanoparticles: From design principles to biomedical applications," *Nano Today*, vol. 13, pp. 61–76, 2017.

[51] Abenojar, Wickramasinghe, Bas-Concepcion and Samia, "Structural effects on the magnetic hyperthermia properties of iron oxide nanoparticles," *Prog. Nat. Sci. Mater. Int.*, vol. 26, no. 5, pp. 440–448, 2016.

[52] Revia and Zhang, "Magnetite nanoparticles for cancer diagnosis, treatment, and treatment monitoring: Recent advances," *Mater. Today*, vol. 19, no. 3, pp. 157–168, 2016.

[53] G. Zhen, B. W. Muir, B. a. Moffat, P. Harbour, K. S. Murray, B. Moubaraki, K. Suzuki, I.

Madsen, N. Agron-Olshina, L. Waddington, P. Mulvaney & P. G. Hartley, “Comparative Study of the Magnetic Behavior of Spherical and Cubic Superparamagnetic Iron Oxide Nanoparticles,” *J. Phys. Chem. C*, vol. 115, no. 2, pp. 327–334, 2011.

[54] C. De Montferrand, L. Hu, I. Milosevic, V. Russier, D. Bonnin, L. Motte, A. Brioude & Y. Lalatonne, “Iron oxide nanoparticles with sizes, shapes and compositions resulting in different magnetization signatures as potential labels for multiparametric detection,” *Acta Biomater.*, vol. 9, no. 4, pp. 6150–6157, 2013.

[55] A. Ali, H. Zafar, M. Zia, I. ul Haq, A. R. Phull, J. S. Ali & A. Hussain, “Synthesis, characterization, applications, and challenges of iron oxide nanoparticles,” *Nanotechnol. Sci. Appl.*, vol. 9, pp. 49–67, 2016.

[56] Lodhia, Mandarano, Ferris, Eu and Cowell, “Development and use of iron oxide nanoparticles (Part 1): Synthesis of iron oxide nanoparticles for MRI,” *Biomed. Imaging Interv. J.*, vol. 6, no. 2, 2010.

[57] Carvalho, Henriques, Ferreira, Godinho and Cruz, “Iron oxide nanoparticles: The Influence of synthesis method and size on composition and magnetic properties,” *J. Solid State Chem.*, vol. 201, pp. 144–152, 2013.

[58] A. F. Alves, S. G. Mendo, L. P. Ferreira, M. H. Mendonça, P. Ferreira, M. Godinho, M. M. Cruz & M. D. Carvalho, “Gelatine-assisted synthesis of magnetite nanoparticles for magnetic hyperthermia,” *J. Nanoparticle Res.*, vol. 18, no. 1, pp. 1–13, 2016.

[59] A. Khan, M. H. Shah, M. Nauman, I. Hakim, G. Shahid, P. Niaz, H. Sethi, S. Aziz & M. Arabdin, “Synthesis and characterization of biocompatible Fe3O4 nanoparticles,” *J. Pak. Med. Assoc.*, vol. 67, no. 8, pp. 1180–1185, 2006.

[60] Carlson and Kawatra, “Factors affecting zeta potential of iron oxides,” *Miner. Process. Extr. Metall. Rev.*, vol. 34, no. 5, pp. 269–303, 2013.

[61] Venkatesan, Anil, Kim and Shim, “Seaweed polysaccharide-based nanoparticles: Preparation and applications for drug delivery,” *Polymers (Basel).*, vol. 8, no. 2, 2016.

[62] Senthilkumar, Manivasagan, Venkatesan and Kim, “Brown seaweed fucoidan: Biological activity and apoptosis, growth signaling mechanism in cancer,” *Int. J. Biol. Macromol.*, vol. 60, pp. 366–374, 2013.

[63] Manivasagan, Bharathiraja, Moorthy, Oh, Seo and Oh, “Marine Biopolymer-Based Nanomaterials as a Novel Platform for Theranostic Applications,” *Polym. Rev.*, vol. 57, no. 4, pp. 631–667, 2017.

[64] Wu, Sun, Su, Yu, Yu and Zhang, “A review about the development of fucoidan in antitumor activity: Progress and challenges,” *Carbohydr. Polym.*, vol. 154, pp. 96–111, 2016.

[65] Deniaud-Bouët, Hardouin, Potin, Kloareg and Hervé, “A review about brown algal cell walls and fucose-containing sulfated polysaccharides: Cell wall context, biomedical properties and key research challenges,” *Carbohydr. Polym.*, vol. 175, pp. 395–408, 2017.

[66] Koyanagi, Tanigawa, Nakagawa, Soeda and Shimeno, “Oversulfation of fucoidan enhances its anti-angiogenic and antitumor activities,” vol. 65, pp. 173–179, 2003.

[67] C. Oliveira, A. S. Ferreira, R. Novoa-Carballal, C. Nunes, I. Pashkuleva, N. M. Neves, M. A. Coimbra, R. L. Reis, A. Martins & T. H. Silva, “The Key Role of Sulfation and Branching on Fucoidan Antitumor Activity,” *Macromol. Biosci.*, vol. 17, no. 5, pp. 1–13, 2017.

[68] B. Jang, M. S. Moorthy, P. Manivasagan, L. Xu, K. Song, K. D. Lee, M. Kwak, J. Oh & J.-

O. Jin, “Fucoidan-coated CuS nanoparticles for chemo-and photothermal therapy against cancer,” *Oncotarget*, vol. 9, no. 16, pp. 12649–12661, 2018.

[69] S. P. Myers, J. O’Connor, J. H. Fitton, L. Brooks, M. Rolfe, P. Connellan, H. Wohlmuth, P. A. Cheras & C. Morris, “A combined Phase I and II open-label study on the Immunomodulatory effects of seaweed extract nutrient complex,” *Biol. Targets Ther.*, vol. 5, pp. 45–60, 2011.

[70] S. Balasubramanian, A. Ravindran Girija, Y. Nagaoka, S. Iwai, M. Suzuki, V. Kizhikkilot, Y. Yoshida, T. Maekawa & S. Dasappan Nair, “Curcumin and 5-Fluorouracil-loaded, folate- and transferrin-decorated polymeric magnetic nanoformulation: A synergistic cancer therapeutic approach, accelerated by magnetic hyperthermia,” *Int. J. Nanomedicine*, vol. 9, no. 1, pp. 437–459, 2014.

[71] Jang, Kang and El-Sayed, “Facile size-controlled synthesis of fucoidan-coated gold nanoparticles and cooperative anticancer effect with doxorubicin,” *J. Mater. Chem. B*, vol. 5, no. 30, pp. 6147–6153, 2017.

[72] M. Santha Moorthy, B. Subramanian, M. Panchanathan, S. Mondal, H. Kim, K. D. Lee & J. Oh, “Fucoidan-coated core–shell magnetic mesoporous silica nanoparticles for chemotherapy and magnetic hyperthermia-based thermal therapy applications,” *New J. Chem.*, vol. 41, no. 24, pp. 15334–15346, 2017.

[73] M. R. A. Abdollah, T. J. Carter, C. Jones, T. L. Kalber, V. Rajkumar, B. Tolner, C. Gruettner, M. Zaw-Thin, J. Baguña Torres, M. Ellis, M. Robson, R. B. Pedley, P. Mulholland, R. T. M. de Rosales & K. A. Chester, “Fucoidan Prolongs the Circulation Time of Dextran-Coated Iron Oxide Nanoparticles,” *ACS Nano*, p. acsnano.7b06734, 2017.

[74] Coimbra, Delgadillo, Waldron and Selvendran, “Isolation and Analysis of Cell Wall Polymers,” *Mod. Methods plant Anal.*, vol. 17, pp. 19–44, 1996.

[75] Selvendran, March and Ring, “Determination of aldoses and uronic acid content of vegetable fiber,” *Anal. Biochem.*, vol. 96, no. 2, pp. 282–292, 1979.

[76] M. Mahdavi, M. Bin Ahmad, M. J. Haron, F. Namvar, B. Nadi, M. Z. Ab Rahman & J. Amin, “Synthesis, surface modification and characterisation of biocompatible magnetic iron oxide nanoparticles for biomedical applications,” *Molecules*, vol. 18, no. 7, pp. 7533–7548, 2013.

[77] Tran, Tran, Vo and Tran, “Effect of pH on the Synthesis of Fucoidan-coated Magnetic Iron Oxide Nanopartciles for Biomedical Apllications,” vol. 46, pp. 5–7, 2015.

[78] Y. P. Yew, K. Shameli, M. Miyake, N. Kuwano, N. B. Bt Ahmad Khairudin, S. E. Bt Mohamad & K. X. Lee, “Green Synthesis of Magnetite (Fe3O4) Nanoparticles Using Seaweed (Kappaphycus alvarezii) Extract,” *Nanoscale Res. Lett.*, vol. 11, no. 1, p. 276, 2016.

[79] ICDD, “Card,” 2018. [Online]. Available: http://www.icdd.com/.

[80] Patterson, “The scherrer formula for X-ray particle size determination,” *Phys. Rev.*, vol. 56, no. 10, pp. 978–982, 1939.

[81] Sing, “Reporting physisorption data for gas/solid systems with special reference to the determination of surface area and porosity (Provisional),” *Pure Appl. Chem*, vol. 54, no. 11, pp. 603–619, 1982.

[82] Eliceiri, Schneider, Rasband and Eliceiri, “NIH Image to ImageJ : 25 years of image analysis HISTORICAL commentary NIH Image to ImageJ : 25 years of image analysis,” *Nat. Methods*, vol. 9, no. 7, pp. 671–675, 2012.

[83] Bini, Marques, Santos, Chaker and Jafelicci, "Synthesis and functionalization of magnetite nanoparticles with different amino-functional alkoxysilanes," *J. Magn. Magn. Mater.*, vol. 324, no. 4, pp. 534–539, 2012.

[84] Berteau and Mulloy, "Sulfated fucans, fresh perspectives: Structures, functions, and biological properties of sulfated fucans and an overview of enzymes active toward this class of polysaccharide," *Glycobiology*, vol. 13, no. 6, pp. 29–40, 2003.

[85] Fernando, Sanjeewa and Samarakoon, "FTIR characterization and antioxidant activity of water soluble crude polysaccharides of Sri Lankan marine algae," *Algae*, vol. 32, no. 1, pp. 75–86, 2017.

[86] Duarte, Cardoso, Noseda and Cerezo, "Structural studies on fucoidans from the brown seaweed Sargassum stenophyllum," vol. 333, pp. 281–293, 2001.

[87] A. Zayed, K. Muffler, T. Hahn, S. Rupp, D. Finkelmeier, A. Burger-Kentischer & R. Ulber, "Physicochemical and biological characterization of fucoidan from fucus vesiculosus purified by dye affinity chromatography," *Mar. Drugs*, vol. 14, no. 4, pp. 1–15, 2016.

[88] Mascolo, Pei and Ring, "Room Temperature Co-Precipitation Synthesis of Magnetite Nanoparticles in a Large ph Window with Different Bases," *Materials (Basel).*, vol. 6, no. 12, pp. 5549–5567, 2013.

[89] M. Thommes, K. Kaneko, A. V. Neimark, J. P. Olivier, F. Rodriguez-Reinoso, J. Rouquerol & K. S. W. Sing, "Physisorption of gases, with special reference to the evaluation of surface area and pore size distribution (IUPAC Technical Report)," *Pure Appl. Chem.*, vol. 87, no. 9–10, pp. 1051–1069, 2015.

[90] M. O. Rocha Amorim, D. Lopes Gomes, L. A. Dantas, R. L. Silva Viana, S. C. Chiquetti, J. Almeida-Lima, L. Silva Costa & H. A. Oliveira Rocha, "Fucan-coated silver nanoparticles synthesized by a green method induce human renal adenocarcinoma cell death," *Int. J. Biol. Macromol.*, vol. 93, pp. 57–65, 2016.

[91] A. C. Pinheiro, A. I. Bourbon, M. A. Cerqueira, É. Maricato, C. Nunes, M. A. Coimbra & A. A. Vicente, "Chitosan/fucoidan multilayer nanocapsules as a vehicle for controlled release of bioactive compounds," *Carbohydr. Polym.*, vol. 115, pp. 1–9, 2015.

[92] Daniel-da-Silva, Trindade, Goodfellow, Costa, Correia and Gil, "In situ synthesis of magnetite nanoparticles in carrageenan gels," *Biomacromolecules*, vol. 8, no. 8, pp. 2350–2357, 2007.

[93] Kallumadil, Tada, Nakagawa, Abe, Southern and Pankhurst, "Suitability of commercial colloids for magnetic hyperthermia," *J. Magn. Magn. Mater.*, vol. 321, no. 10, pp. 1509–1513, 2009.

[94] Ludwig, Stapf, Dutz, Müller, Teichgräber and Hilger, "Structural properties of magnetic nanoparticles determine their heating behavior - an estimation of the in vivo heating potential," *Nanoscale Res. Lett.*, vol. 9, no. 1, 2014.

[95] Gonzales-Weimuller, Zeisberger and Krishnan, "Size-dependant heating rates of iron oxide nanoparticles for magnetic fluid hyperthermia," *J. Magn. Magn. Mater.*, vol. 321, no. 13, pp. 1947–1950, 2009.

[96] Giri, Pradhan, Sriharsha and Bahadur, "Preparation and investigation of potentiality of different soft ferrites for hyperthermia applications," *J. Appl. Phys.*, vol. 97, no. 10, pp. 10–14, 2005.

[97] R. Ghosh, L. Pradhan, Y. P. Devi, S. S. Meena, R. Tewari, A. Kumar, S. Sharma, N. S.

Gajbhiye, R. K. Vatsa, B. N. Pandey & R. S. Ningthoujam, “Induction heating studies of Fe3O4magnetic nanoparticles capped with oleic acid and polyethylene glycol for hyperthermia,” *J. Mater. Chem.*, vol. 21, no. 35, pp. 13388–13398, 2011.

[98] P. B. Shete, R. M. Patil, N. D. Thorat, A. Prasad, R. S. Ningthoujam, S. J. Ghosh & S. H. Pawar, “Magnetic chitosan nanocomposite for hyperthermia therapy application: Preparation, characterization and in vitro experiments,” *Appl. Surf. Sci.*, vol. 288, pp. 149–157, 2014.